AD-A118 752 AIR FORCE GEOPHYSICS LAB HANSCOM AFB MA F/G 7/4
DEVELOPMENT OF AN ION MASS SPECTROMETER AND SOUNDING ROCKET SYS--ETC(U)
JAN 82 A BAILEY, R NARCISI, L WLODYKA
UNCLASSIFIED AFGL-TR-82-0022 NL

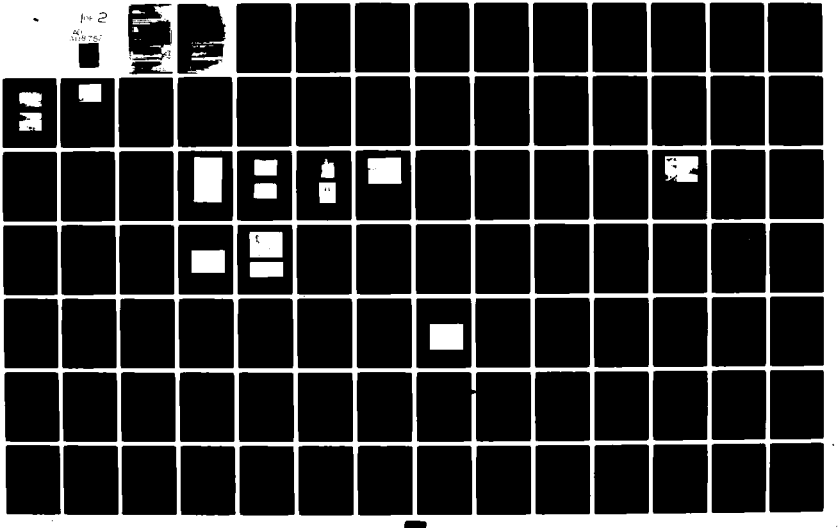

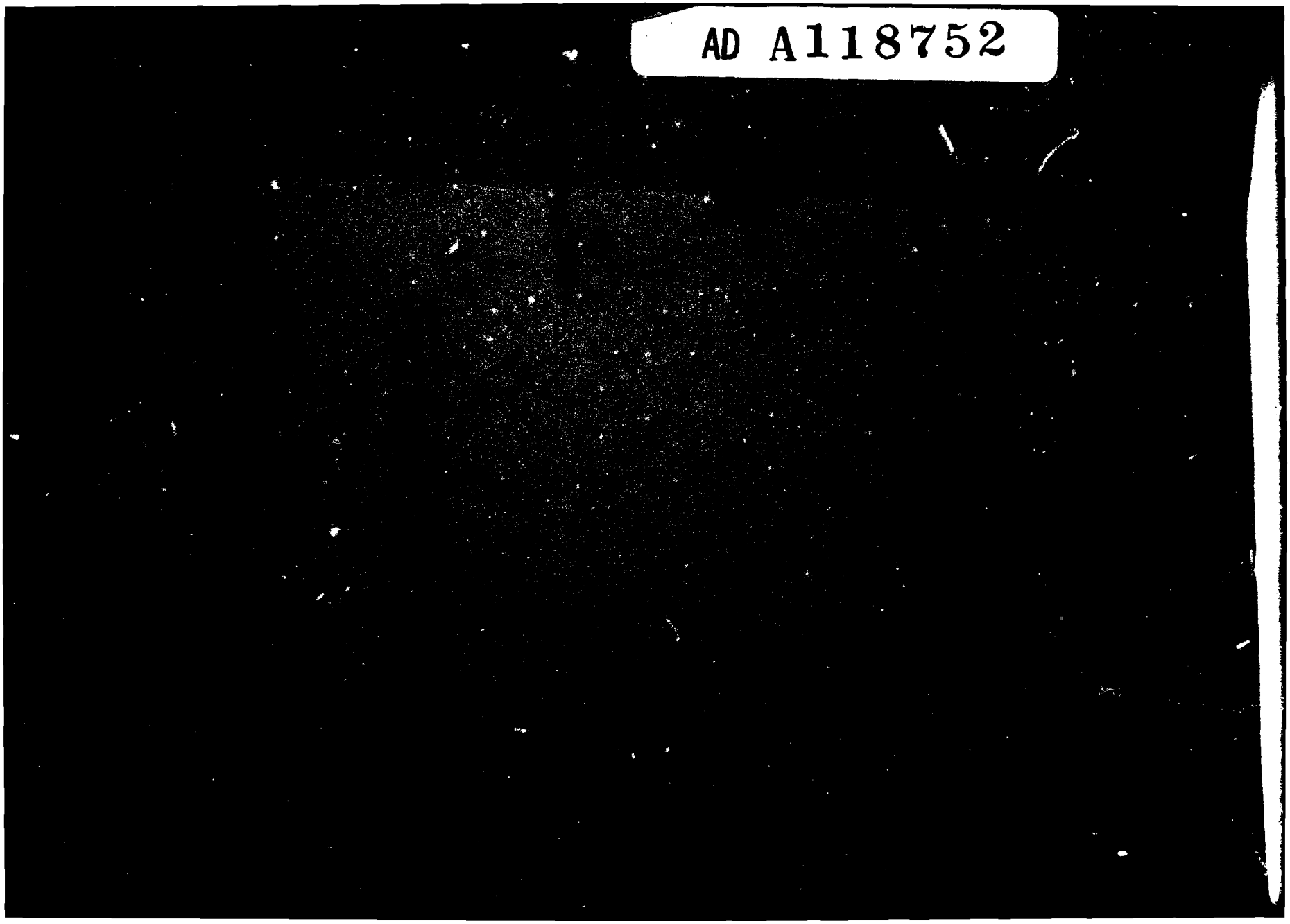

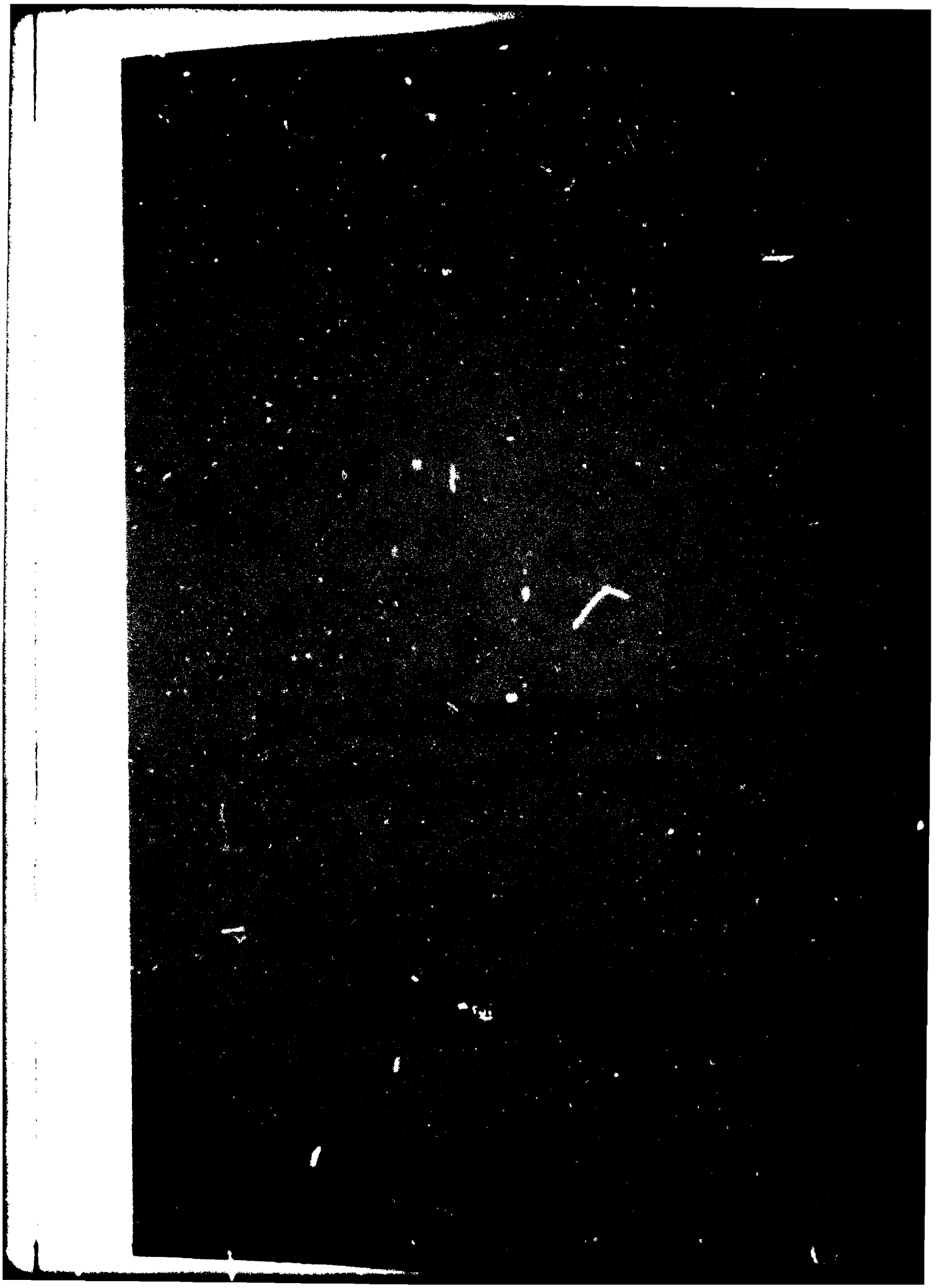

Unclassified

SECURITY CLASSIFICATION OF THIS PAGE (When Data Entered)

REPORT DOCUMENTATION PAGE		READ INSTRUCTIONS BEFORE COMPLETING FORM
1. REPORT NUMBER AFGL-TR-82-0022	2. GOVT ACCESSION NO. AD-A118752	3. RECIPIENT'S CATALOG NUMBER
4. TITLE (and Subtitle) DEVELOPMENT OF AN ION MASS SPECTROMETER AND SOUNDING ROCKET SYSTEM FOR D-REGION CLUSTER-ION MEASUREMENTS		5. TYPE OF REPORT & PERIOD COVERED Scientific. Final. 6. PERFORMING ORG. REPORT NUMBER IP, No. 309
7. AUTHOR(s) A. Bailey G. Federico R. Narcisi E. McKenna L. Wlodyka		8. CONTRACT OR GRANT NUMBER(s)
9. PERFORMING ORGANIZATION NAME AND ADDRESS Air Force Geophysics Laboratory (LKD) Hanscom AFB Massachusetts 01731		10. PROGRAM ELEMENT, PROJECT, TASK AREA & WORK UNIT NUMBERS 61102F 2310G304
11. CONTROLLING OFFICE NAME AND ADDRESS Air Force Geophysics Laboratory (LKD) Hanscom AFB Massachusetts 01731		12. REPORT DATE 27 January 1982 13. NUMBER OF PAGES 103
14. MONITORING AGENCY NAME & ADDRESS(if different from Controlling Office)		15. SECURITY CLASS. (of this report) Unclassified 15a. DECLASSIFICATION DOWNGRADING SCHEDULE
16. DISTRIBUTION STATEMENT (of this Report) Approved for public release; distribution unlimited.		
17. DISTRIBUTION STATEMENT (of the abstract entered in Block 20, if different from Report)		
18. SUPPLEMENTARY NOTES		
19. KEY WORDS (Continue on reverse side if necessary and identify by block number) Cluster ion Ion composition Ion mass spectrometer D-region Ionosphere Sounding rocket		

20. ABSTRACT (Continue on reverse side if necessary and identify by block number)

An Ion Mass Spectrometer and supporting Sounding Rocket System were developed to make in situ measurements of cluster-ions in the D-region of the ionosphere. A cryogenically vacuum-pumped quadrupole mass filter and secondary emission ion counter are coupled to make mass spectral measurements of positive and negative ion composition in ambient gas sampled at the apex of a cone designed to attach the shock wave induced by supersonic sounding rocket speeds. A Gerdien Condenser and Retarding Potential Analyzer are

DD FORM 1 JAN 73 1473

Unclassified

SECURITY CLASSIFICATION OF THIS PAGE (When Data Entered)

20 Abstract (Continued)

are also integrated with attitude control and payload recovery units into a complete two-stage sounding rocket system. Salient details of instrument are presented and referenced, and preparation and calibration procedures are discussed. Comparisons of calibration data and early-flight data are made with similar data from earlier blunt-nosed instruments.

Preface

The preparation of this report was possible only because of the manifold extra contributions of the following:

R. Sukys	Northeastern University
R. Anderson	Northeastern University
R. Eng	Northeastern University
C. Kuczon	Tricon Associates
R. Wilton	AFGL/LCR
J. Griffin	AFGL/LCR
R. Rossi	AFGL/LKD
J. Borghetti	AFGL/LKD
P. Beardsley	AFGL/LKD

Contents

Contents

Illustrations

Illustrations

Tables

Development of an Ion Mass Spectrometer and Sounding Rocket System for D-Region Cluster-Ion Measurements

1. GENERAL BACKGROUND

1.1 Objectives and Foundations

The objective of the AFGL work unit reported herein was to develop and test instrumentation with which to make in situ measurements of both positive and negative ion composition and densities in the D and lower E regions of the ionosphere. Measurement emphasis was to be placed on determination of the mass, quantities, and distribution of large cluster ions, especially between 40 and 90 km above sea level. Consequently, the label "Cluster Ion Mass Spectrometer" (CIMS).

The altitude range-of-interest for these measurements effectively limited the choice of instrument vehicle to a sounding rocket that must travel at supersonic speeds to maintain altitude for sufficiently long intervals to make substantive measurements over most of the whole range.*

The measurement objectives have come about as an extension of sounding rocket measurement efforts which have been actively pursued by AFGL(AFCRL) and others since 1961. The developments summarized here are a combination of

(Received for publication 18 January 1982)

*The lower fringe of this range can be reached with high-altitude balloons. Higher altitudes could also be reached with a battery of sounding rockets, each designed to operate at a different apogee, to cover the full range with subsonic sampling.

the better techniques, with added improvements, that have evolved from these efforts. The CIMS instrument concept resulting from these developments is illustrated in block form by Figure 1.

Several phases of parallel development effort are involved, and are discussed in varying degrees in the following report. Extensive detail is deferred or referenced to other reports where they exist.

1.2 Phases of Development, CIMS

As a consequence of the altitude access problem previously mentioned, a significant element of the CIMS instrument development was the design of a shock-attaching sampling aperture which would not introduce shock-induced disruptions to the ion composition of the sample.[1] Other crucial areas wherein instrument development was needed included:

a. Vacuum pump adaptation to the conical sampling aperture requirements[2] (see Appendix A, and Section 2.2).

b. Improved CIMS design to provide for dual polarity ion measurements over an extended amu range.

1.3 Phases of Development, Other

This work unit also encompassed significant development effort on a broader scale than just the CIMS instrument. A complete payload system had to be developed to support the CIMS. The most important development was a vehicle attitude control system that would maintain alignment of the sampling axis with the vehicle velocity vector (see Section 3.2.5). Without such control the shock-attachment requirement would be defeated. Other new supporting system development efforts included:

a. Provision for supporting supplementary experiments to provide reference data for CIMS calibration and data interpretation.

b. Trajectory tracking capability.

c. Payload recovery capability (see Figures 2-4).

2. CIMS DEVELOPMENT

The following description of the mass spectrometer instrument development effort is divided into four separate areas of concern, three of which have entailed

1. Burke, R.R., and Miller, W.J. (1970) Study of Mass Spectrometer Ion Sampling Processes, AerChem-TP-247, AFCRL-TR-70-0550, AD 725149.
2. Philbrick, C.R., Faucher, G., and Bench, P. (1978) Composition of the mid-latitude winter mesosphere and lower thermosphere, COSPAR: Space Research Volume XVIII, Pergamon Press, Oxford and New York.

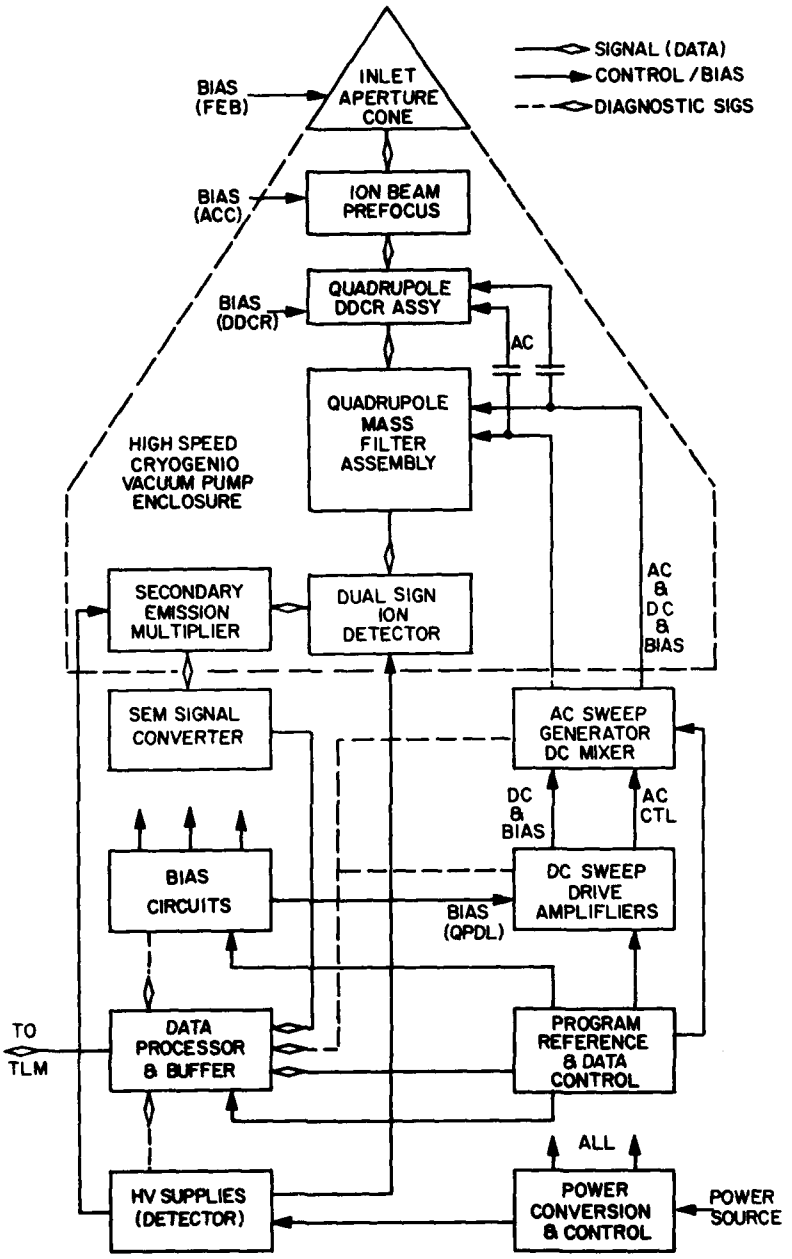

Figure 1. Block Diagram CIMS

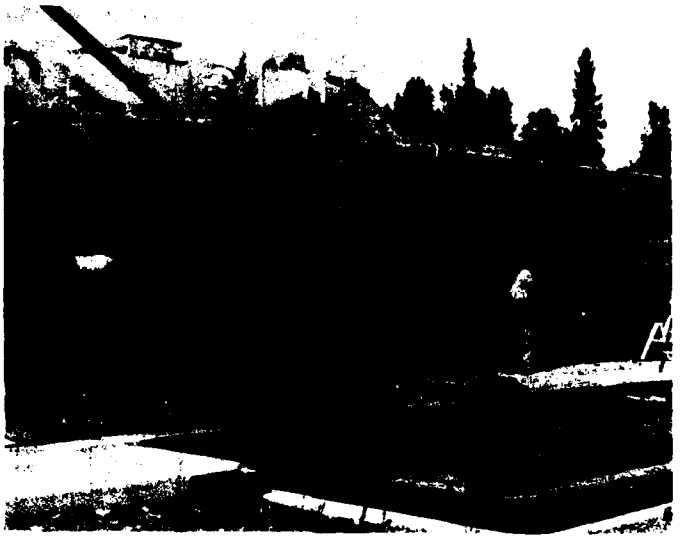

Figure 2. Mounted CIMS Rocket, Univ. of Alasks, PFRR Fairbanks, Alaska

Figure 3. CIMS Payload With Cryogen Fill Line

Figure 4. Portable Pumping System

some new approaches. The fourth, a cryogenically activated liquid helium (LHe) vacuum pump (cryopump), has not been previously reported in detail but has been used successfully by Philbrick et al, of AFGL in 1975.[2]

2.1 Cryopump

There was no extensive cryopump development effort undertaken within the time frame scheduled for this work unit. Consequently, the pumps used in the CIMS instruments flown to date, built by Excalibur Corporation, have incorporated no improvement over those used in experiments previously referenced. Later experience suggests this was an inappropriate tactic, and is discussed in Sections 4 and 5.

Although the Excalibur-designed pump provides the essential pumping performance for these applications, the blunt-nose configuration results in serious shock wave-induced effects which compromise the value of measurements. The pump design problem is extended in scope in this application because of a reconfiguration of the sampling inlet system and the need to operate the CIMS at lower altitudes than had been successfully accommodated before. Results of experiments to date suggest that important modifications to the internal configuration are crucial to adequate performance, especially below 65 km.

Some tentative modifications to the pump design are indicated in Appendix B. In laboratory tests, these modifications have resulted in significant improvements

in pumping capacity and holding time. They employ an inherently greater pumping cross section, and added chilled surfaces in the conical volume, chilled by the LHe boil-off vapors. However, to date, even the evaluation efforts in this area are incomplete. Comments regarding appropriate directions for further work are discussed in Section 5.

For the first CIMS instruments, the Excalibur pump vacuum chamber was simply extended forward by attaching a conical front-end assembly as depicted in Figure 5. The quadrupole mass filter assembly was extended to fill the breach by installing a separate quadrupole "delayed-dc-ramp" assembly (DDCR).[3] Several problems become apparent, though ill-defined, with only a cursory examination of the resulting geometry.

Serious constrictions (A) and (D) exist in the pumping path between the pumping surfaces (B) and the conical expansion region (C). When sampling at 50 km (0.5 torr), through a 0.040-in. aperture, gas throughputs as high as 5×10^{-2} torr-liter/sec may be expected in the forward conical region. The constricted pumping rate has been estimated at about 100 liter/sec; suggesting pressures near 5×10^{-4} torr after expansion. This is clearly an area of concern that requires serious further studies. Early flights have been limited to altitudes about 65 km, in an attempt to avoid the lowest altitude performance shortcomings.

2.2 Sampler/Prefocuser

The design of the shock-attaching sampling aperture is based on exploratory work under DNA Project 5710(1970)[1] and AFCRL Project 8605(1977).[4,5] In the adopted design, the sampling aperture is a 0.04-in. (1 mm) diameter hole in the apex of a cone of 70° total included angle. Figure 6 shows dimensional details of the sampling and prefocusing region.

The main cone is electrically sliced 2.5 in. (6.25 cm) behind the apex (see Appendix E, Figure 5). This permits an ion-attractive bias to be applied, relative to system ground (see "FEB", Table 1). Typical bias voltages in the positive ion mode are -4 V and -10 V. In the negative ion mode, this voltage has typically been switched between +5.8 and +40 V. The higher-magnitude positive voltage has been programmed to explore the impact on spectral distributions (as might result from cluster breakup, etc.) for comparison with blunt-nose instruments

3. Brubaker, W.M. (1968) Advances in Mass Spectrometry, Vol. 4, Elsevier, Amsterdam.

4. Haldeman, C.W., Kraemer, R.A., and Ziph, B. (1977) Wind Tunnel Tests of the Upstream Influence of a Conical Mass Spectrometer Probe, MIT-TR-197, AFGL-TR-77-0210, ADA 047739.

5. Alt, R.E., Price, L.L., Campbell, D.H., Stephenson, W.B., and Powell, H.M. (1980) Temperature and Density Measurements Near a 1/4 Scale Model Upper Atmospheric Probe at Mach Number 3.5, AEDC-TSR-80-V19.

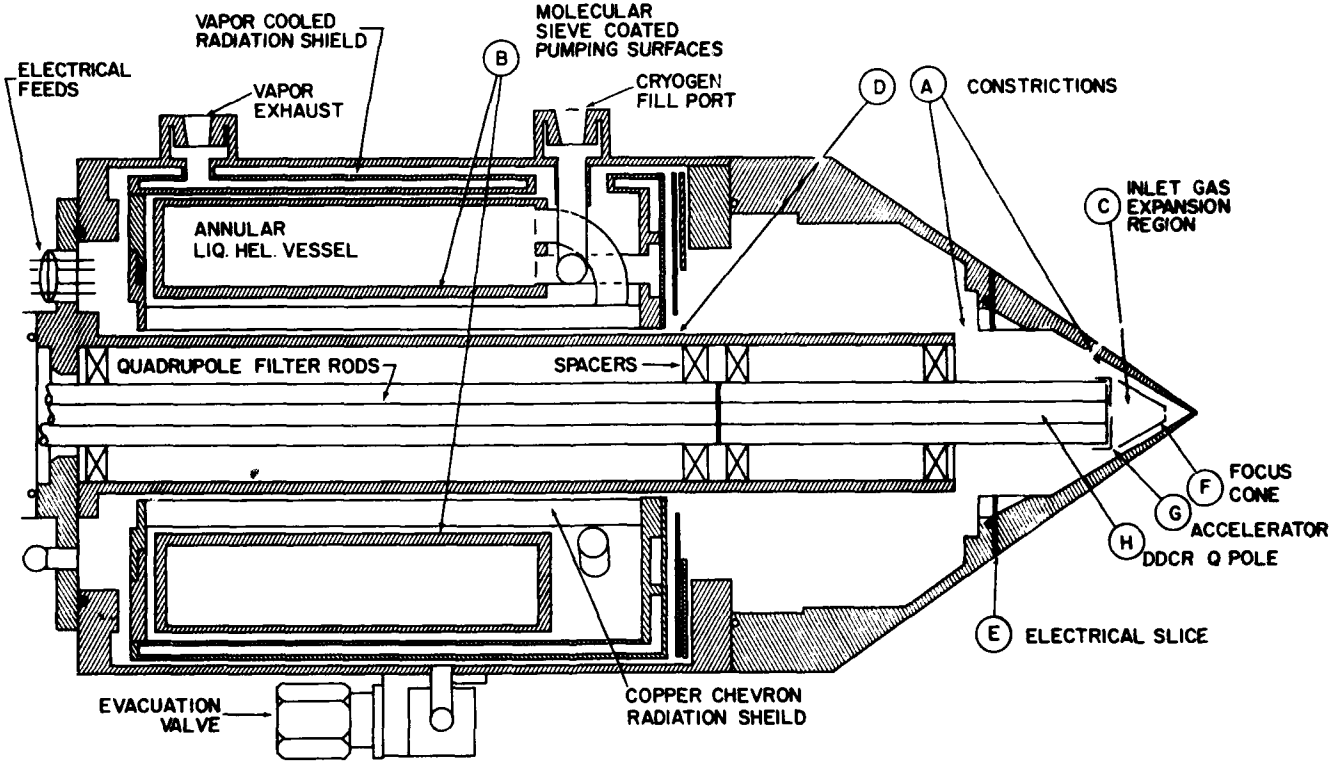

Figure 5. Cryopump Crossection, With Quadrupole Showing Salient Features of Flight Hardware

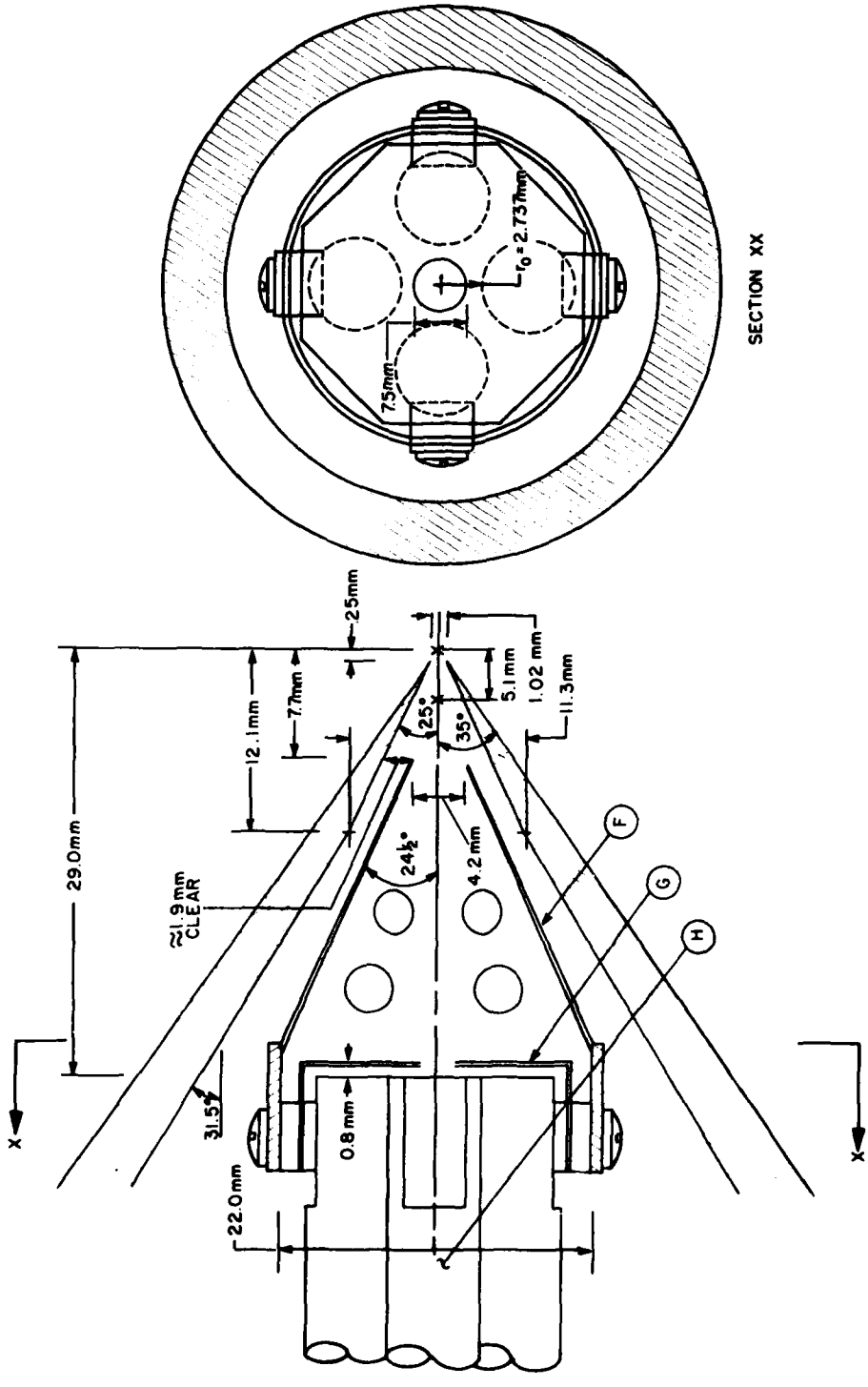

Figure 6. Sampling Aperture Specifications

Table 1. Parameter Comparisons

	WSMR-78	ECLIPSE No. 1	ECLIPSE No. 2	PFRR-80
Electrometer amplifier range:				
min.	1×10^{-11}	1×10^{-11}	1×10^{-11}	5×10^{-12}
max.	1×10^{-6}	1×10^{-5}	1×10^{-5}	1×10^{-5}
Detector biases (both modes):				
SEM anode	+3.47 kV	+3.68 kV	+3.70 kV	+3.83 kV
SEM cathode	+1.0 kV	+0.65 kV	+0.68 kV	+0.86 kV
Target shield	-0.75 kV	-0.80 kV	-0.75 kV	-0.95 kV
Ion target	-2.95 kV	-3.0 kV	-2.9 kV	-2.85 kV
Element biases (+ion mode):				
FEB	-10 V, -3.8 V	-4.04 V	-3.96 V	-4.05 V
ACC	-43 V	-37.2 V	-39.6 V	-44 V
DDCR	-10 V	-10.1 V	-10.7 V	-10.6 V
QPOLE	-10 V	-10.1 V	-10.2 V	-10 V
Element biases (-ion mode):				
FEB	+20 V, +5.6 V*	+39.7 V, 5.7 V	+41.6 V, 5.4 V	+41.9 V, 5.5 V
ACC	+42 V	+37.7 V	+38.6 V	+83 V**
DDCR	+41 V	+40.4 V	+41.05 V	+41.3 V
QPOLE	+20 V	+19.2 V	+20.3 V	+20.9 V

*TI mode stepped through 0 to +40 V. See program Table 2.
**Cone added to ion-focus region.
Typical ac frequency is 2.7 MHz.

where high voltages were required to penetrate a sheath field created by the negative vehicle-to-plasma potential.[6]

Typical focusing voltages applied to electrodes (F) and (G), and to the DDCR reference node (H), are listed in Table 1 and discussed in Appendix C. Section 5.1.1 comments on the urgent need to redesign this prefocuser. This remains one of the more pressing needs for achievement of good negative ion measurements that have eluded success to this writing, as discussed in Section 4.2.

2.3 Dual Polarity Ion Detector

The technique for ion detection was chosen to address the need to sense ions of either polarity. It is an extension of the method used in earlier AFGL work to

6. Sherman, C., and Parker, L.W. (1970) Potential Due to a Circular Double Disk, Physical Sciences Research Paper No. 431, AFCRL-70-0568, AD 715889.

Table 2, Flight Program Sequence, WSMR-78

Line	Mode	Bias (FEB) Nominal	AMU
1	Scan +ions	-3.5	14^+ to 150^+
2	Stepped bias, total +ions	+2,+1,+0 V -1,-2,-3.5,-5,-10 V	$>16^=$
3	Step -ions	+5.5 V	16^-, 32^-
4	Scan -ions	+5.5 V	52^- to 235^-
5	Stepped bias, total +ions	0,+2,+3,+4,+5.5 V +10,+20,+40 V	$>50^-$
6	Scan +ions	-10 V	14^+ to 150^+
7	Step -ions	+20 V	16^-, 32^-
8	Scan -ions	+20 V	52^- to 235^-

measure negative ions.[7] The signal levels of interest require sensitivity from 100 ions/sec to as many as 10^6 ions/sec with sampling intervals of 10 msec. This requires the use of charge multiplications of 10^7 prior to circuit processing (using circuits typically sensitive to inputs > 1 pC). The Johnson Labs Inc. "focused mesh" wide aperture, high gain, CuBe secondary emission multiplier (SEM) was chosen because all of its distinctive characteristics promised to contribute to a solution.

The detection chamber is configured as shown in Figure 7. Applied voltages are typically as indicated.* The objective is to form an accelerating field, which intercepts and is transverse to the ion entry path. Negative ions are attracted directly to the first stage (K) of the SEM. Positive ions are attracted by and pass through the grid (G), then are accelerated sufficiently by the high negative potential on the target (T) to produce emission of electrons which ultimately reach the SEM for detection. Processing of the SEM output signal requires translation from the nominal 3.6 kV SEM anode bias level to ground. The approach employed is discussed in Section 2.4.2.

*Voltages employed for each mission to date are listed in Table 1.

7. Narcisi, R.S., Bailey, A.D., Della Lucca, L., Sherman, C., and Thomas, D.M. (1971) Mass spectrometric measurements of negative ions in the D and lower E regions, J. Atmos. Terr. Phys. 33:1147-1159, Pergamon Press, Northern Ireland.

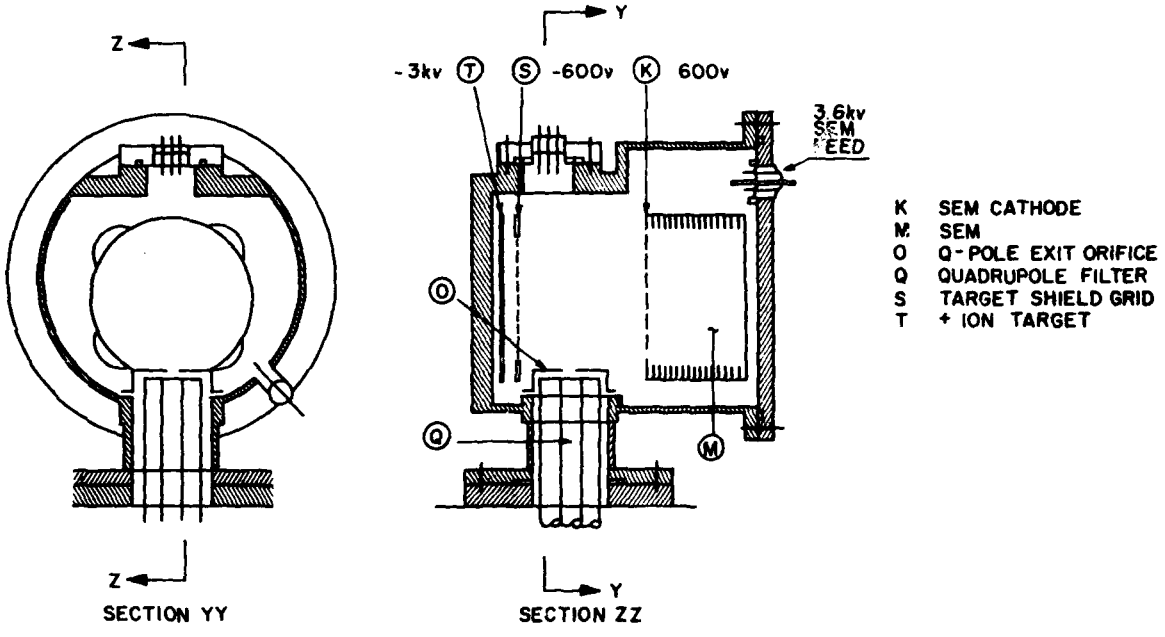

Figure 7. Detection Chamber Showing SEM and Other Electrodes

It may be noted that the energies acquired by the negative ions at the SEM cathode K, are dramatically less than those acquired by positive ions at the target T. This difference is based on the observation that less energy is required to free a detectable electron from the negative ion than to release a free emitted electron from the target by positive ion impact. Clearly, one may suspect variations in performance of this system as a function of ion mass and structure. Just as clearly, little is known about the relative sensitivity of the SEM cathode to electrons of high energy, (2 keV to 4 keV) such as are emitted at the target and the other intermediate electrodes.

No discussion is offered here, nor has any important attempt been made to analyze or investigate the potential effects of these uncertainties on flight data. However, laboratory calibration data have not yet shown evidence of dominant sign or mass dependent effects of these particle-energy characteristics. Consequently, investigation awaits the acquisition of important quantities of perplexing flight data in order to provoke such an investigation. Operation of the SEM in the pulse-counting mode is called for here. Some increase in electronic complexity would be the only price.

2.4 Mass Spectrometer Circuits

Figure 1 is a functional block diagram of the several typical instrument components. Excitation circuit components are: the bias circuits, the dc drive amplifier, the ac generator,* and the high-voltage SEM detector supplies. The bias circuits serve to control the ion flow from inlet to detector. Mass selective focusing of ions is accomplished in the quadrupole assembly by applying the combined outputs of the ac generator and dc drivers (see Appendix C). The high-voltage supplies provide appropriate operating biases for the ion-detecting SEM system.

Detection circuit components are the SEM output current-to-voltage converter (preamplifier), the isolator, and buffers. Control circuit components make up the balance, that is, the reference generator, control-information latches, logic, and memory.

Four important areas of circuit redevelopment were combined into this instrument which provide improvements and extensions of performance over that of its predecessors.

1. The ac generator, discussed in Section 2.4.1, was redesigned in an attempt to achieve: a) higher output voltages; b) improved efficiency; c) improved frequency stability and amu precision; d) more effective shielding; and e) reduced volume.

2. A new, isolated input, current-voltage converter with 5 kV isolation capability was designed to permit operation of the detector SEM in the current mode, at high offset bias levels as described in Section 2.4.2.

*Sometimes referred to as "r-f generator" or "r-f oscillator."

3. Mass scan programming flexibility was greatly enhanced by the design of a new controller, based on LSI technology, which u_es a NMOS EPROM as an instruction storage medium.[8,9] As many as eight separate program sequences, each of up to 16 breakpoints, can be implemented, or one with up to 128 breakpoints. Table 3 describes a 56-breakpoint program used in October 1980.

4. Data precision and processing possibilities have been extended by the integration of a pulse-coded (PCM) data generator with the program controller. This feature has also proved useful at signal-to-noise improvement since, on one occasion, it has permitted extraction of flight data from high telemetry-noise levels that had nearly obliterated analog data carried on other FM subcarrier channels.

In addition to the above listed major areas, other circuits have been improved by taking advantage of recent advances in the state-of-the-component arts and market.

2.4.1 AC GENERATOR

This development effort is reported in detail by Palasek.[10] The single most distinctive feature of the generator is the innovative toroidal core design that permits generation of higher voltages in less space, and is freer from external shield loading effects than preceding designs. A typical ac frequency for the CIMS is 2.7 MHz.

Other improvements in circuit design include the adoption of capacitively/coupled feedback for amplitude control, and protective power shutdown and recovery circuits. Capacitive feedback coupling avoids the high harmonic component feedback experienced with inductive coupling, resulting in improved ac/dc ratio control over the full amplitude range. Temperature stabilization is achieved with detector compensation circuitry, but remains an area of concern because of the necessity to trim as part of the setup process when high-precision amu identification is desired. Protective shutdown/recovery alleviates oscillator lockup problems. See Figures 8 through 10.

Capacitive ac coupling in the amplitude control loop requires that care be exercised in the selection of the type of coupling capacitors (C1 through C4, Fig ure 10). This is to assure tracking of their ratios as a function of environment. Corning CYR glass capacitors are specified.

---

8. Rochefort, J.S., and Sukys, R. (1978) A Digital Control Unit for a Rocketborne Quadrupole Mass Spectrometer, AFGL-TR-78-0106, ADA 057251.
9. Rochefort, J.S., and Sukys, R. (1978) Electronics For A Rocketborne Quadrupole Cluster Ion Mass Filter, AFGL-TR-78-0292, ADA 066289.
10. Palasek, T.A. (1979) An R-F Oscillator for Rocketborne and Balloonborne Quadrupole Mass Spectrometers, AFGL-TR-79-0226, ADA 078797.

Table 3. Flight Program Sequence, PFRR-80

Line	Mode	Bias (FEB) Nominal	AMU
1	Scan +ions	-4 V	14^+ to 43^+
2	Step -ions	+5.8 V	$32^-, 80^-, 98^-, 134^-$
3	Scan +ions	-4 V	42^+ to 100^+
4	Step total +ions	-4 V	$>80^+, >14^+$
5	Step -ions	+5.8 V	16^-
6	Scan -ions	+5.8 V	27^- to 39^-
7	Scan -ions	+5.8 V	45^- to 105^-
8	Scan -ions, dc/ac*	+5.8 V	93^- to 105^-
9	Step +ions	-4 V	$30^+, 32^+, 37^+, 55^+, 73^+$
10	Scan -ions	+5.8 V	104^- to 207^-
11	Step bias, total ions	+5.8, 20, 40 V	$>160^-$
12	Step bias, total ions	+5.8, 20, 40 V	$>14^-$
13	Scan +ions	-4 V	14^+ to 43^+
14	Step -ions	+40 V	$32^-, 80^-, 98^-, 134^-$
15	Scan +ions	-4 V	42^+ to 100^+
16	Step total +ions	-4 V	$>80^+, >14^+$
17	Step -ions	+40 V	16^-
18	Scan -ions	+40 V	27^- to 33^-
19	Step -ions	+40 V	$35^-, 37^-, 46^-$
20	Scan -ions	+40 V	58^- to 64^-
21	Scan -ions	+40 V	75^- to 105^-
22	Scan -ions, dc/ac*	+40 V	93^- to 105^-
23	Step +ions	-4 V	$30^+, 32^+, 37^+, 55^+, 73^+$
24	Scan -ions	+40 V	104^- to 154^-
25	Step bias, total -ions	+40, +20, +5.8 V	$>160^-$
26	Step bias, total -ions	+40, +20, +5.8 V	$>14^-$

*dc/ac ratio set for higher resolution

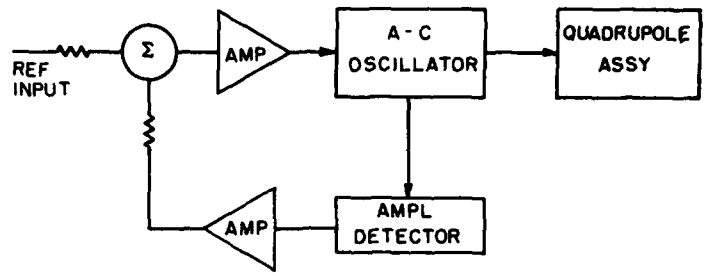

Figure 8. AC Generator Block Diagram

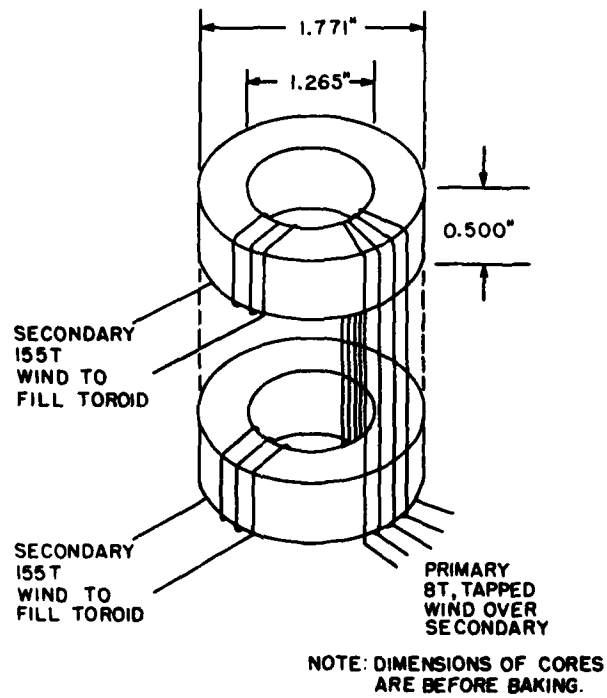

Figure 9. Toroid Winding

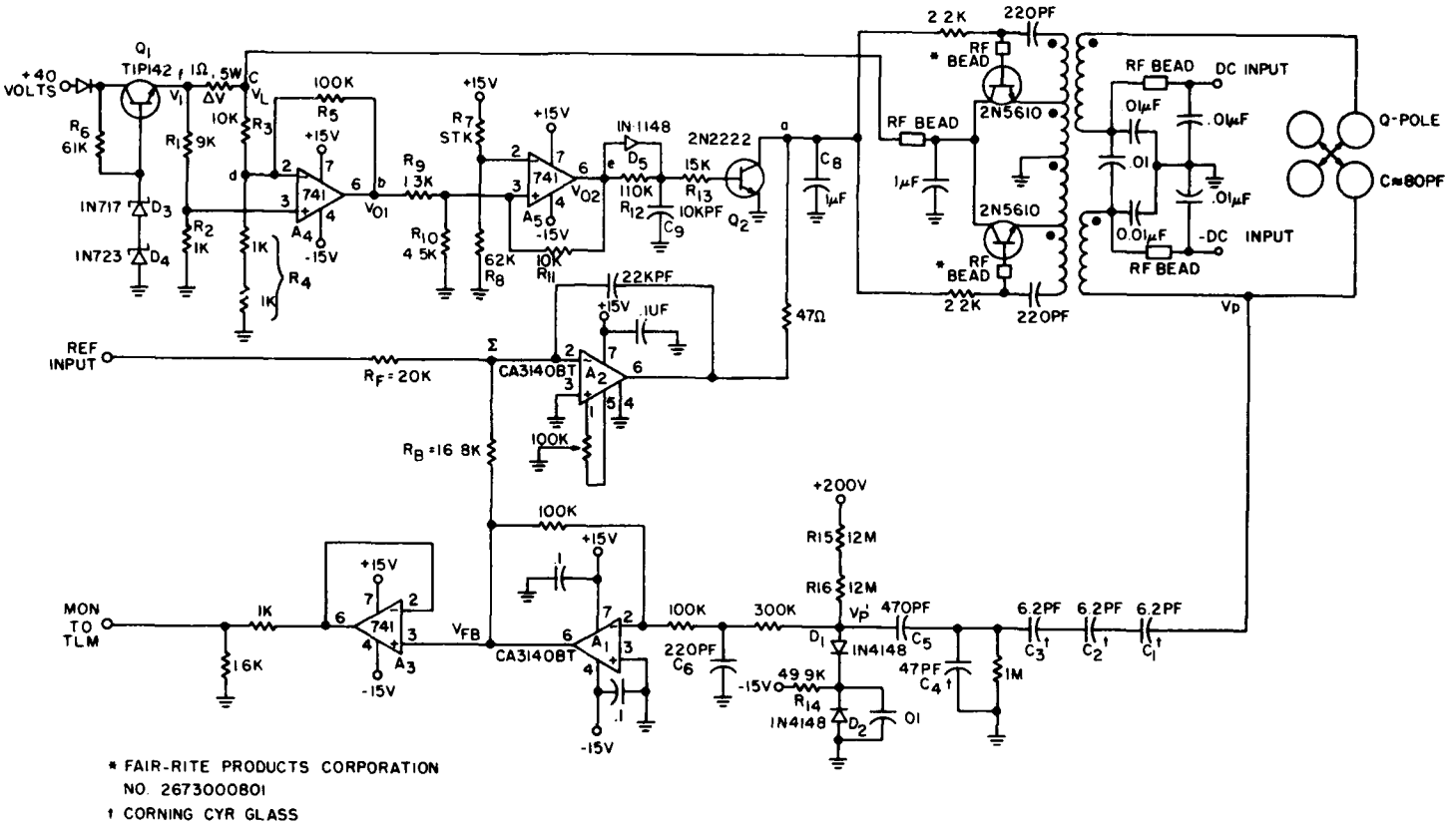

* FAIR-RITE PRODUCTS CORPORATION
NO. 2673000801

† CORNING CYR GLASS

Figure 10. Circuit Schematic, ac Generator

The need for protective shutdown/recovery of the ac generator was established by unhappy experiences with unprotected circuits that self-destructed whenever oscillation ceased. Such difficulties could be triggered by any of a variety of uncontrolled circumstances, that is, transistor overheating, ac circuit arcing or breakdown, or other intermittent effects.

2.4.2 INPUT CONVERTER

This unit provides for the isolation and output-translation of a current-sensitive SEM signal amplifier (see Figure 11). The isolated signal amplifier is a modification and extension of designs used in predecessor systems. Commercially available isolated-output ac/dc converter modules, and an optical signal isolator, permit isolated operation of the entire current-to-voltage converter along with a volt-frequency pulse driver (VFC), at a bias up to 5 kV above ground.

The VFC pulse signal is transferred to dc ground through the optical coupler. This frequency-modulated pulse train is reconverted to an analog of the SEM current-to-voltage converter output. The transfer function of the system is logarithmic, as illustrated in Figure 12, a plot of voltage-out vs current-in.

The resulting signal is outputed for observation, and also applied to an ADC for insertion into the PCM data train. The PCM system is discussed in Section 2.4.4.

2.4.3 PROGRAMMER

This unit offers a significant extension of those capabilities provided by its predecessors by utilizing digital generation techniques. These digital methods have been enhanced by utilizing newly available LSI technology. Programming flexibility and complexity have been advanced by employing user-programmable semiconductor memory devices as the instruction storage medium. Figure 13 illustrates the programmer architecture. A detailed description of the controller is provided in reference 8.

2.4.4 DATA CONDITIONER (PCM)

The data system for the CIMS includes the traditional analog voltage outputs, typically telemetered by FM subcarriers, which further frequency modulate the r-f carrier of the radiotelemetry transmitter. All parameters of special interest, plus several diagnostic monitors, are available in this form. In addition, the CIMS utilizes an integrated pulse-coded (PCM) digital data capability.

In this system, prime signal information is converted to a 10-bit digital word format, and combined with information derived from the digital controller that defines the amu, dc/ac ratio, and biases. Note that the coded PCM does not include diagnostic capabilities since no monitoring of circuits performance is provided. Figure 13 includes a functional block diagram of the PCM data organizer. A detailed description of the system is provided in reference 8.

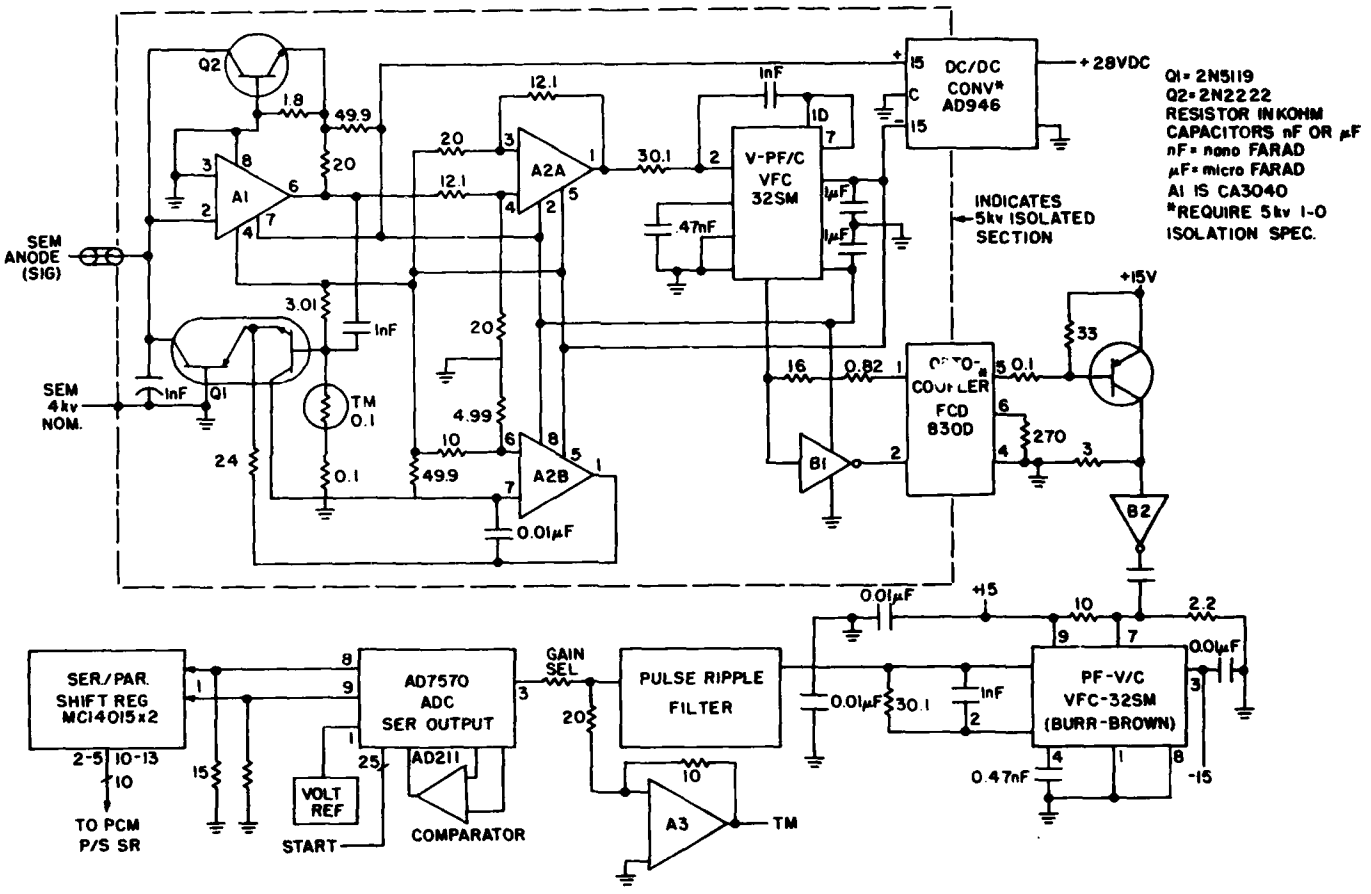

Figure 11. Signal Input Converter

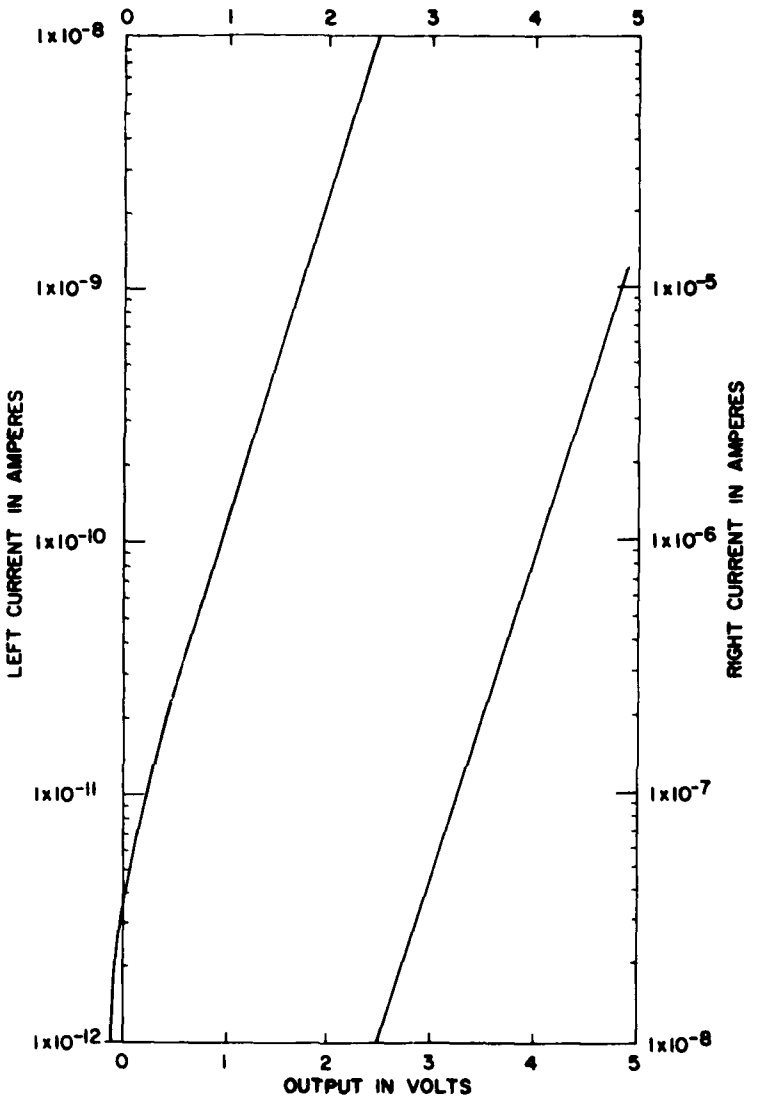

Figure 12. Input Converter Transfer Curve

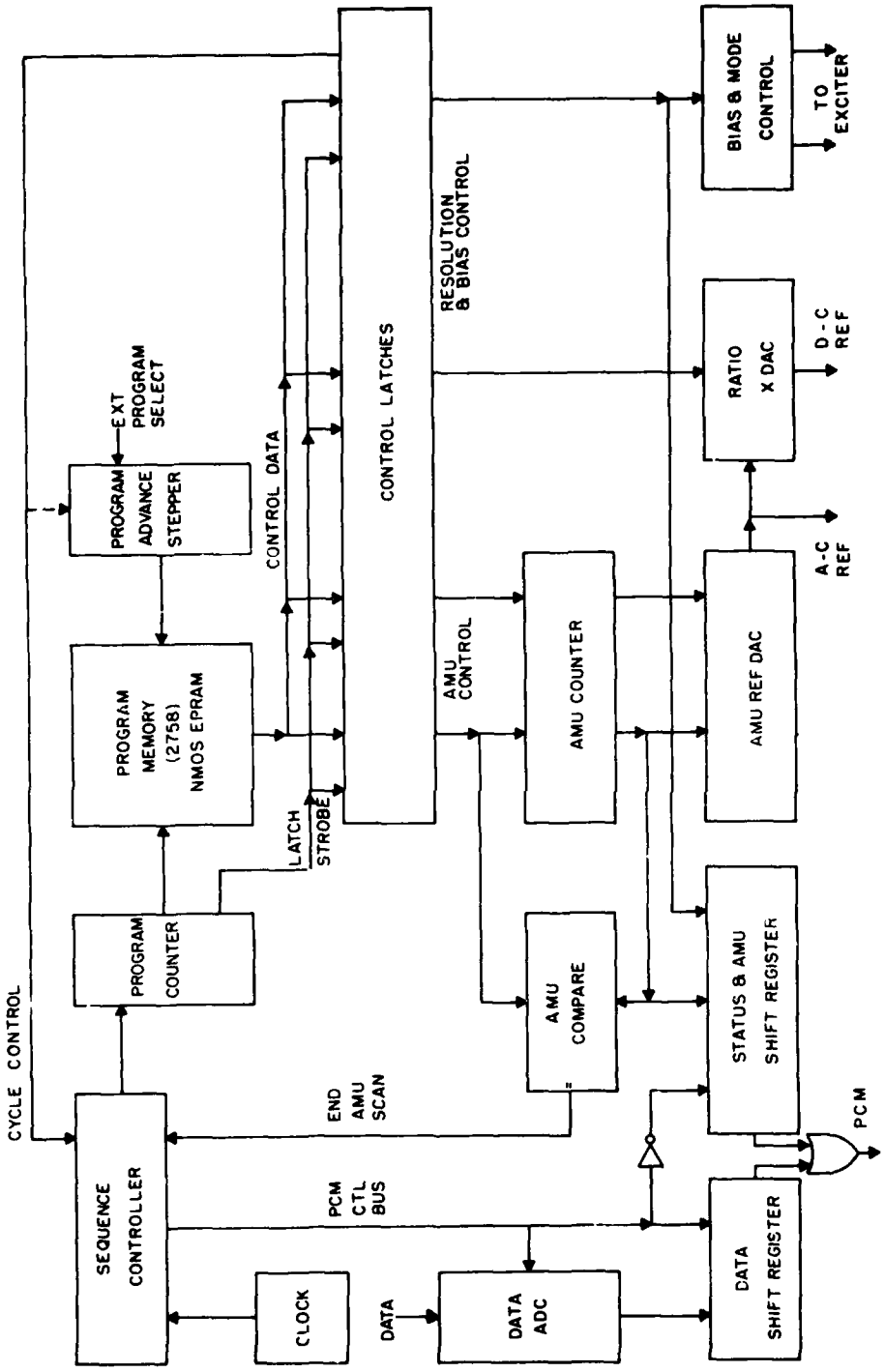

Figure 13. Programmer Block Diagram, Including PCM

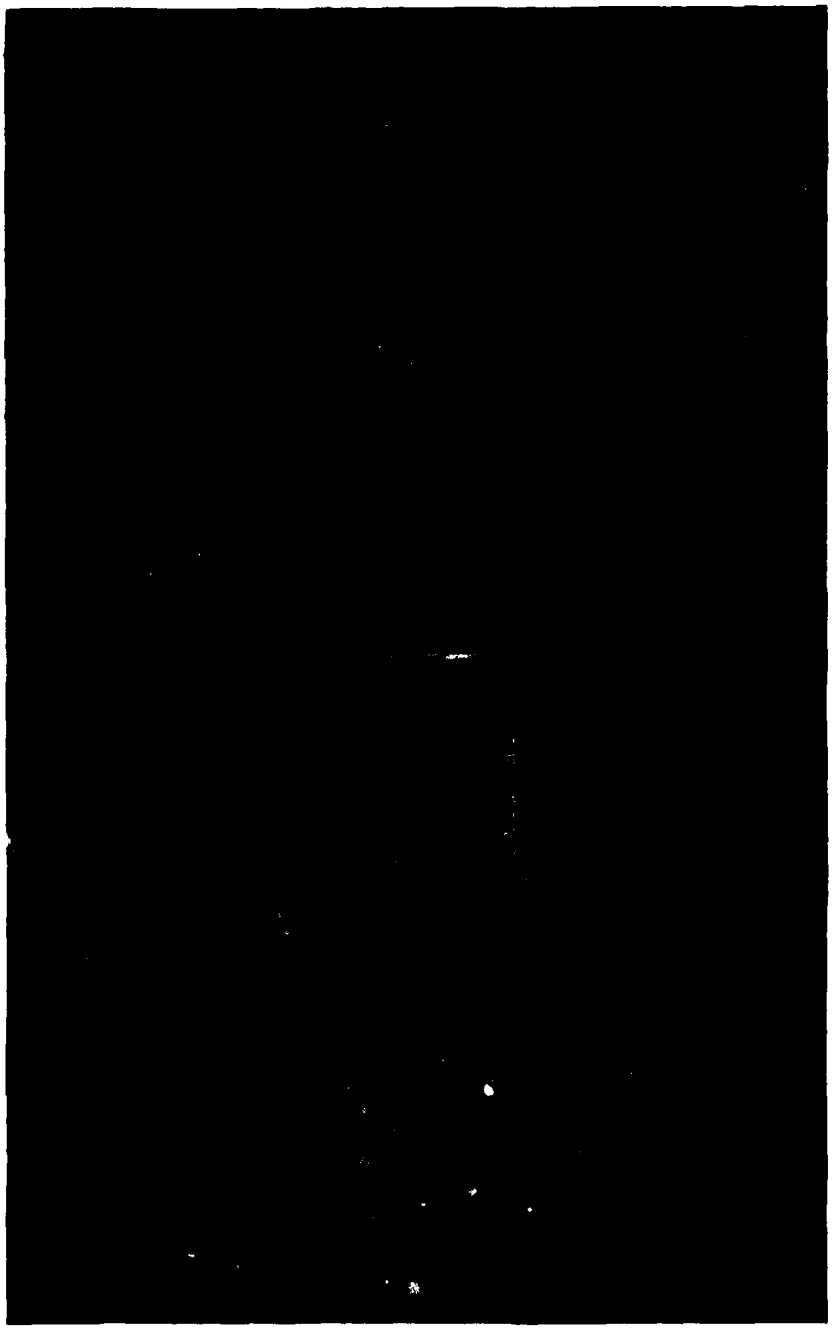

Figure 14. Artists Crossectional View

Figure 15. Inlet Closeup

Figure 16. Quadrupole DDCR Closeup

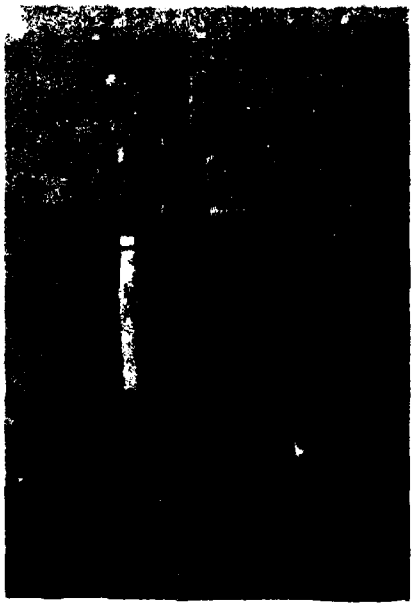

Figure 17. Quadrupole in Cryopump

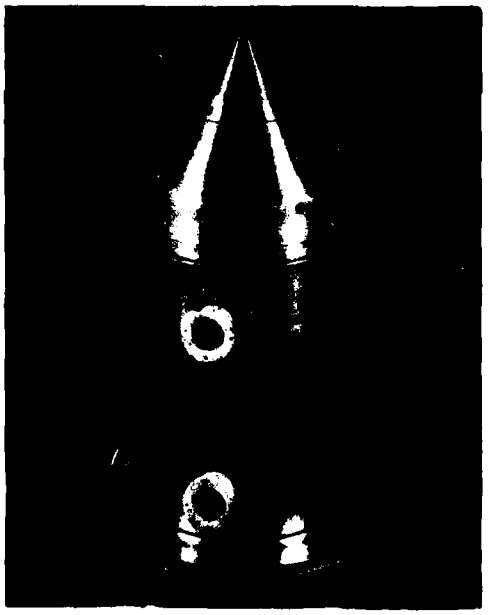

Figure 18. CIMS, Mounted to Payload Structure

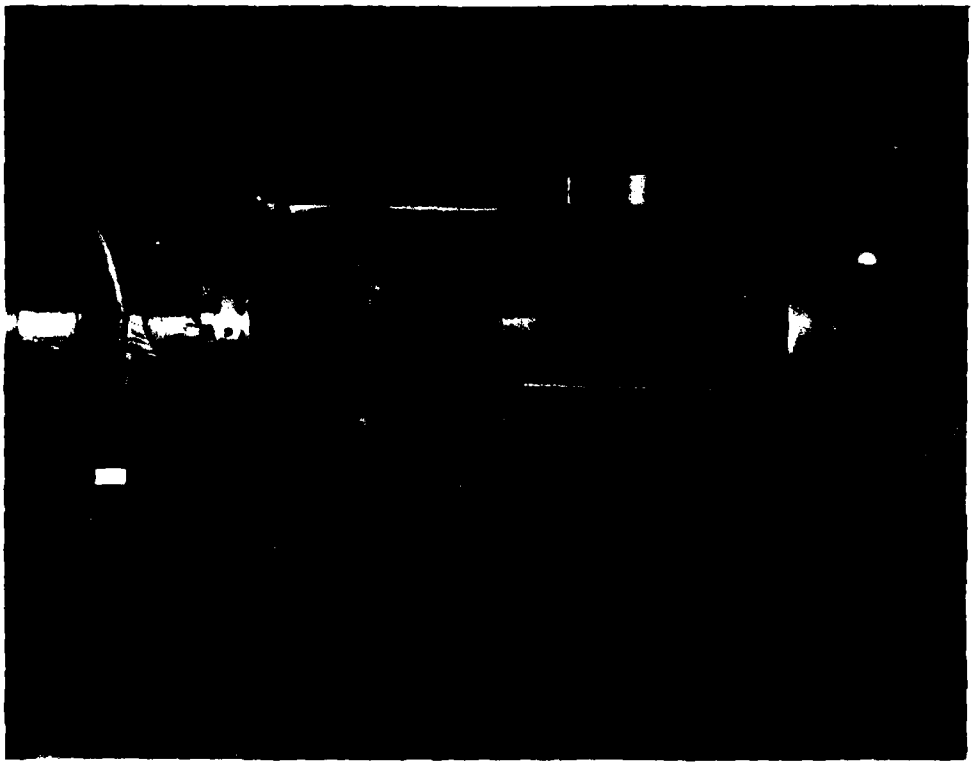

Figure 19. CIMS Electronics, Open View

3. DEVELOPMENT, OTHER

3.1 Objectives

The total payload development objective was to produce a suitable support system for the CIMS. Such "suitable support" had to include the following capabilities:

a. Carry the instrumentation into the 40- to 120-km altitude range
b. Maintain instrument alignment to the velocity vector
c. Provide for complimentary instrumentation (see Section 3.2.3)
d. Provide "appropriate" deployment capabilities
e. Provide data telemetry and trajectory tracking.

Also, payload recovery was considered highly desirable because of the high cost of instrumentation and the expectation of experiment repetition.

Most of these objectives have been met, but largely at the expense of the first. The size and weight of the CIMS and GC instruments has placed demands on the

support system which tend to multiply their normal loading effects. The result has been a payload of extraordinary size and weight for the rocket-booster system originally intended for use.

Because of the excess weight, the first successfully recovered flight of this system was limited to 88 km at apogee. Earlier flights, carrying a smaller parachute recovery unit, achieved altitudes of about 115 km, but recovery failed. Altitudes above 90 km will be achieved by weight reduction of various payload components.

3.2 Payload Architecture

The total sounding-rocket payload system has been developed by AFCL/LCR and incorporates the following major elements, listed in order of their location according to station as illustrated in Figure 20:

a. Tip ejector and CIMS
b. Payload control section
c. Complementary experiment bay with deployment system
d. Telemetry and tracking unit
e. Vehicle attitude control system
f. Despinner
g. Recovery unit (including parachute and locator beacon)
h. Booster separator.

3.2.1 TIP AND CIMS

The "tip" is the conical section at the forward end of the payload. Its function during vehicle ascent is apparent. As measurement altitudes are approached, it must be ejected to expose the sampling orifice of the CIMS. Until this point is reached, the tip protects the CIMS and serves to retain a vacuum-seal cap over the sampling orifice. The analyzer chamber is thereby maintained at high vacuum until opened for operation.

The ejection mechanism operates in two stages. First, a pyrotechnically operated piston releases a spring-loaded yoke which detaches the pressure sealing cap, and then a similar activation hurls the two halves of a split cone assembly aside, as illustrated in Figures 20 and 21. Figures 22 and 23 show some detail of the tip eject mechanism and its interface with the CIMS vacuum seal.

3.2.2 PAYLOAD CONTROL SECTION

This section contains power supplies (NICAD batteries), switching relays, a data commutator, and flight control timers, to name a few of its elements. It is the control center for all other payload functions. Design details are referenced in various status reports submitted under contract F19628-C-73C-0152.

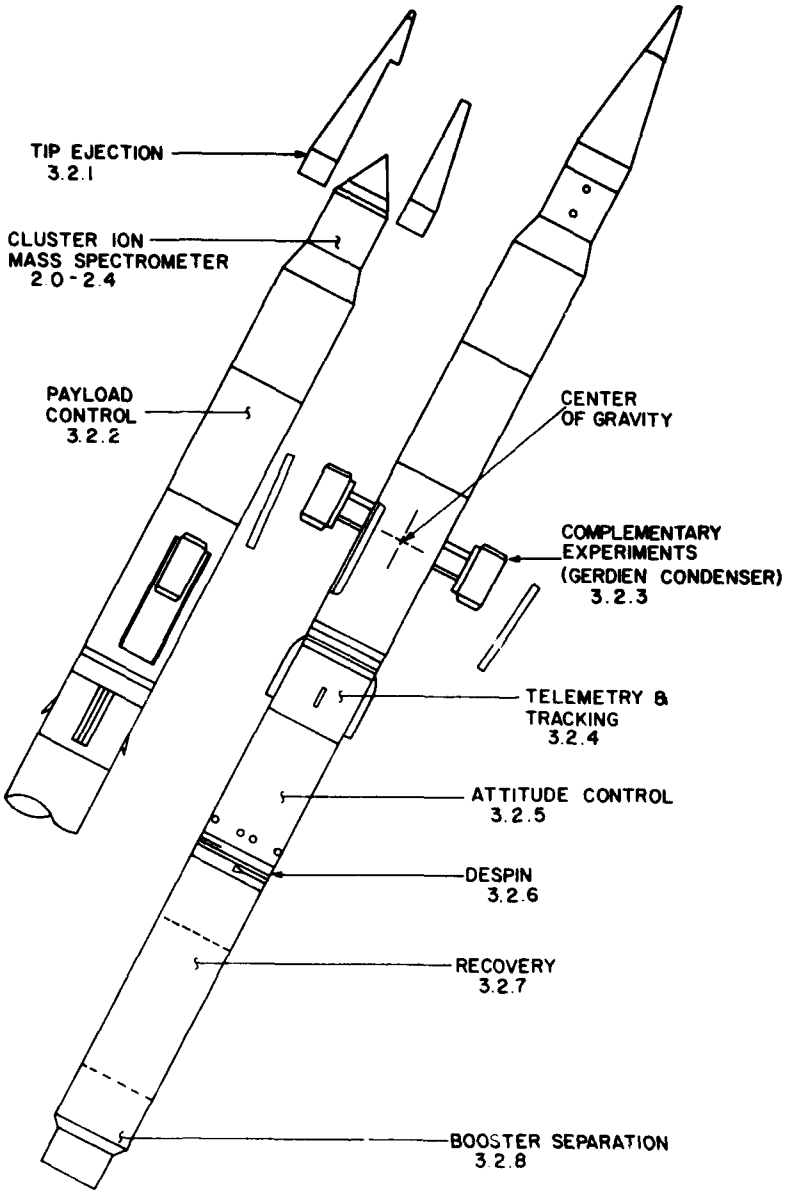

Figure 20. Payload Overview With Sectional Indicators

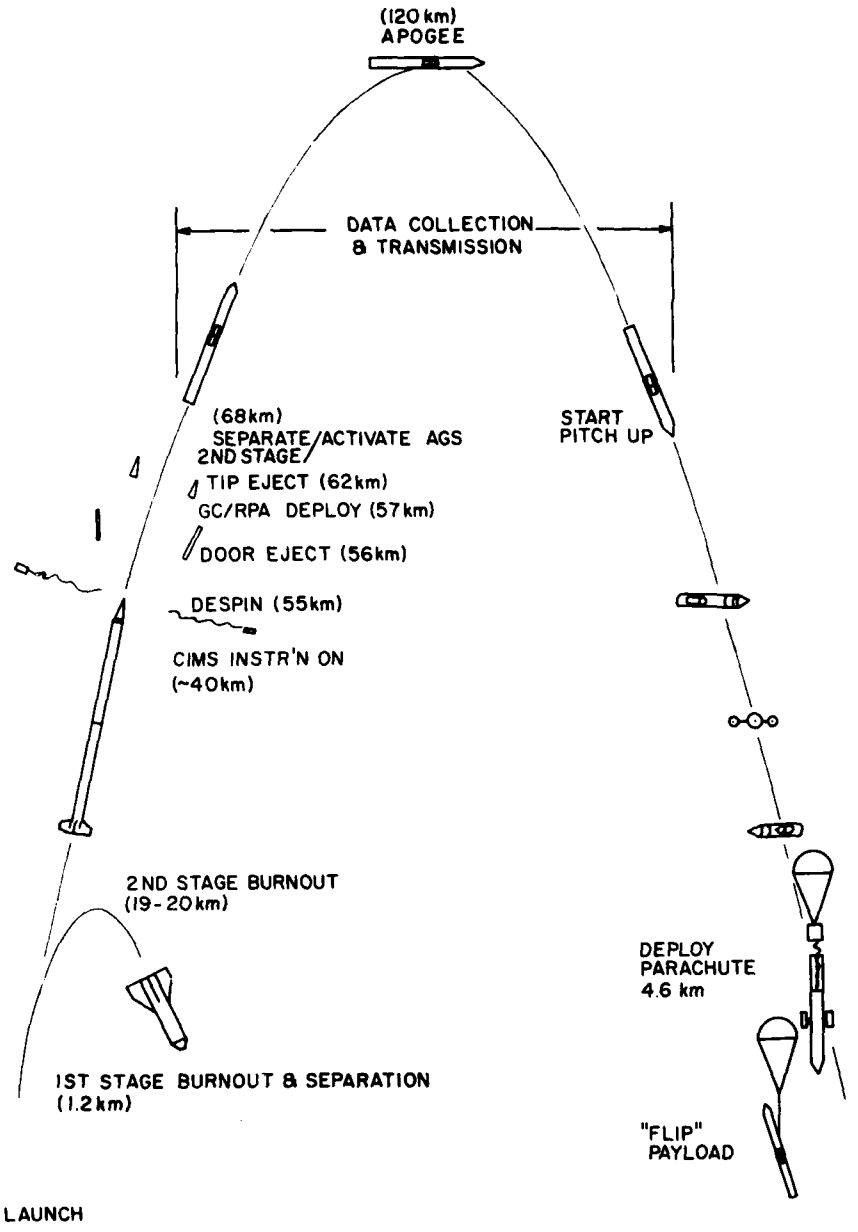

Figure 21. Event Sequence "Pictorial"

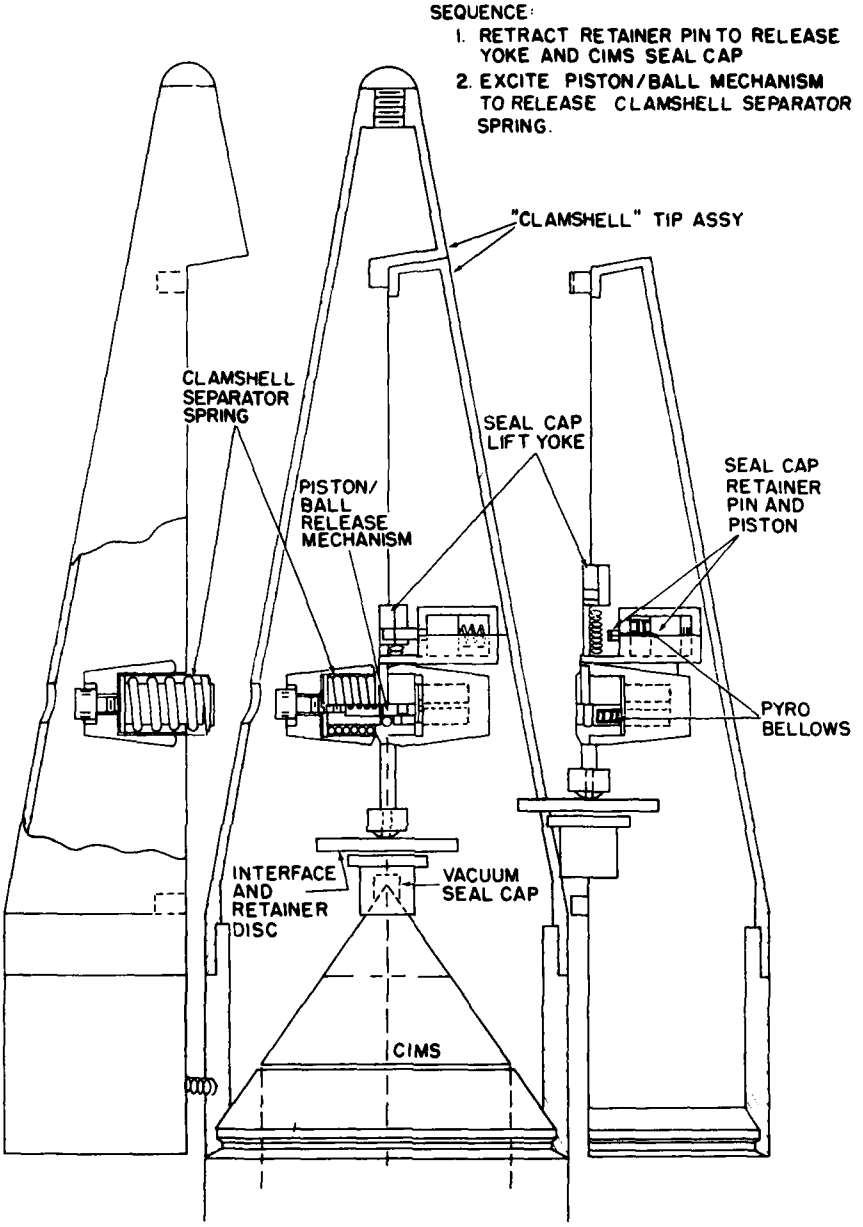

Figure 22. Tip Ejection System

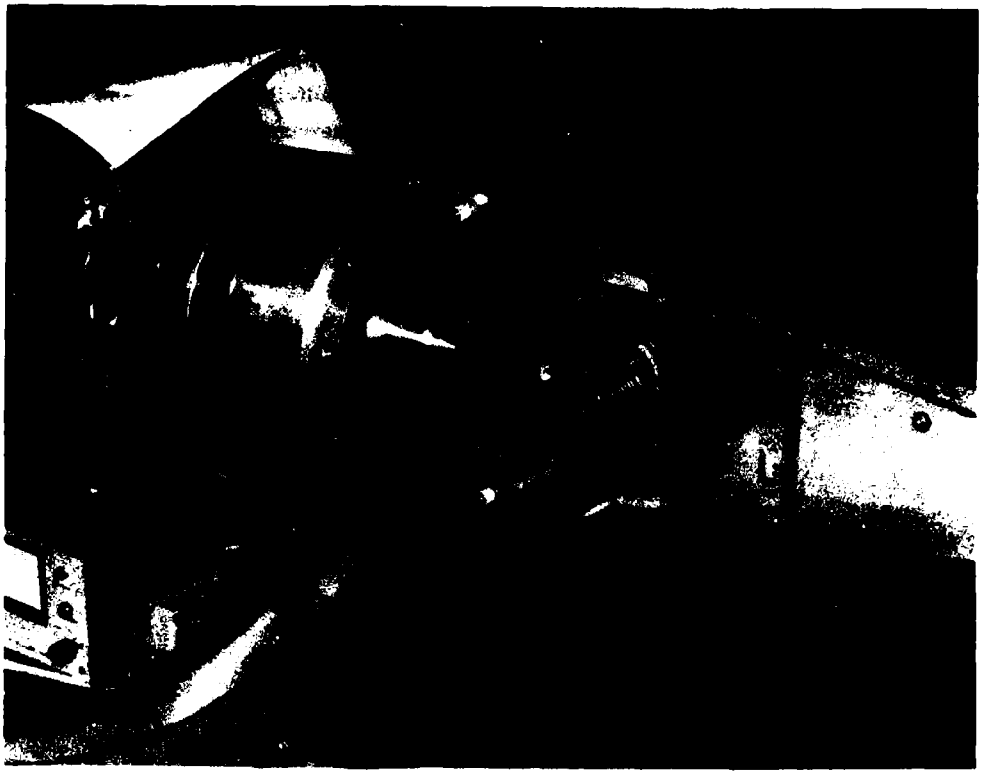

Figure 23. Tip System

3.2.3 COMPLEMENTARY EXPERIMENTS

Ion composition measurements obtained by the CIMS must be adjusted not only in accord with supporting information regarding vehicle position and altitude, but also with data on plasma density and other related information. Such data are obtained from complementary experiments flown on the same vehicle.

A Gerdien Condenser (GC) has been designed into the CIMS payload system for lower altitude (40 to 75 km) plasma measurements. This has subsequently been supplemented by adapting a Retarding Potential Analyzer (RPA) to obtain measurements at higher altitudes.

Wind tunnel calibrations of the GC in the CIMS payload configuration are reported by Haldeman.[11, 12] Both instruments, GC and RPA, have been used extensively by AFGL and other workers. The devices were supplied by Tricon Associates Inc., and are described diagrammatically in Appendices D and E.

References 11 and 12 will not be listed here. See References, page 67.

The GC and RPA deployment mechanism, is characterized in Figure 24. Each instrument, prior to launch, is stowed on a pivoted dual parallel-arm assembly. This assembly is spring-loaded to extend each device radially through, and forward of, a doorway in the vehicle skin. Orientation of the instruments' sensing axis is maintained parallel to the vehicle axis. Deployment is done in the Yaw plane of the attitude controlled vehicle. Launch phase protective doors are ejected immediately prior to deployment as indicated in Figure 21.

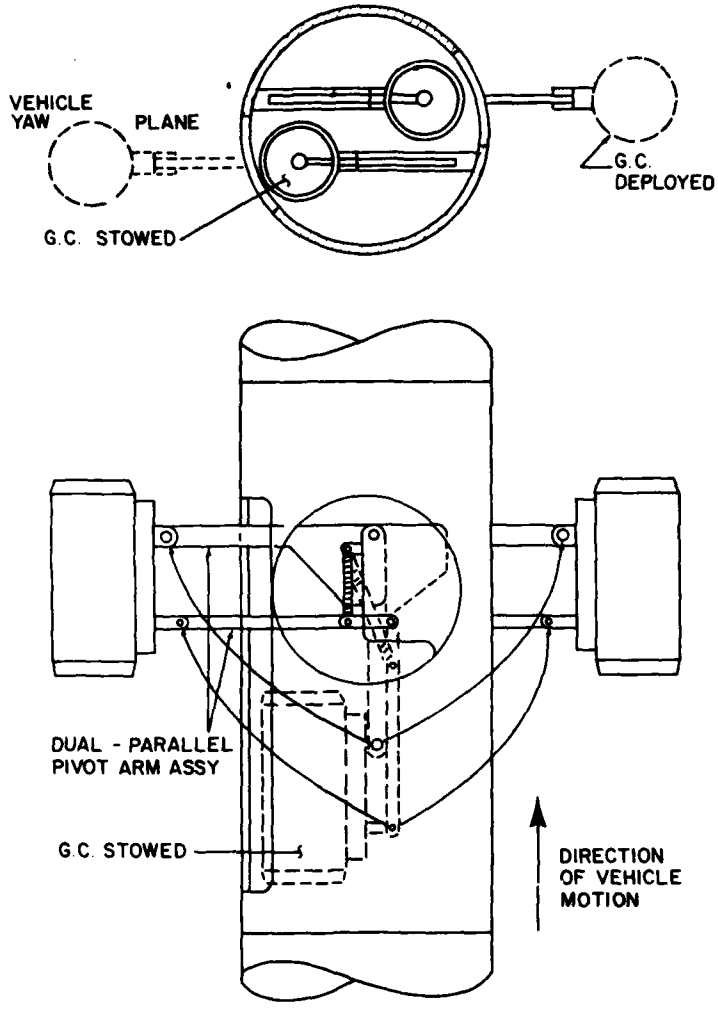

Figure 24. GC Deployment System

3.2.4 TELEMETRY AND TRACKING UNIT

This unit provides for data and tracking communication with the ground. Two radio down-links telemeter scientific and diagnostic data. These are S-band AM-FM IRIG-standard systems. Link I carries all information derived from the scientific instrumentation, for example, the CIMS, GC, and RPA. Link II carries support systems diagnostic data and the return link of the TRADAT ranging system. Pulse-coded data are injected as PCM-FM subcarriers in each case.

Tracking is provided by the Oklahoma State University-developed TRATEL/TRADAT system.[13, 14] An autotracking telemetry-receiving antenna system (TRATEL) is supplemented by the ranging data system (TRADAT) illustrated in Figure 25. A 14-bit PCM code, synchronized with a time-interval counter "start" pulse, modulates a 430-MHz ranging transmitter, feeding a helix antenna. This antenna is mounted to and pointed by the S-band TRATEL antenna system.

The demodulated output from an airborne ranging receiver is mixed with other telemetered data as a PCM-FM subcarrier. At the ground telemetry receiver the ranging code is retrieved to produce a "stop" pulse to the interval counter. This round trip time interval information is scaled to provide range data that is combined with TRATEL azimuth and elevation angle data. Trajectory coordinates are computed for printout and display as a function of time from launch.

3.2.5 ATTITUDE CONTROL SYSTEM

This is a time-programmed, three-axis gyro-referenced, gas-jet activated, orientation controlling system. It functions to maintain alignment of the vehicle axis close to its velocity vector by following a time dependent reference program, which has been designed to match the predicted trajectory. A zero roll rate is maintained, with the GC (or other) sensors held in the Yaw plane. It utilizes a miniature inertial gyro platform to provide pitch and roll data, referenced from an uncaged attitude prior to launch; and Yaw data, referenced to the Yaw position at the time of the first in-flight command. Pitch rate is controlled by a ramp-generated pitch reference. The system thereby nulls continuously against an approximation of the predicted trajectory flight path angle. The ACS also does a "pitchup" maneuver at mission end, in preparation for reentry and recovery. See Figure 26.

---

13. Fike, R.M. (1973) Mobile S-band Trajectory Determination and Telemetry Receiving Systems, AFGL-TR-73-0716, AD 775748.

14. Buck, R.F., Gwinn, C.M., and Fike, R.M. (1975) Instrumentation for Research Rockets, AFGL-TR-75-0216, ADA 012552.

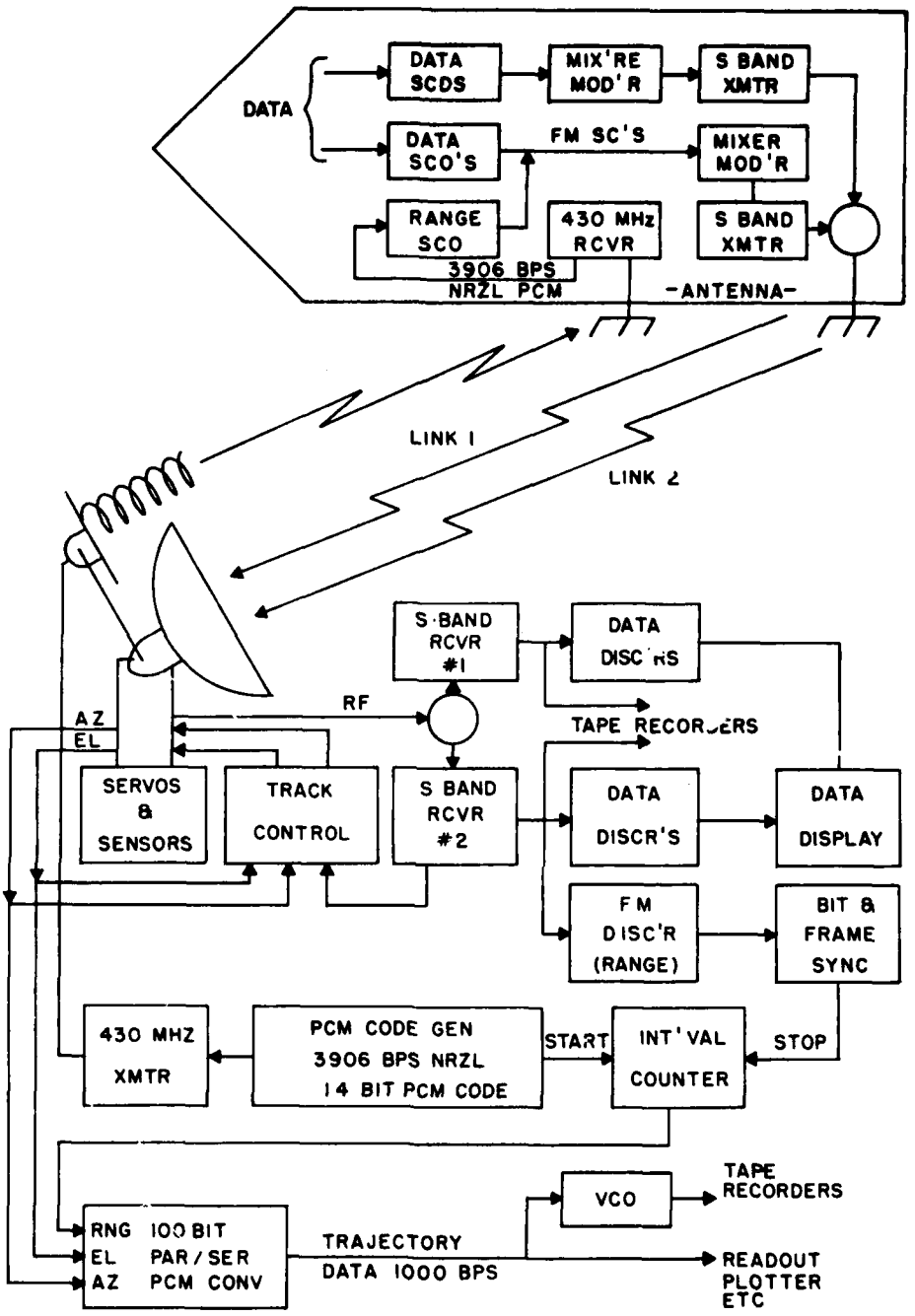

Figure 25. TLM/Tracking System Diagram

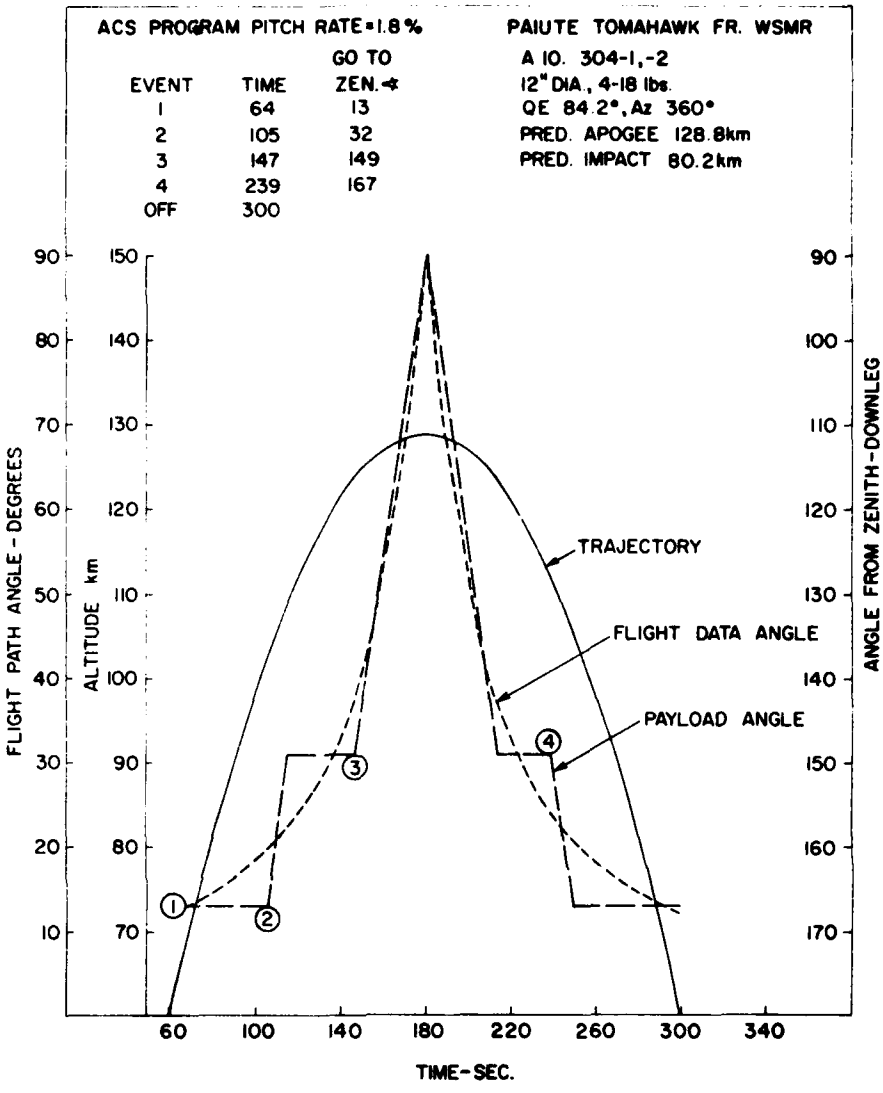

Figure 26. ACS Flight Path Angle vs Time

3.2.6 DESPIN

At launch, a rocket system of this type is typically stabilized by virtue of its spin, the rate determined by booster fin settings. However, experiments such as these frequently require zero or minimal spin. Despin to near zero is accomplished by discarding weighted cables, wrapped about the payload body (yo-yo), which absorb and dispense with the vehicle's angular momentum.

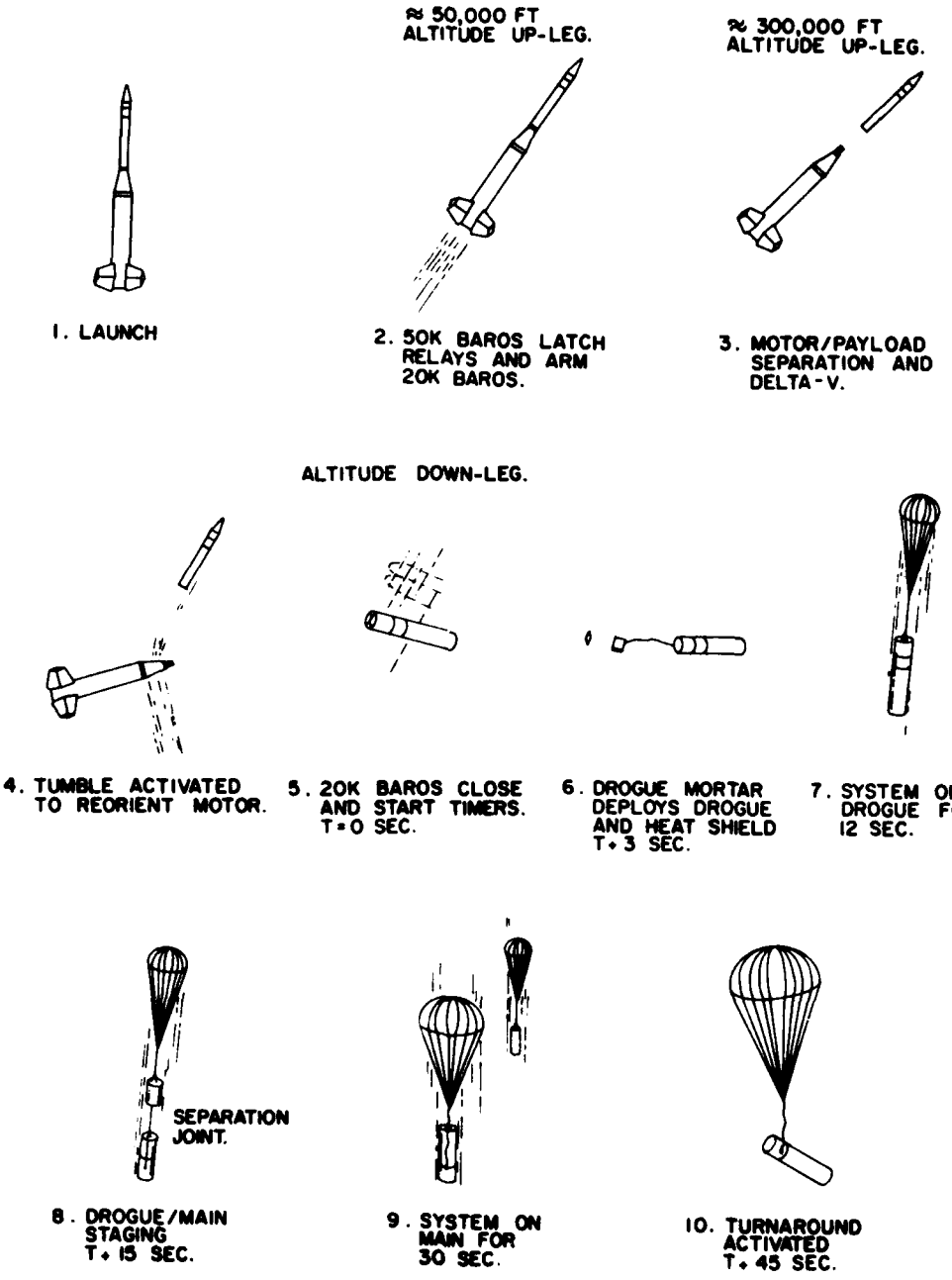

Figure 27. Recovery System, Sequence of Events

3.2.7 RECOVERY UNIT

A new recovery parachute system, developed for AFGL/LCR for heavy 12-in. diameter payload systems,[15, 16] has been employed successfully in the latest (October 1980) flight. This unit employs new variations on standard techniques for parachute deployment. It also includes provision to reorient the payload noseup after deployment in order to protect expensive instrumentation in the nose section from ground-impact damage. Figure 27 shows the operating sequence for deployment.

3.2.8 BOOSTER SEPARATOR

Prior to ACS activation, the vehicle and payload are despun and the rocket second stage motor is disengaged from the payload, using compressed gas to impart a high-axial separation velocity (delta-v). ACS initiation is programmed to occur simultaneously with payload-vehicle separation. (See Figures 28-30.)

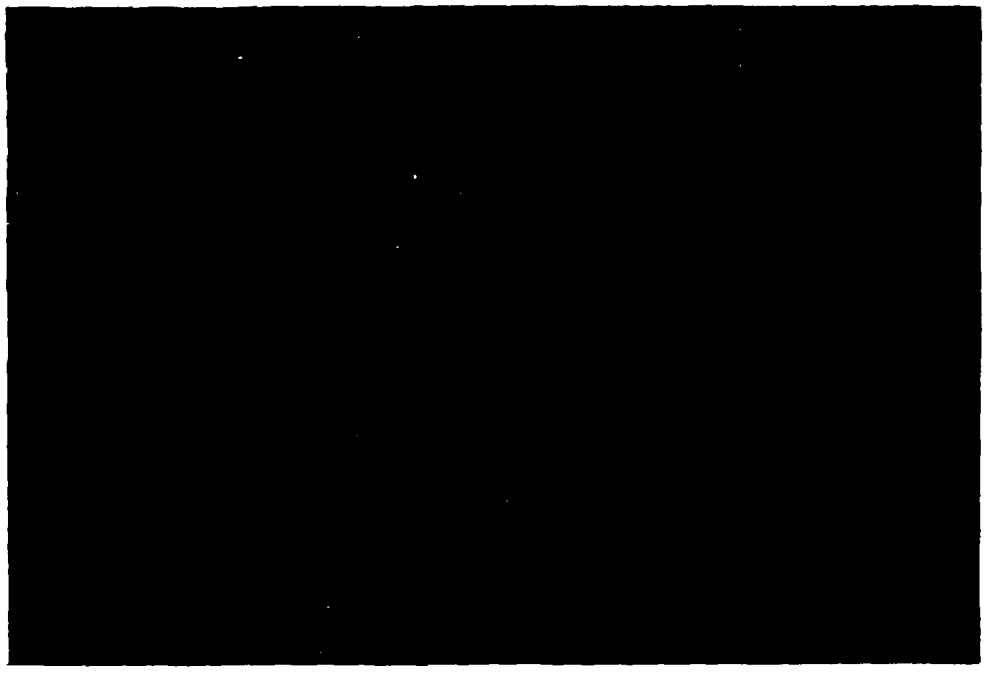

Figure 28. GC in Deployed Position

15. Space Data Corp. (1980) AFGL 12-inch Recovery Development & Design Report, SDC-TM-1791.
16. Space Data Corp. (1980) 12-inch Recovery Test Report, SDC-TM-1730-A.

Figure 29. Overview of Payload

Figure 30. CIMS Payload Sector

4. PERFORMANCE AND RESULTS

This section comments briefly on preparation aspects of the CIMS instruments that have been flown to date, points to the salient short comings of the results, and speculates on the prospects for future improvement.

4.1 Preparation and Calibration

The laboratory preparation procedures for the CIMS do not differ appreciably from those used for predecessor flight systems. However, little has been reported on these procedures, and so a short summary follows.

4.1.1 THE SETUP FACILITY

Figure 31 illustrates, in schematic form, a typical preparation and calibration setup. The sampling end of the flight instrument is adapted to a port of a high vacuum pumping system. An ionizer of suitable design (A) is installed in the throat of the port immediately next to the instrument sampling orifice (B). A controlled gas leak (C) is mounted next to the ionizer, as is a Baird-Alpert density gauge tube (D). Two design variations of the ionizer are used, both assembled from kit parts. One design, Figure 32 (a) was developed to provide positive ions by conventional techniques. The other design, Figure 32 (b), was developed to optimize negative ion generation.

In the positive ion unit, an ion forming region (E) (labelled "box"), is bombarded with an electron stream from a hot tungsten filament (F). Electron emission is regulated to maintain a constantly defined current to the "collector" (G). Ions formed in the box are drawn out by a bias voltage applied between the box and the "exit aperture" plate (H). The other electrodes (J) are biased to obtain some suitable indication of optimum electron beam formation. The "shield" (K) is intended to function as a shield against stray electron currents to the system under test. In CIMS preparations this function has been ignored, and it is connected to the exit aperture.

In the negative ion unit, special precautions are required to control internal generation of ions. This problem arises because of the obvious effects of biasing for negative ion extraction. Electrons will be attracted into the CIMS, forming positive ions by impact within. These will be detected as negative ion aliases. To avoid this, this device employs a magnetic field, in conjunction with an electrostatic ion lens. The magnetic field is aligned with the ionizing electron beam, and normal to the ion extraction path.

This arrangement enhances electron beam focusing while also serving to deflect most electrons in the lens area away from the CIMS input aperture. The heavier negative ions are only slightly affected by the magnetic field. The

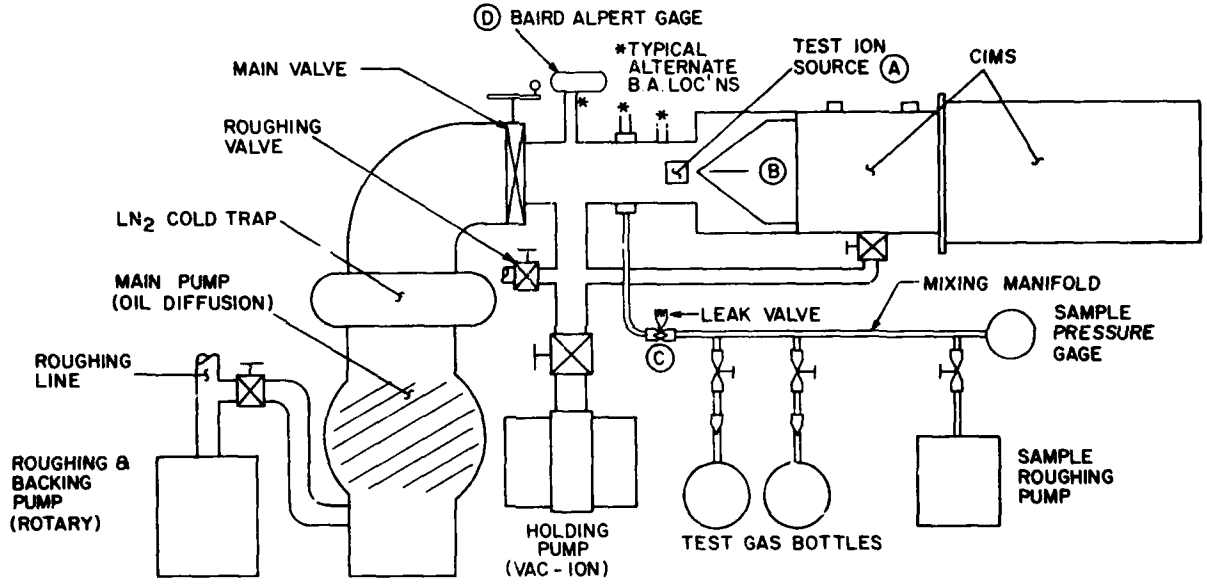

Figure 31. Preparation and Calibration Facility

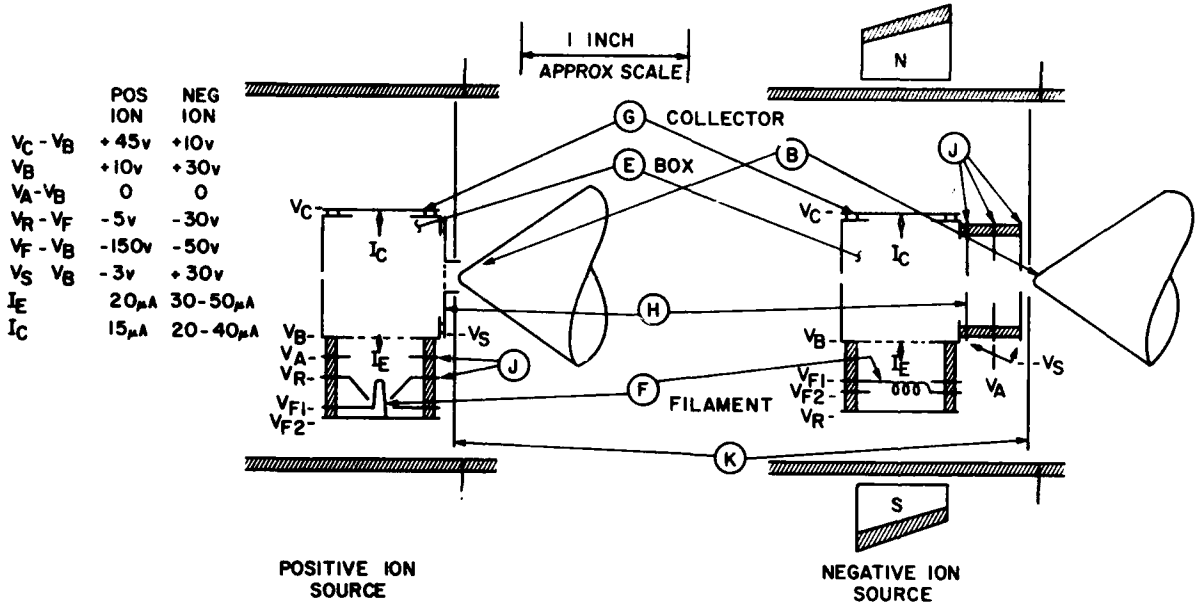

Figure 32. Ion Sources; (a) Positive Ion and (b) Negative Ion

electrostatic ion lens provides some focusing to limit ion losses from dispersion, while lengthening the path over which electrons may be diverted. The negative ion source must be biased carefully and selectively, since different optimum bands of ion production as a function of electron energy exist for each sample gas. The tables in Figure 32 list typical biases applied to each ion source for typical calibration gases.

Complete discrimination against alias signals must be accomplished by appropriate biasing of the DDCR sector internal to the instrument. Figure 33 shows the alias phenomenon observed in flight data.

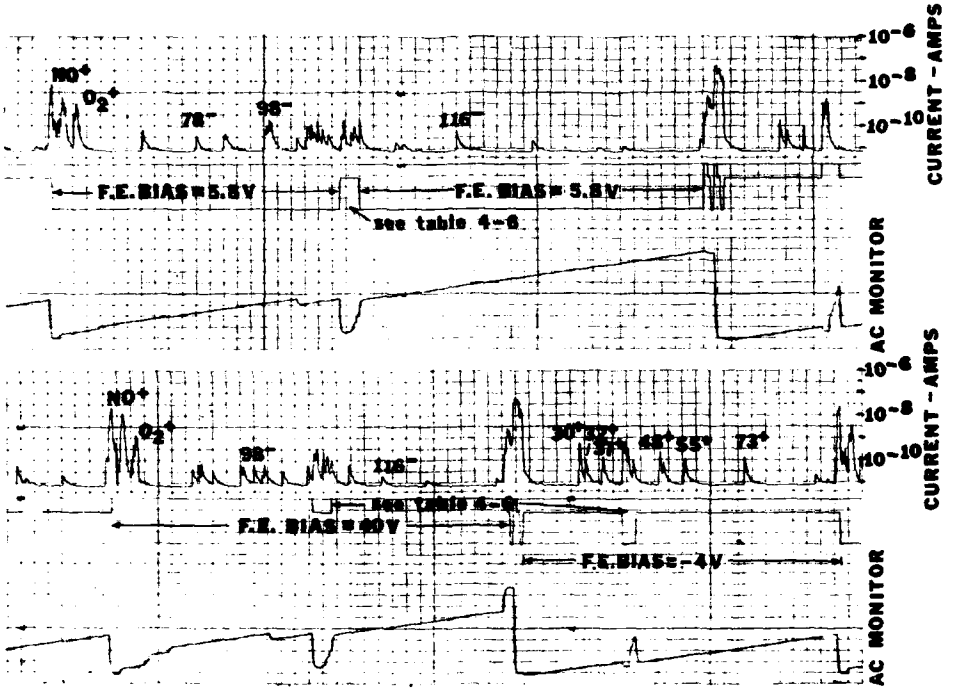

Figure 33. PFRR-80 Flight Data Samples

4.1.2 SETUP PROCEDURE

After the instrument is baked, cleaned, and found leakless, the electrometer is calibrated, the biases adjusted, SEM high voltage set to nominal values, the dc and ac balances and dc/ac ratio are checked and trimmed as necessary. The mass

range is adjusted by using test gases that provide signals close to the desired upper and lower limits of amu.

After the amu range is set, sensitivity and resolution are trimmed by adjusting the SEM voltage and the dc/ac ratio. Iterative adjustments may be required. Several gases are used to accomplish these adjustments and to obtain an evaluation of mass discrimination. Generally, nitrogen and air are the principle gases used for sensitivity measurements for positive ions (N_2^+), while oxygen and sulfur hexafluoride are used for negative ions (O^-), and (SF_n^-). Table 4 lists other common test gases.

Table 4. Calibration Gases

WSMR-78	ECLIPSE-79	PFRR-80	AMU
N_2	N_2	N_2	$14^+, 28^+$
N_2/CH_4	N_2/CH_4	N_2/CH_4	$14^+, 15^+, 16^+$ (resolution)
-	N_2/Ar	N_2/Ar	$28^+, 40^+$ (discrimination)
-	Ar/Kr	Ar/Kr	$40^+, 85^+$ etc. (resolution)
Ar	-	-	40^+
Ar/Kr/Xe	-	-	$40^+, 85^+$ etc., 135^+ etc.
-	-	Air	(discrimination)
O_2	O_2	O_2	$16^-, 32^-$ (sensitivity, transmission)
SF_6	SF_6	SF_6	$19^-, 127^-, 146^-$ (calibration, discrimination)

While a variety of gases are available for positive ion generation, there are very few that produce useful negative ions. Only two of these, oxygen (O_2), and surfur hexafluoride (SF_6) are used for the CIMS calibration. Others, such as chlorine (Cl) compounds, are too toxic, or "dirty", or both. O_2 provides convenient low mass references at 16^- and 32^- amu. SF_6 provides strong ion peaks at 19^-, 127^-, and 146^- as well as a wealth of small intermediate peaks specifically 38^-, and at 19-amu intervals from 51^- through 108^-. SF_6 does not produce a positive ion at 146^+, which is helpful in isolating aliases, since 146^- is the largest of

the $127^-/146^-$ pair. If the 127^- is larger, it is probably an alias peak, and biasing is adjusted to enhance 146^- and reduce the 127^- alias. O_2 produces large 32^+ with small 16^+ peaks, and small 32^- with large 16^-.

Both O_2 and SF_6 still have drawbacks. O_2 causes ion source and density gauge filament deterioration while SF_6, a liquid at storage pressure, is difficult to get rid of and tends to "reappear" in the test facility. However SF_6 can be cleaned out of the CIMS instrument by baking, in contrast to Cl compounds, which have long residence times and are difficult to bake out.

Calibration reference runs are conducted, starting with light gases first. Typically, 300 mTorr of test gas is loaded into the source manifold. A run begins with a recording of background spectra, typically 1×10^{-7} torr or less, and procedes with a gradually incremented increase of test gas pressure. Recordings of spectra are made with each increment, over the desired pressure range, typically to 3×10^{-5} torr for positive ions, and to 3×10^{-4} torr for negative ions.

Figures 34 through 39 are examples of calibration reference spectra obtained in the preparation of instruments for three missions described below. Mixtures of argon (Ar) and krypton (Kr) are used for positive ion display, while SF_6 displays negative ion performance. Flight data are shown for comparison in Figures 40 and 33, and in Appendix F.

Because the test controls for each of the data runs shown were not fully standardized, it is a little difficult to draw immediate conclusions from a visual inspection of these spectra. However, the salient differences are observable. A good comparison of sensitivity in the total-ion (high mass pass) mode may be made between the WSMR-78 and ECLIPSE-79 instruments. Similarly a comparison in the resolving mode may be made between the ECLIPSE-79 and the PFRR-80 units. This comparison is less direct, however, since the resolution settings differ appreciably.

Because negative ion sensitivity was so poor, the dc/ac ratio for negative ions was programmed in all three instruments to sacrifice resolution in order to conserve all available sensitivity. This is clearly seen in Figure 37 and Figure 39. Consequently, negative ions in the ECLIPSE-79 data of Appendix F, appear as very broad peaks (note especially 98^- and 116^-). This of course, defeats the objective to make high resolution determinations of negative ion species.

More precise sensitivity comparisons may be made from Table 5. However, no indication of the resolving performance is included. Low resolution settings were used where sensitivity was a premium, especially for negative ions.

Table 1 lists a variety of parameter values used in each experiment. Tables 2, 6, and 3 describe the CIMS flight program sequence for the three experiments referenced in the next section.

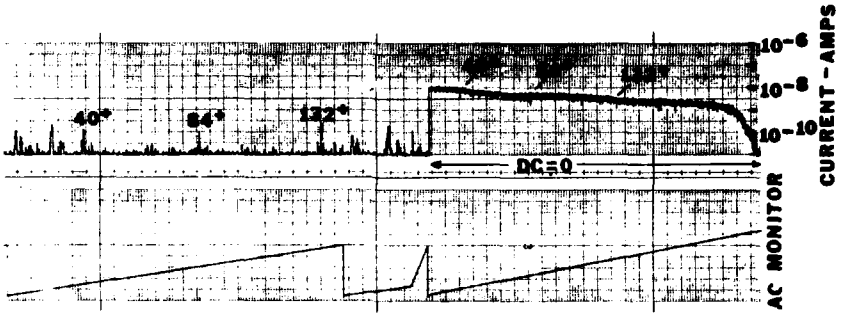

Figure 34. WSMR-78 +Ion Reference Spectrum

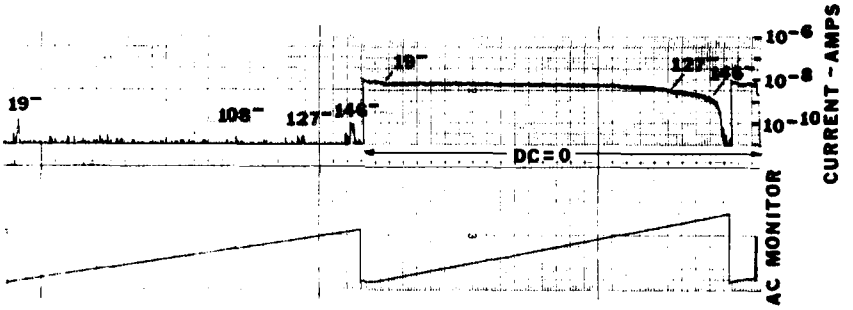

Figure 35. WSMR-78 -Ion Reference Spectrum

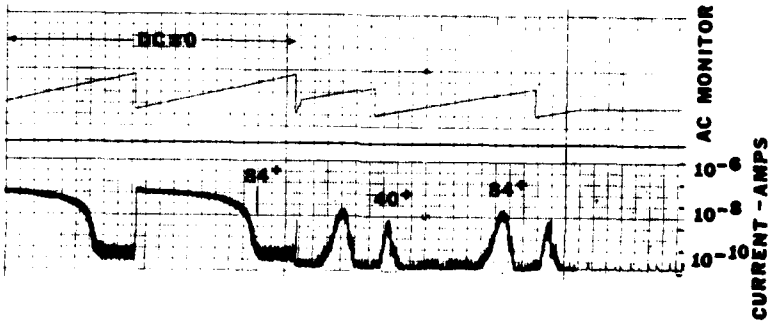

Figure 36. ECLIPSE-79 +Ion Reference Spectrum

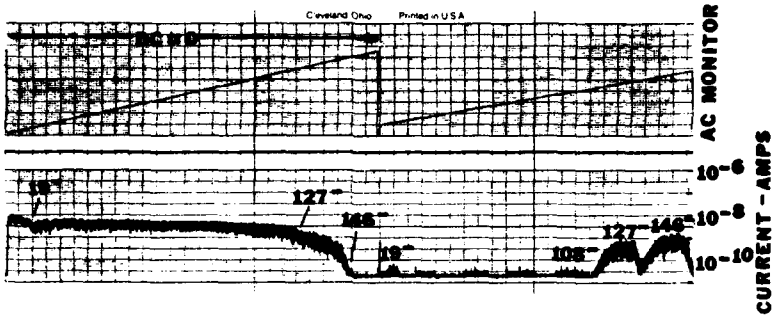

Figure 37. ECLIPSE-79 -Ion Reference Spectrum

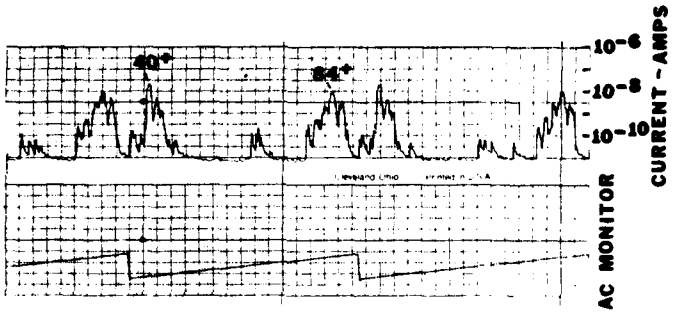

Figure 38. PFRR-80 +Ion Reference Spectrum

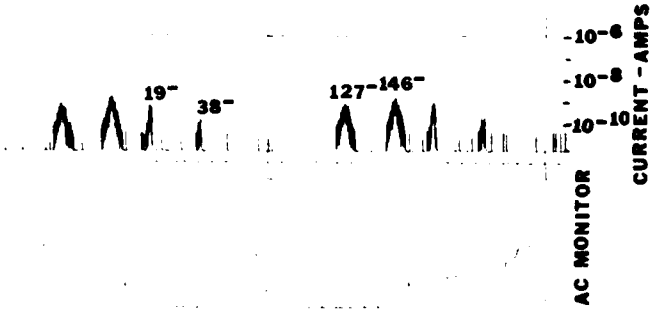

Figure 39. PFRR-80 -Ion Reference Spectrum

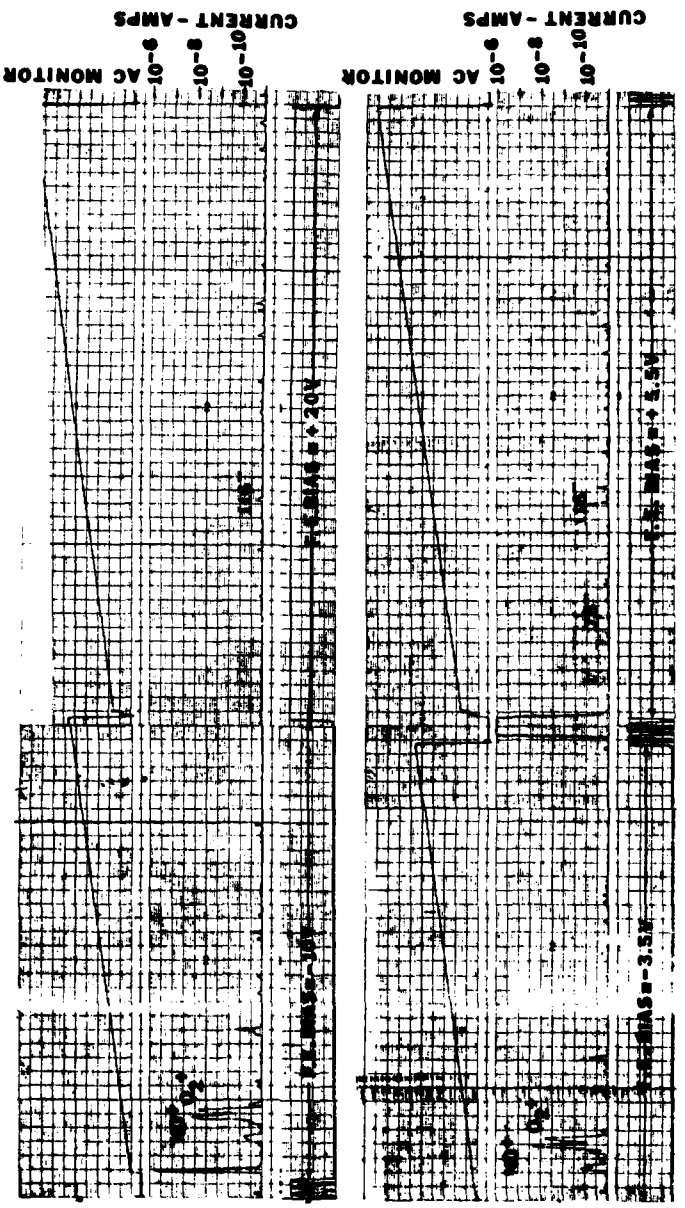

Figure 40. WSMR-78 Flight Data Samples

Table 5. Sensitivity Comparison

Sensitivities expressed in Amp/torr; using procedures described.				
Special Conditions	WSMR-78	ECLIPSE-79 Unit 1	ECLIPSE-79 Unit 2	PFRR-80
Positive Ions: Nitrogen (Emission = 20 μA)				
High FEB				
TI > 20^+	8.3×10^{-5}	4×10^{-2}	2.65×10^{-2}	2×10^{-1}
AMU = 28^+	2×10^{-5}	6.3×10^{-3}	3.2×10^{-3}	2×10^{-2}
Low FEB				
TI > 20^+	1.55×10^{-5}			
AMU = 28^+	6×10^{-6}			
Negative Ions: Oxygen (Emission = 31 μA)				
High FEB				
TI > 10^-	3.8×10^{-6}	9×10^{-4}	2.5×10^{-4}	1.05×10^{-3}
AMU = 16^-	8×10^{-7}	1.35×10^{-4}	3.9×10^{-5}	4.6×10^{-4}
Low FEB				
TI > 10^-	2.65×10^{-6}	6.4×10^{-4}	2.15×10^{-4}	1.5×10^{-3}
AMU = 16^-	5×10^{-7}	9.7×10^{-5}	3.9×10^{-5}	2.25×10^{-4}
Approximate SEM Gain at 3 kV, from manufacturers calibration certificate.				
	1×10^7	5×10^7	1×10^7	2×10^7

4.2 Results

As of this writing, three field operations have been conducted with varying degrees of success. The first, from WSMR New Mexico on September 1978, (WSMR-78) was to be a two-payload experiment seeking normal diurnal difference data. The second, was a two-payload launch into the February 1979 Solar Eclipse (ECLIPSE-79) at Chukuni River near Red Lake, Canada. The third (PFRR-80), was again planned to be a two-payload launch into a Solar Proton Event (SPE) looking for diurnal differences, during the fall of 1980 from the Poker Flat Research Range at Fairbanks, Alaska.

The first experiment (WSMR-78) was scrubbed after the first launch because of a recovery system failure. Data were obtained however, although results have

Table 6. Flight Program Sequence, ECLIPSE-79

Line	Mode	Bias (FEB) Nominal	AMU
1	Scan +ions	-4 V	14^+ to 42^+
2	Step -ions	+40 V	$32^-, 80^-, 98^-, 134^-$
3	Scan +ions	-4 V	42^+ to 100^+
4	Step total +ions	-4 V	$>80^+, >14^+$
5	Step -ions	+40 V	16^-
6	Scan -ions	+40 V	32^- to 37^-
7	Scan -ions	+40 V	46^- to 104^-
8	Step +ions	-4 V	$30^+, 37^+, 55^+, 73^+$
9	Scan -ions	+40 V	104^- to 200^-
10	Total -ions	+40 V	$>160^-$
11	Total -ions	+5.8 V	$>160^-$
12	Total -ions	+40 V	$>14^-$
13	Total -ions	+5.8 V	$>14^-$
14-17	Repeat lines 1-4		
18	Step -ions	+5.8 V	$16^-, 32^-$
19	Scan -ions	+5.8 V	78^- to 104^-
20	Step +ions	-4 V	$30^+, 37^+, 55^+, 73^+$
21	Scan -ions	+5.8 V	104^- to 154^-
22-24	Repeat lines 10-13		

not yet been published. Sensitivity to negative ions, in line with laboratory observations, was much lower than hoped for.

The second, into the Solar Eclipse (ECLIPSE-79), was completed. Although recovery systems failed to carry the load, some instrumentation was recovered. Instrument performance was excellent and some data were presented at the 1980 American Geophysical Union, Spring Meeting at Toronto, Canada.[17] Excerpts are

17. Bailey, A., Narcisi, R. Federico, G., Wlodyka, L. (1980) Positive and negative ion composition measurements in the D&E regions during the 26 February 1979 solar eclipse, Presented to AGU, E.O.S. Vol. 61, pg 312, 22 April 1980.

reprinted here as Appendix F. Sensitivity to negative ions was still far below expectations in spite of hopeful efforts to improve it in laboratory preparation, for example, addition of the conical electrode shown in Figure 6.

The third experiment was not fully accomplished, since no SPE occurred during the available waiting period. However, one payload (PFRR-80), was launched into the trailing edge of a significant Auroral Zone Absorption (AZA) event, with nearly complete operational success. The newly-developed recovery unit, described in Section 3.2.7, worked perfectly, but predicted altitude was not achieved. Indications of poor negative ion sensitivity persisted in spite of promising design modifications.

4.2.1 POSITIVE ION PERFORMANCE

Performance of the CIMS in the positive ion mode has been encouraging. Comparison with positive ion data from predecessor blunt-nose instruments indicate that the attempt to avoid heavy cluster breakup has been successful. Although it is impossible to find two experiments with identical ionospheric conditions, some indicative parallels are suggested between the ECLIPSE-79 (post-totality) flight, and an AZA positive ion experiment from Fort Churchill, Canada, in 1973 (AZA-73). Both experiments were launched into energetic particle events, although the Eclipse experiment did not anticipate such a happening.

Table 7, makes comparisons between the calibration data for these instruments and the atomic oxygen O^+ and total cluster $H^+(H_2O)_n$ signals for each flight. Figures 41 (a,b) and 42 (a,b) provide the reader with some indications of CIMS success at avoiding heavy cluster breakup. Note that the ECLIPSE-79 data exhibit higher proportions of the heavier clusters, $H_9O_4^+$, $H_7O_3^+$, and $H_5O_2^+$ (37^+, 55^+, 73^+) than the AZA-73 data.

4.2.2 NEGATIVE ION PERFORMANCE

An important discrepancy arises when flight and calibration data from pre-CIMS negative ion experiments are compared with similar CIMS data. Even when one makes an allowance for dissimilarities in experimental conditions, ratios of flight-signal to calibration-reference levels from CIMS flights appear to be significantly lower than pre-CIMS similar ratios, as indicated in Table 8.

This table compares flight observations of the negative ion 98^-, $[NO_3(H_2O)_2]$ from two CIMS experiments, with a blunt-nosed instrument launched from Fort Churchill, Canada, in 1974 (CHILL-74). The 98^- peak was the most prominent and easily identified. No adjustments are made to account for differences in ionospheric or latitude conditions. All observations were made near 83^+_3 km, and the CIMS' were both launched into unexpected energetic particle events. The CHILL-74 was launched into an AZA event. Sensitivity comparisons are based on

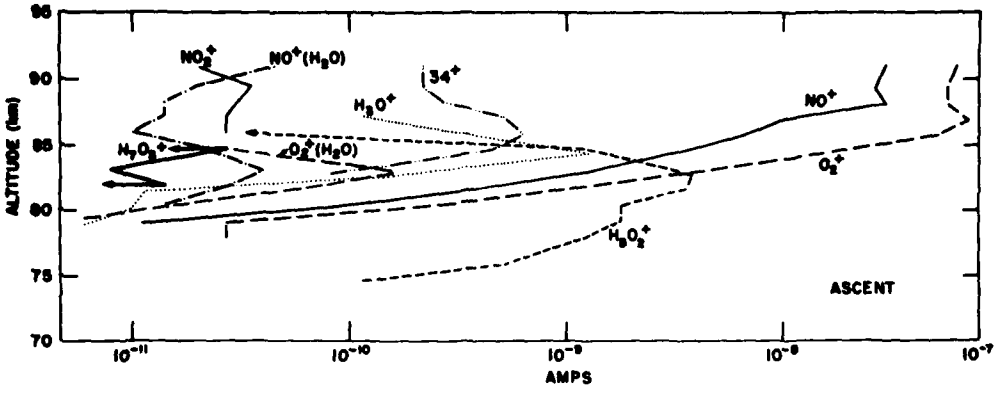

(a)

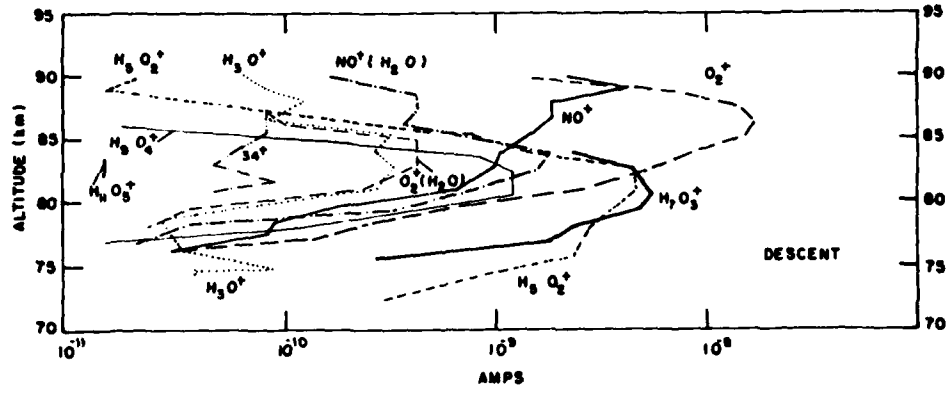

(b)

Figure 41. Pos-ion Flight Data vs Altitude AZA-73; a = Ascent, b = Descent

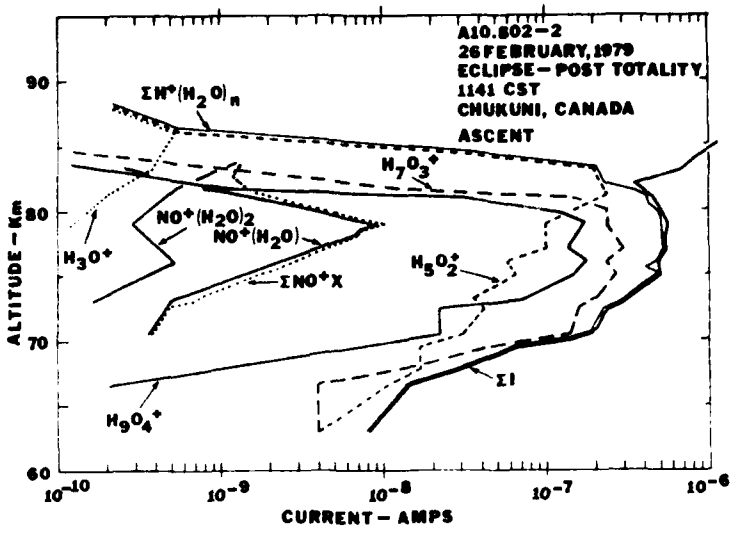

(a)

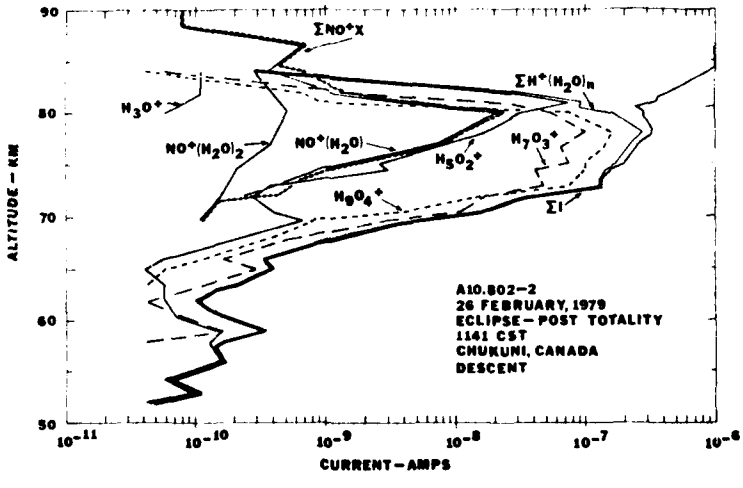

(b)

Figure 42. Pos-ion Flight Data vs Altitude ECLIPSE-79/2; a = Ascent, b = Descent

Table 7. Positive Ion Performance Comparison. Positive ion (flight signal)/(calibration sensitivity) comparison of CIMS-79 vs pre-CIMS, AZA-73 blunt-nose instrument data

Line No.	ECLIPSE-79	AZA-73	CIMS/AZA
1. Sensitivity to N_2^+	3.2×10^{-3}	4.3×10^{-4}	7.4
2. Max. signal, $H^+ (H_2O)_n$	(at 79 km)	(at 82 km)	
2a. Ascent	5×10^{-7}	5×10^{-9}	100.0
2b. Descent*	3×10^{-7}	1×10^{-8}	30.0
2c. Mean	4×10^{-7}	7.5×10^{-9}	53.3
3. Yield** = line 2c/line 1	1.2×10^{-4}	1.7×10^{-5}	7.2
4. Max. signal, O_2^+	(at 87 km)	(at 87 km)	
4a. Ascent	1.2×10^{-6}	3×10^{-9}	400.0
4b. Descent*	4×10^{-7}	1.5×10^{-8}	26.7
4c. Mean	8×10^{-7}	9×10^{-9}	88.9
5. Yield** = line 4c/line 1	2.5×10^{-4}	2.1×10^{-5}	11.9

*ECLIPSE-79 was attitude controlled with the vehicle axis aligned to the velocity vector. AZA-73 attitude was not controlled, resulting in a backdown attitude on descent.

**The concept of "Yield" is offered in an attempt to provide an indicator of the relative effectiveness of the conical nose "shock attaching" configuration, when compared with the earlier blunt-nose configurations. The calibration procedures used to date, as described in Section 4.1, do not include the effects of density discontinuities (shock fronts) in the sensitivity determinations. All calibration has been done under conditions of free molecular flow. Consequently, the only available data that may indicate the effectiveness of the new design is in situ flight data. "Yield" compares in situ flight data with laboratory calibration data, for a particular instrument. An obvious weakness in the application of such data to comparative analysis, is the difficulty of making valid comparisons between measurements taken under somewhat different conditions. For example, the relative amounts of the cluster species are dependent on ion production rate, total density, and various chemical processes.

laboratory calibrations using the oxygen 16^- reference. This is the only available negative ion that exhibits a nearly linear correlation with pressure.

The sensitivity numbers in Table 8 are taken from the earlier negative ion experiment. Figure 43 shows a sample of data from that experiment. This is representative of several such negative ion measurements, including reported attempts in 1967.[7]

Note especially the laboratory sensitivity of the CIMS' were apparently less than the CHILL-74 instrument by a ratio of $\approx 10^{-2}$, and appear less sensitive in flight by $\approx 10^{-4}$, clearly indicating a need for further design studies.

Table 8. Negative Ion Performance Comparison. Negative ion (flight signal)/(calibration sensitivity) comparison of CIMS-79, 80 vs pre-CIMS, Churchill (1974) blunt-nose instrument data

Line No.	ECLIPSE-79	CHILL-74[a]	CIMS/CHILL
1. Sensitivity to 16^-	3.9×10^{-5}	5×10^{-3} *	7.8×10^{-3}
2. Max. signal, 98^-	2×10^{-10}	1.2×10^{-6} **	1.6×10^{-4}
3. Yield*** = line 2/line 1	5×10^{-6}	2.4×10^{-4}	2×10^{-2}
PFRR-80			
4. Sensitivity to 16^- at 5.8 V (at 40.0 V)	2.2×10^{-4} (4.6×10^{-4})[b]	1×10^{-2} *	2.2×10^{-2} (4.6×10^{-2})[b]
5. Max. signal, 98^-	1×10^{-10}	2.4×10^{-6} **	4.2×10^{-5}
6. Yield*** = line 5/line 4	4.5×10^{-7} (2.2×10^{-7})[b]	2.4×10^{-4}	1.9×10^{-3} (9.1×10^{-4})[b]

[a]The CHILL-74 instrument utilized pulse counting as the data collecting technique. Consequently, comparisons with CIMS data requires an adjustment to equivalent SEM current. Because SEM gain differed among the several CIMS instruments, different equivalent CHILL-74 sensitivity numbers are shown for comparison to each CIMS instrument. The calculation used to obtain these numbers is:

$$S = \frac{\text{Count} \times \text{CIMS-SEM gain} \times 1.6 \times 10^{-19}}{\text{Sample time} \times \text{Test pressure}} \quad : \text{Amp/torr} .$$

[b]The PFRR instrument calibration yielded different sensitivity numbers at each front-end bias (5.8 V, 40 V). The 40 V number and related calculations are indicated in parentheses. Highest signals from the CIMS were with 5.8 V. The CHILL unit required +40 V to penetrate the vehicle potential sheath around the blunt-nose.

*Based on $16^- = 3 \times 10^3$ counts/0.01 sec/1×10^{-4} torr oxygen. Emission = 31 μA.

**Based on $98^- = 7.7 \times 10^3$ counts/0.01 sec at altitude.

***See note, Table 7.

There is some basis to believe that negative ion sensitivity loss is a consequence of thermal gas expansion effects in the new conical CIMS configuration, ion-focusing losses at the inlet, or other instrument design shortcomings. Note in Figure 33, that aliases NO^+ and O_2^+ show up very strongly in the negative ion mode of the PFRR-80 flight. This may be an indication of excessively high pressures inside the instrument. (See Figure 44.)

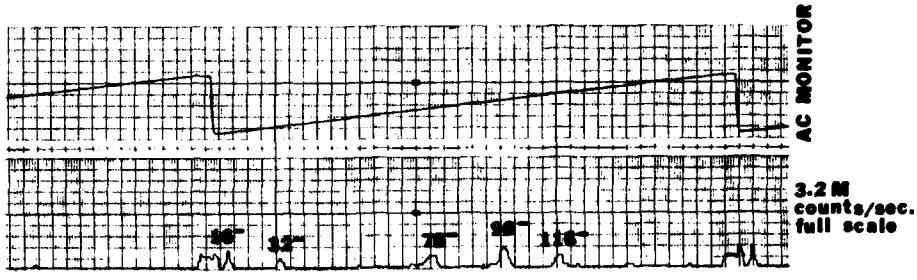

Figure 43. Neg-ion Flight Data Sample From CHILL-74

Figure 44. Photo of Prep/Cal Facility

5. CONCLUSIONS/RECOMMENDATIONS

Although some success can be claimed at the development of an instrument and payload system according to the documented objectives of this work unit, in fact the few glaring weaknesses reported in Section 4 need more attention. One of the principal objectives for development of the shock-attach configuration was to get measurements of cluster ions, unmodified by the pressure and temperature transitions across a shock wave. Consequently, the failure to date to obtain any substantive negative cluster measurements with the CIMS configuration is seen as a major disappointment, although not necessarily without prospect for resolution.

The most crucial of these weaknesses are the shortcomings of low negative ion sensitivity, and of inadequate pumping near the expansion region for low altitude measurements. It is believed that poor pump design is a factor in both problems.

5.1 Proposed Action

Two high priority areas in which to continue directed effort are recommended, (a) a concerted laboratory study of the ion-focusing problem in that expansion region between the sampling aperture and the mass filter inlet; and (b) the design and manufacture of a totally revised cryopump unit that provides for the correction of those several shortcomings noted in Section 2.2. Lower priority areas of development that will improve performance cabapilities include reductions in weight and size of elements of the overall payload.

5.1.1 ION FOCUSING STUDIES

A study of the ion-focusing problem must include the design and development of viable laboratory simulation hardware. First there is the need to generate a plasma in the 10 to 100 mTorr range to simulate in situ conditions. Secondly, an adaptable simulator of the instrumental sampling system is needed that can be readily modified and manipulated to test exploratory focusing techniques. See Figure 45.

The ion-focusing study may best be undertaken in-house or under close in-house supervision. Some preliminary effort in this direction was initiated in 1976. The need for resumption of this effort is clearly indicated.

5.1.2 CRYOPUMP

The design of a new cryopump may be relatively straightforward, if done by experienced cryogenic engineers, since the problems are identified and viable concepts for solution are known (see Figure 46). The cryopump lends itself to an R and D contract.

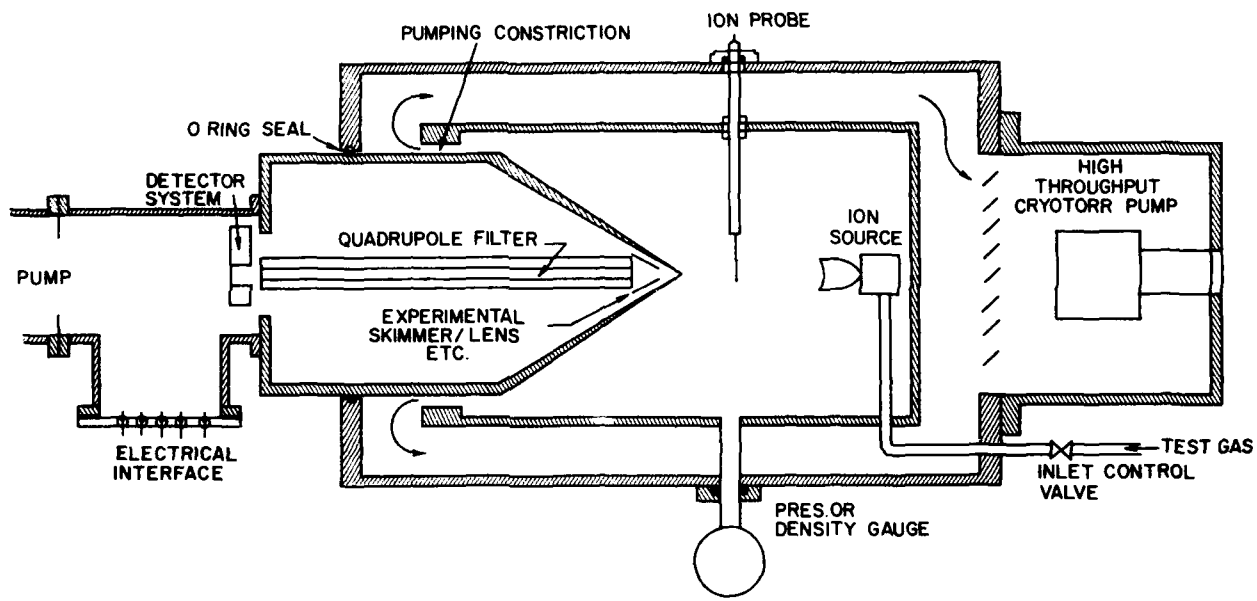

Figure 45. Suggested Simulator for Sampling/Focusing Studies

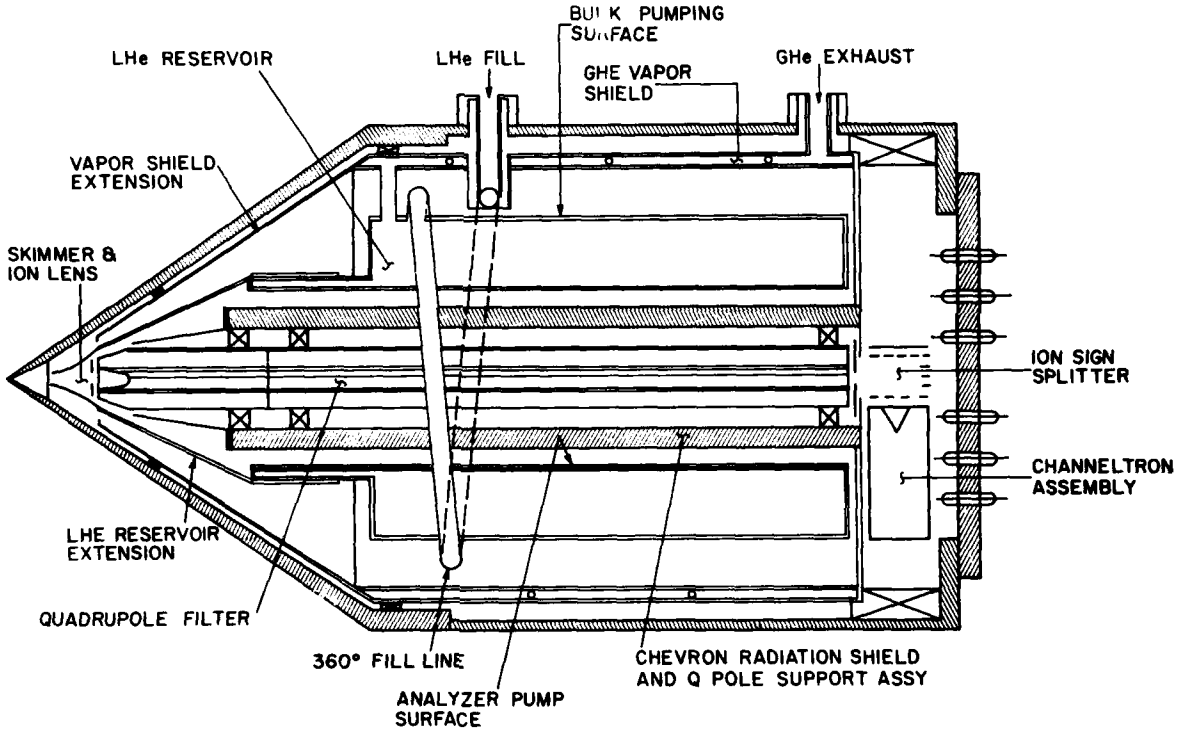

Figure 46. Proposed New Cryopump

5.1.3 SIZE AND WEIGHT REDUCTION

The present payload system is too heavy to achieve altitudes above 90 km, when using the booster system that it was designed around. Although this is adequate for D-region measurements, specific possibilities for weight reduction to achieve higher altitudes center around the scientific instruments. The electronics control unit of the CIMS has promising potential for compaction, and might permit a reduction of nearly a foot in payload length, with the corresponding saving in weight. The GC design is also under informal review with some hope for similar success, as are other areas which have been identified where materials can be removed.

References

1. Burke, R.R., and Miller, W.J. (1970) Study of Mass Spectrometer Ion Sampling Processes AerChem-TP-247, AFCRL-TR-70-0550, AD 725149.
2. Philbrick, C.R., Faucher, G., and Bench, P. (1978) Composition of the mid-latitude winter mesosphere and lower thermosphere, COSPAR:Space Research Volume XVIII, Pergamon Press, Oxford and New York.
3. Brubaker, W.M. (1968) Advances in Mass Spectrometry, Vol. 4, Elsevier, Amsterdam.
4. Haldeman, C.W., Kraemer, R.A., and Ziph, B. (1977) Wind Tunnel Tests of the Upstream Influence of a Conical Mass Spectrometer Probe, MIT-TR-197, AFGL-TR-77-0210, ADA 047739.
5. Alt, R.E., Price, L.L., Campbell, D.H., Stephenson, W.B., and Powell, H.M. (1980) Temperature and Density Measurements Near a 1/4 Scale Model Upper Atmospheric Probe at Mach Number 3.5, AEDC-TSR-80-V19.
6. Sherman, C., and Parker, L.W. (1970) Potential Due to a Circular Double Disk, Physical Sciences Research Paper No. 431, AFCRL-70-0568, AD 715889.
7. Narcisi, R.S., Bailey, A.D., Della Lucca, L., Sherman, C., and Thomas, D.M. (1971) Mass spectrometric measurements of negative ions in the D and lower E regions, J. Atmos. Terr. Phys. 33:1147-1159, Pergamon Press, Northern Ireland.
8. Rochefort, J.S., and Sukys, R. (1978) A Digital Control Unit for a Rocketborne Quadrupole Mass Spectrometer, AFGL-TR-78-0106, ADA 057251.
9. Rochefort, J.S., and Sukys, R. (1978) Electronics For A Rocketborne Quadrupole Cluster Ion Mass Filter, AFGL-TR-78-0292, ADA 066289.
10. Palasek, T.A. (1979) An R-F Oscillator for Rocketborne and Balloonborne Quadrupole Mass Spectrometers, AFGL-TR-79-0226, ADA 078797.
11. Haldeman, C.W., Bus, R.H., and Prey, S.W. (1978) Some Effects of Field Flow on the Capture Efficiency of a Gerdien Capacitor Atmospheric Probe, MIT-TR-204, AFGL-TR-79-0009, ADA 067710.

12. Haldeman, C.W. (1980) Wind Tunnel Tests of a Gerdien Capacitor-Vehicle Combination, MIT-TR-206, AFGL-TR-80-0179, ADA 091719.

13. Fike, R.M. (1973) Mobile S-band Trajectory Determination and Telemetry Receiving Systems, AFGL-TR-73-0716, AD 775748.

14. Buck, R.F., Gwinn, C.M., and Fike, R.M. (1975) Instrumentation for Research Rockets, AFGL-TR-75-0216, ADA 012552.

15. Space Data Corp. (1980) AFGL 12-inch Recovery Development & Design Report, SDC-TM-1791.

16. Space Data Corp. (1980) 12-inch Recovery Test Report, SDC-TM-1730-A.

17. Bailey, A., Narcisi, R., Federico, G., Wlodyka, L. (1980) Positive and negative ion composition measurements in the D&E regions during the 26 February 1979 solar eclipse, Presented to AGU, E.O.S. Vol. 61, pg 312, 22 April 1980.

Appendix A

Excalibur Cryopump Specification

The Excalibur Corporation
Waltham, Massachusetts
Los Altos, California

1. GENERAL DESCRIPTION

This Cryo-Vacuum pumping device utilizes the pumping action of zeolite (molecular sieve), which is bonded to the walls of a LHe container by a proprietary process. This bonding process is patented by the Linde Division of Union Carbide Corp., and licensed exclusively to The Excalibur Corporation. Use of this process permits the LHe-cooled zeolite to pump all gases, including He, H, and Ne with a high-sticking coefficient and in large enough quantities to permit fabrication of practical pumping units.

The Excalibur Model N873C Pump is a miniaturized and ruggedized version of The Excalibur Corporation line of ultra-high vacuum cryo pumps. This Model is sized to fit in a small rocket package, and constructed to withstand the severe vibrational and shock loadings of rocket flight, while still maintaining the minute heat leakage required for a cryogenic dewar. The materials of construction are primarily stainless steel with nickel plated copper, where thermal conductivity is of prime importance, and a small quantity of Teflon for thermal isolation. All vacuum walls and joints are stainless steel heliarc-welded for integrity. The pump is bakeable to 200°C, and will contribute no contaminants to the enclosed instrumentation. (See Figure A1.)

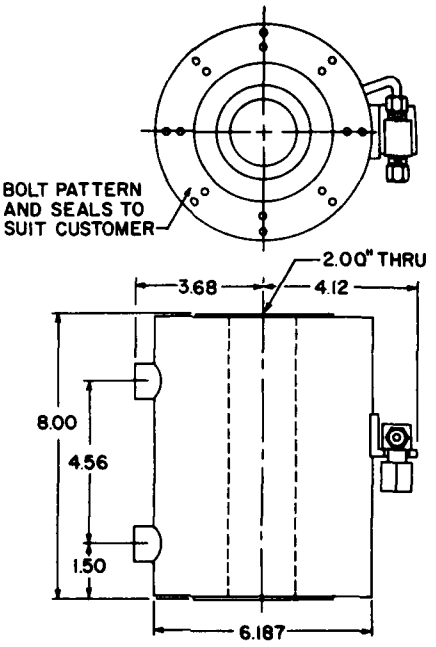

Figure A1. *Excalibur*

PERFORMANCE SPECIFICATIONS

a) Pumping speed	
Directed (at aperture)	1000 l/sec for Air 500 l/sec for He
b) Ultimate pressure	less than 10^{-8} torr (dependent on seals used)
c) Pumping capacity	greater than 200 cc (STP) Air greater than 100 cc (STP) He, H_2
d) LHe requirements	
To cool and fill	4 liters (from 80°K)
Hold time between refills	2 hours, min
e) Vibrational loading (longitudinal)	
Sinusoidal	5-20 CPS (0.25" displacement) 20-2000 CPS (±5 Gs)
Random	5 Gs RMS (1 min)
f) Shock loading	
+60 Gs peak amplitude (half sine pulse, 11 msec)	
-20 Gs peak amplitude (half sine pulse, 11 msec)	
g) Temperature capability	200°C
h) Cryogen level indication	Three level sensing by internal resistors (readout not included)

Appendix B

Powers Cryopump Drawing

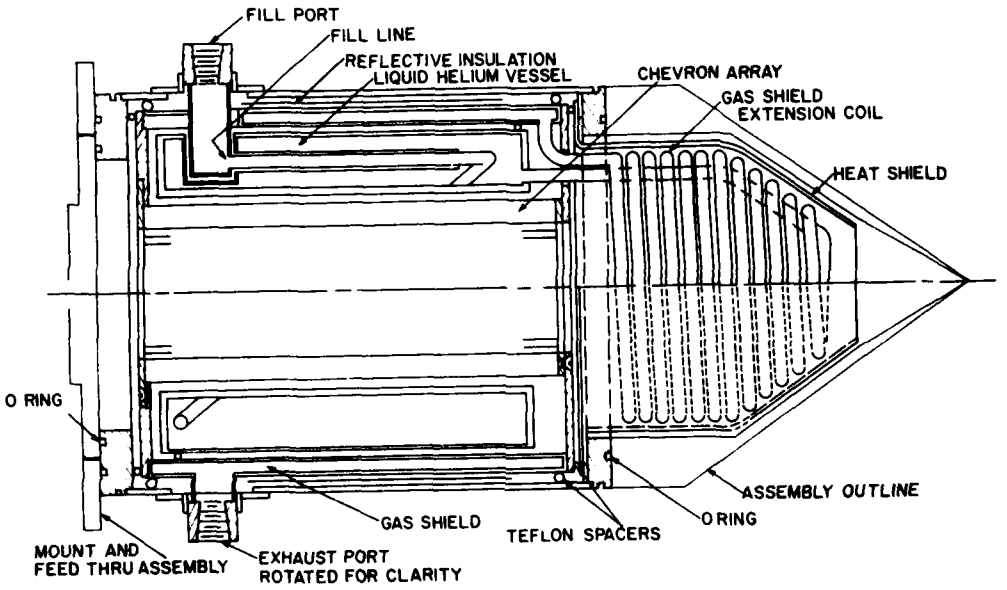

Figure B1. Power Cryopump

Appendix C

Electric Quadrupole Mass Filters

The quadrupole mass filter is constructed ideally of four electrically-conducting parallel hyperbolic cylindrical surfaces described by the equation

$$x^2 + y^2 = {}^{+}/_{-} A \qquad (1)$$

where A is a constant. In the most common mode of operation, opposite electrodes of the filter are connected together, and to one pair is applied a potential

$$\theta\,(t) = U + V \cos(2\pi ft)\ , \qquad (2)$$

where U is a dc voltage and V is the peak amplitude of a radio frequency ac voltage at the frequency f. To the other pair of electrodes the same potential, but of opposite sign, is applied, so that the equipotential surfaces are symmetric hyperbolic cylinders and the potential on the z-axis is zero. If one replaces the hyperbolic cylinders with circularly cylindrical rods, of radius 1.1486 times the inscribed circle radius, the fields near the axis closely approximate hyperbolic.

Important factors that determine the transmission and ultimate resolution of the quadrupole filter include ion energy, ion entrance optics, purity and stability of the U and V potentials, the U/V ratio, suppression of scattered ions, and the physical accuracy of the pole dimensions.

If an ion is injected at the entrance end of this assembly with motion generally parallel to the z-axis, the ac and dc field, which are perpendicular to the z-axis, will cause it to undergo transverse motion. The differential equations of motion in the x-y plane are Mathieu equations. The solutions contain either an exponential factor or an oscillatory factor, depending on the charge-to-mass ratio e/m of the ion. With proper selection of U and V, ions of a given e/m will have stable trajectories and the ions will oscillate about the z-axis, ultimately emerging from the opposite end of the assembly. Ions with other values of e/m will have unstable trajectories and move away from the z-axis, ultimately being removed.

For mass separation to occur, any ion of the incorrect e/m must remain in the transverse fields sufficiently long that it will be rejected. This requires that a maximum axial ion energy exists for a filter of given length L. If E_{ion} is in electron volts, then

$$E_{ion} < 0.04\, f^2 L^2\, (\Delta m/m)m \tag{3}$$

where m is the mass in amu, f is the ac frequency in MHz, and L is in centimeters.

The mass resolution of such a device is expressed by

$$\frac{m}{\Delta m} = \frac{0.126}{0.16784 - U/V} \tag{4}$$

from which, by making the ratio U/V = 0.16784, one achieves a theoretical infinite mass resolution, and the resolution can be varied by controlling the ratio U/V. For infinite resolution the values of U and V are given by

$$U\,(\text{volts}) = 1.212\, mf^2 r_o^2 \tag{5a}$$

$$V\,(\text{volts}) = 7.219\, mf^2 r_o^2 \tag{5b}$$

where r_o is the radius, in centimeters, of the circle tangent to the electrode surfaces.

Variation of the mass to be transmitted can be accomplished through either the variation of U and V, or the variation of f. Equation (4) indicates that constant resolution $m/\Delta m$ is maintained if U and V are always held in the same ratio. In the CIMS, as in most Quadrupole Systems, the frequency is held constant while U and V are varied simultaneously.

If ions are injected either off axis or with a transverse initial velocity component, (as in virtually every real situation), the following analysis applies. For

ions injected parallel to the axis, the maximum injection aperture to insure that none of the ions will strike the electrodes has a radius, a, given by

$$a \approx \frac{2}{3} r_o (\Delta m/m)^{1/2} \quad . \tag{6}$$

Similarly, the maximum transverse energy, E_t, of an ion injected at the axis can have to assure transmission is given by

$$E_t \approx \frac{m}{2} f^2 r_o^2 (\Delta m/m) \quad , \tag{7}$$

where E_t is in electron volts. It is evident that as $\Delta m/m$ is decreased, the transmission will diminish until only ions injected exactly on the axis parallel to it, will emerge from the filter.

Note that to operate in a constant $m/\Delta m$ resolution mode, the maximum aperture for entrance of the ions is independent of the mass, but the maximum transverse energy of ions to be transmitted increases with mass. Heavy ions with a given transverse energy E_t will be transmitted while light ions will not. The mass filter will show a mass-dependent transmission with discrimination against the lighter ions.

Operation in a mode with U and V controlled for constant Δm would result in all centrally injected ions below a given E_t to be transmitted, while the maximum radius for transmission of paraxially injected ions would decrease with mass. This results in a mass-dependent transmission that discriminates against heavier ions.

A mixed mode may be achieved if U and V are controlled so that

$$U = gV - h \quad , \tag{8}$$

where g and h are selected constants. Then Eq. (4) becomes

$$\frac{m}{\Delta m} = \frac{0.126}{(0.16784 - g) + hV} \quad . \tag{9}$$

In this case if $h = 0$, then g determines a constant $m/\Delta m$, and if $g = 0.16784$, then h determines a constant Δm. It is then possible to select values of g and h that avoid the mass discrimination associated with either mode, over a selected mass range, of about 10:1 or less.

Analyses of the effects of the entrance fringe fields on ion transmission have shown a great dependence on the injection angle in the y-z plane (the plane of the

pole pair that is biased with negative dc for positive ions).[C1] A useful technique to reduce this loss of ions incorporates a set of auxiliary poles, located at the entrance to the main set. By applying the full ac voltage but no dc voltage to this set, the dc field component is delayed for ions entering the filter system. This is called the "delayed dc ramp" technique (DDCR). This technique has shown dramatic improvements in ion transmission at high resolutions, especially for ions of low injection energy.

The CIMS not only utilizes the DDCR technique, but also takes advantage of the possibility to bias the two sets of poles to different references. In the negative ion mode, electrons are drawn into the quadrupole field at sufficiently high energies to generate positive ions. The CIMS uses a positive ion-retarding bias differential between the two pole sets to discriminate against those formed within the first set.

The influence of pole length on the mass resolution depends on the choice of ion injection velocity (energy) and ac frequency, as indicated by Eq. (3). This expression suggests that either frequency or length may be adjusted with equally proportional effect, but this choice should be weighed with due consideration of other factors. For example, the length-to-diameter ratio should be great enough to reduce the relative distortions of the end fringe fields, and the relative impact on the exciter power requirements should be considered.

In practice it is found that the resolution increases with the ion mass, with a simultaneous drop in the transmission efficiency. This is attributed to the number of ac cycles seen by the ion as it passes through the filter. An empirical expression that describes this effect is,

$$(m/\Delta m)_{max} \approx B\, N^{1.7} \quad , \tag{10}$$

where B is a constant, and N is the number of ac cycles. This evolved from experiments based on the observation of the resolution as a function of ion kinetic energy. For an ion injection potential V

$$eV = \frac{1}{2} m v^2 \quad . \tag{11}$$

In traversing a filter of length L, an ion sees N cycles as

$$N = f L/v \quad . \tag{12}$$

C1. Brubaker, W. M. (1968) Advances in Mass Spectrometry, Vol. 4, Elsevier, Amsterdam.

If N must remain constant for fixed resolution and transmission, then v must also be held constant. This is achieved if D is a constant and

$$V = D m \quad . \tag{13}$$

Another approach to constant $m/\Delta m$ operation is to vary f as the square of $1/m$

$$f^2 = k m \tag{14a}$$

$$N^2 = k L^2/m v^2 \tag{14b}$$

$$N^2 = k L^2/2 eV \quad . \tag{14c}$$

This method has not generally been used, probably because of equipment complexity and the inconvenience of the nonlinear mass scale that results.

In cylindrical rod mass filters, the fields are not hyperbolic near the electrodes, and the ion trajectories far off the axis are not the ideal trajectories for filter operation. To most closely approximate hyperbolic fields, it is desirable to have as large an r_o as practicable, in order to offer an adequate entrance aperture to obtain the desired sensitivity. A large r_o may also help to avoid problems associated with maintaining accuracy of the pole dimensions. The achievement of good resolution requires both high voltage purity and stability, and high physical dimensional precision. Realistic manufacturing tolerances can have less impact with larger pole diameters. Fractional radial dimensional requirements are nominally $(\Delta m/4m)$.

Large radial dimensions also increase demands on the exciter circuitry. Applied voltages must be increased as the square of r_o. Consider the following where C = capacitance pole-to-pole in picofarads, including shunt to ground; Q is the normal figure of merit of the ac generator; and P is the power dissipated by the power supply, in watts.

$$P = 6.5 \times 10^{-4} \, C \, M^2 f^5 r_o^4 / Q \quad . \tag{15a}$$

For any given diameter structure, C is proportional to length L (typically 2 pf/cm). Q is typically 100 to 150. Consequently where room is available, and exciter power economy is important, an increase in L (and C) would appear preferable to an increase in f, as a means to improve ultimate resolution. Other factors such as mean free path, and ion energy spread must also be considered. If typical values for C and Q are substituted in Eq. (15a),

$$P \approx M^2 f^5 L r_o^4 \times 10^{-5} \quad . \tag{15b}$$

It is clear from the previous discussions that high performance as a sensitive mass filter depends heavily on the ion entry conditions. Instruments intended for high performance analysis incorporate some means to control the injection conditions. The nature of such means is a function of the application. Generally an electrostatic lens arrangement will be mounted at the inlet of the mass-filter with potentials applied that establish optimum limits on injection energy, angle and radius. Ion entry into the lens will be from an ion generator with suitably chosen potentials, or from a sampling orifice through which ions travel from a separate test chamber.

Any application of the device to aeronomic measurement from a sounding rocket must encounter special problems of sensitivity and resolution, because control over ion entry conditions is complicated by special sampling problems. These arise from variations in velocity, and the pressure differentials across the inlet orifice and the shock-front ahead of the orifice.

Experience with blunt-nose payloads suggest that sufficient ion number injection rates are readily obtainable. D-Region (65 to 110 km) measurements of positive ions have been routinely obtained with this configuration with the simple expedient of a three bias sequence applied as follows:

a. The exposed blunt circular forward surface of the cylindrical instrumented vehicle is biased slightly (-10 V) with respect to the main vehicle surface.

b. Internally, a flat apertured accelerator plate is located immediately behind the centered inlet orifice. A significant ion accelerating potential (-50 V) is applied to aid ion extraction from the bulk expanding gas. The aperture limits the ion injection radius into the filter.

c. The mass filter is mounted immediately behind the accelerator plate with a reference bias (-15 V) chosen only to assure ion transmission through the filter.

Attempts to avoid shock-front effects ahead of the blunt surface utilize a conical sampling configuration to attach the shock at the sampling inlet orifice at the apex. However, a special problem arises as a consequence of the restrictions imposed by the cone, against placing the mass-filter inlet at the sampling orifice, especially without obstructing neutral gas flow and expansion. This enlarges the problem of extracting and focusing ions of the bulk gas into the mass filter inlet.

Efforts to design an ion-focusing lens that is effective in the transitional flow region have not yet been successful. Such designs require empirical verification through well-designed experimental testing.

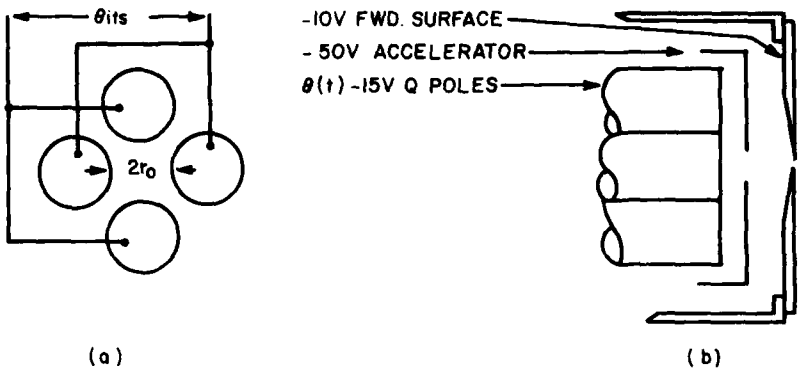

Figure C1. Q-pole

Appendix D

Gerdien Condenser (GC)

SPE GERDIEN SYSTEM NO. 1 (Figures D1-D6)

Electrometer calibration

I	$E_{o(+)}$	$E_{o(-)}$
10^{-12}	-0.12	-0.14
3x 10^{-12}	-0.06	-0.21
10^{-11}	+0.08	-0.34
3x	0.38	+4.92
10^{-10}	0.83	4.39
3x	1.29	3.87
10^{-9}	1.79	3.31
3x	2.25	2.78
10^{-8}	2.75	2.32
3x	3.20	1.69
10^{-7}	3.70	1.12
3x	4.14	0.60
10^{-6}	4.65	0.02
3x	5.08	-0.50
10^{-5}	5.41	-0.63

V_R Sweep	V_R	V_{RTM}
Small sweep	+43.4 V	1.62 V
	-43.4	3.48
Duration	0.83 sec/slope	
Large sweep	+88.0	0.67 V
	-88.0	4.42
Duration	1.7 sec/slope	

Calibrations	E_{oTM}
Mode	
1	3.3 and 1.8 V
2	0
3	0
4	1.5 and 3.3

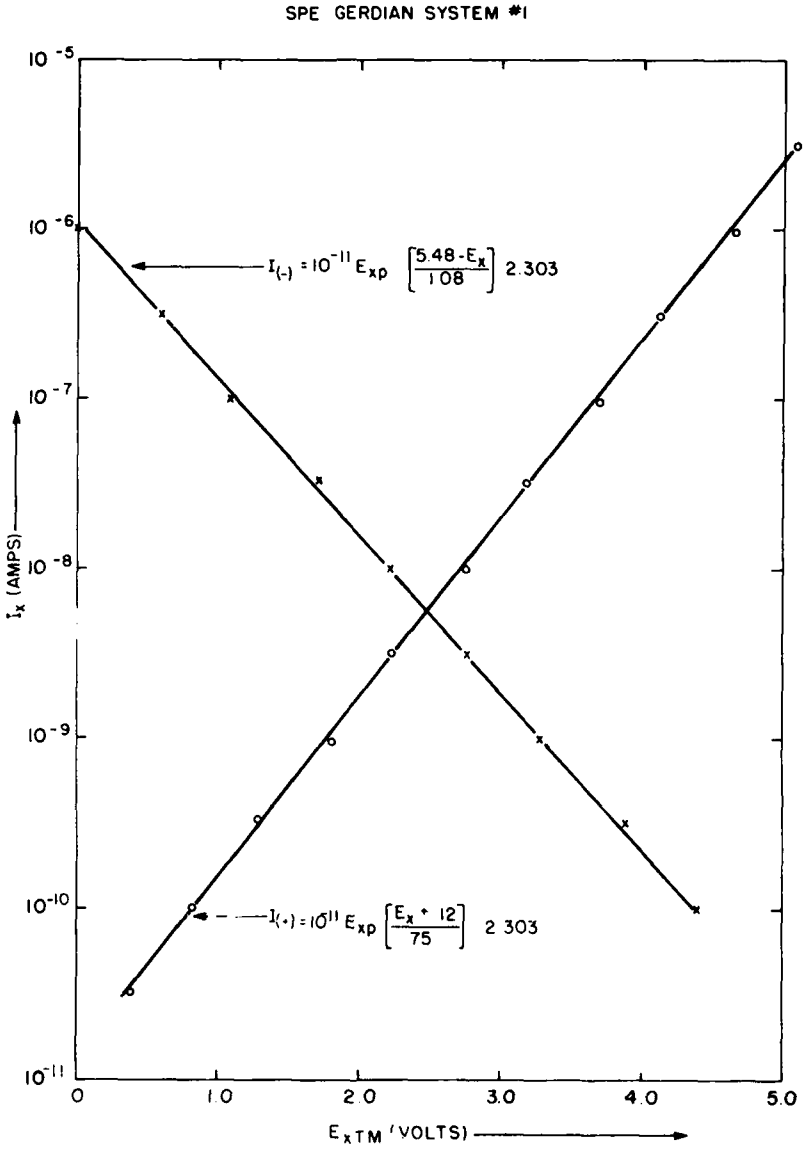

Figure D1. Gerdien Condenser (Capacitor) GC

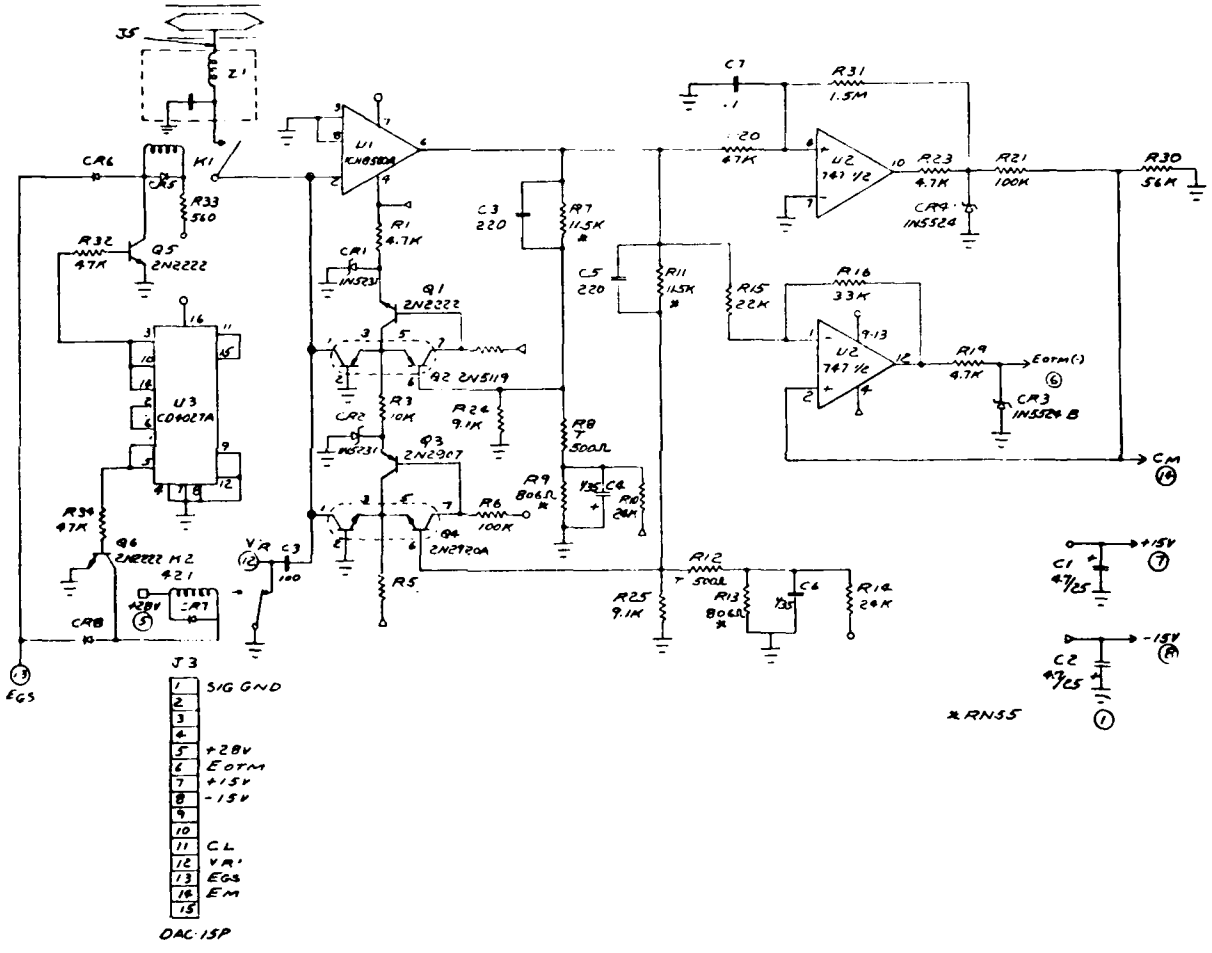

Figure D2. Bipolar Log Amp Gerdien Condenser

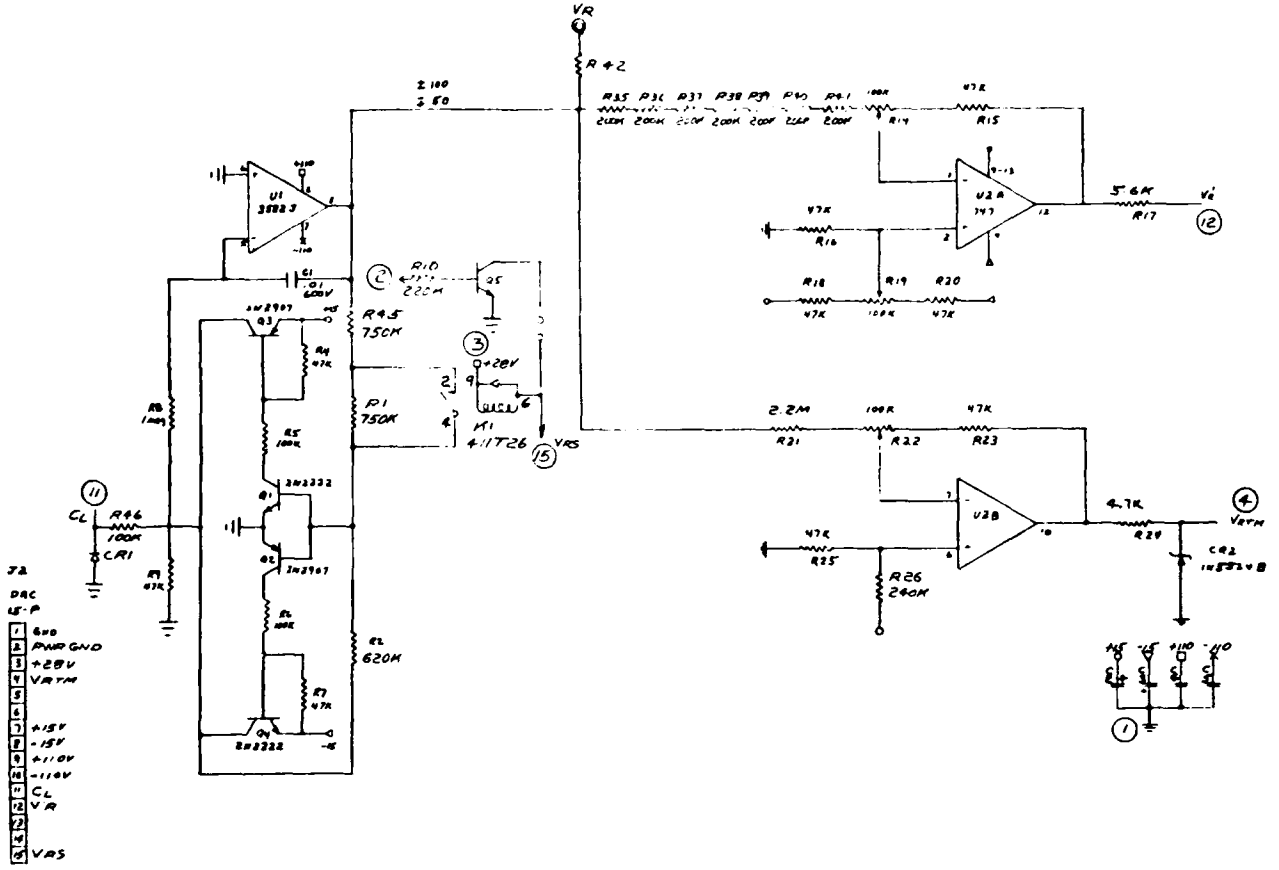

Figure D3. (+) and (-) Gerdien Sweep

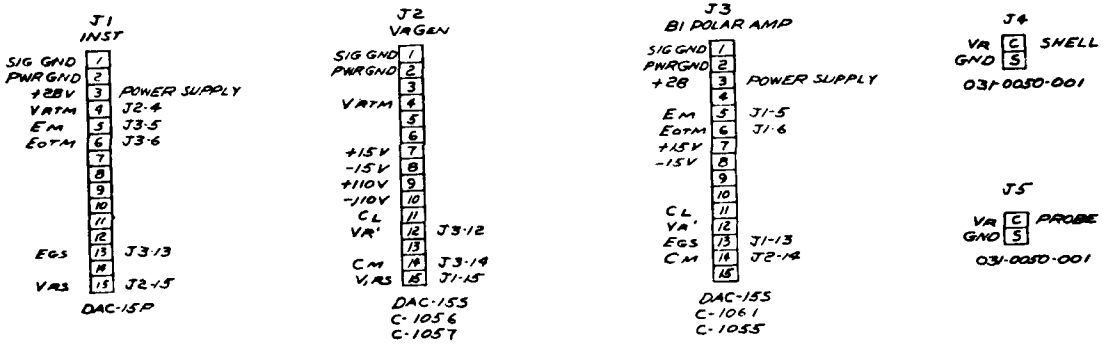

Figure D4. Wiring Harness Gerdien Condenser

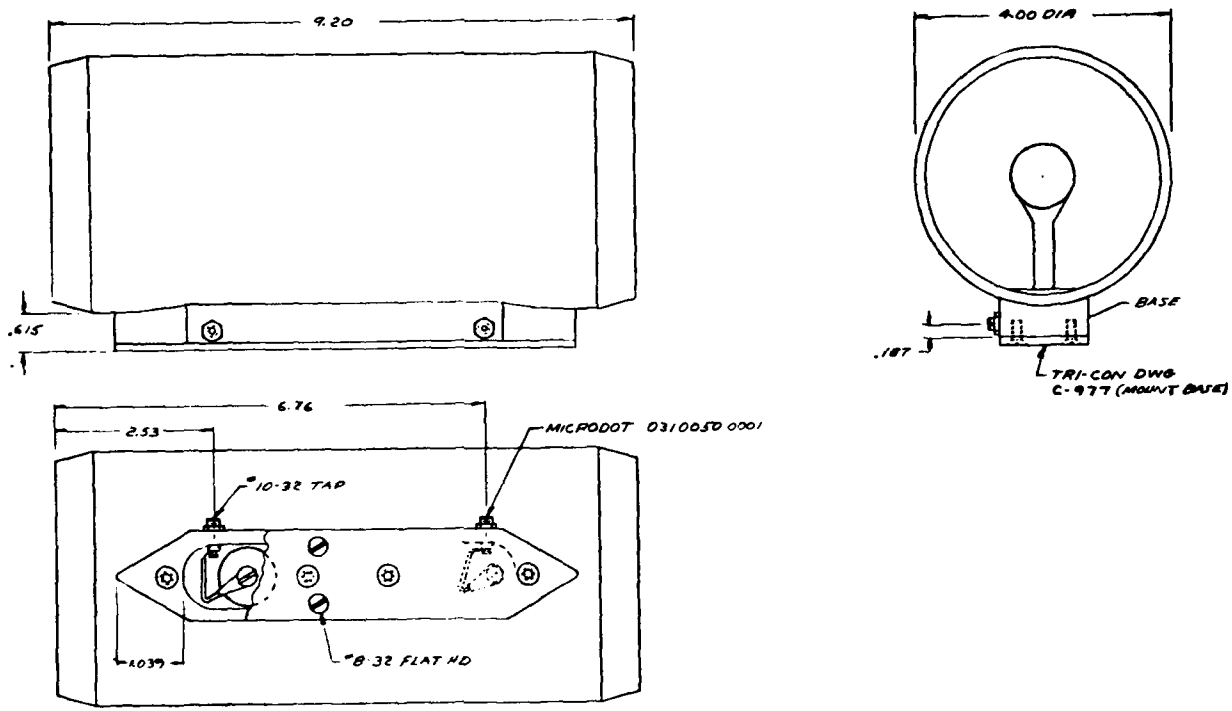

Figure D5. Gerdien Outline

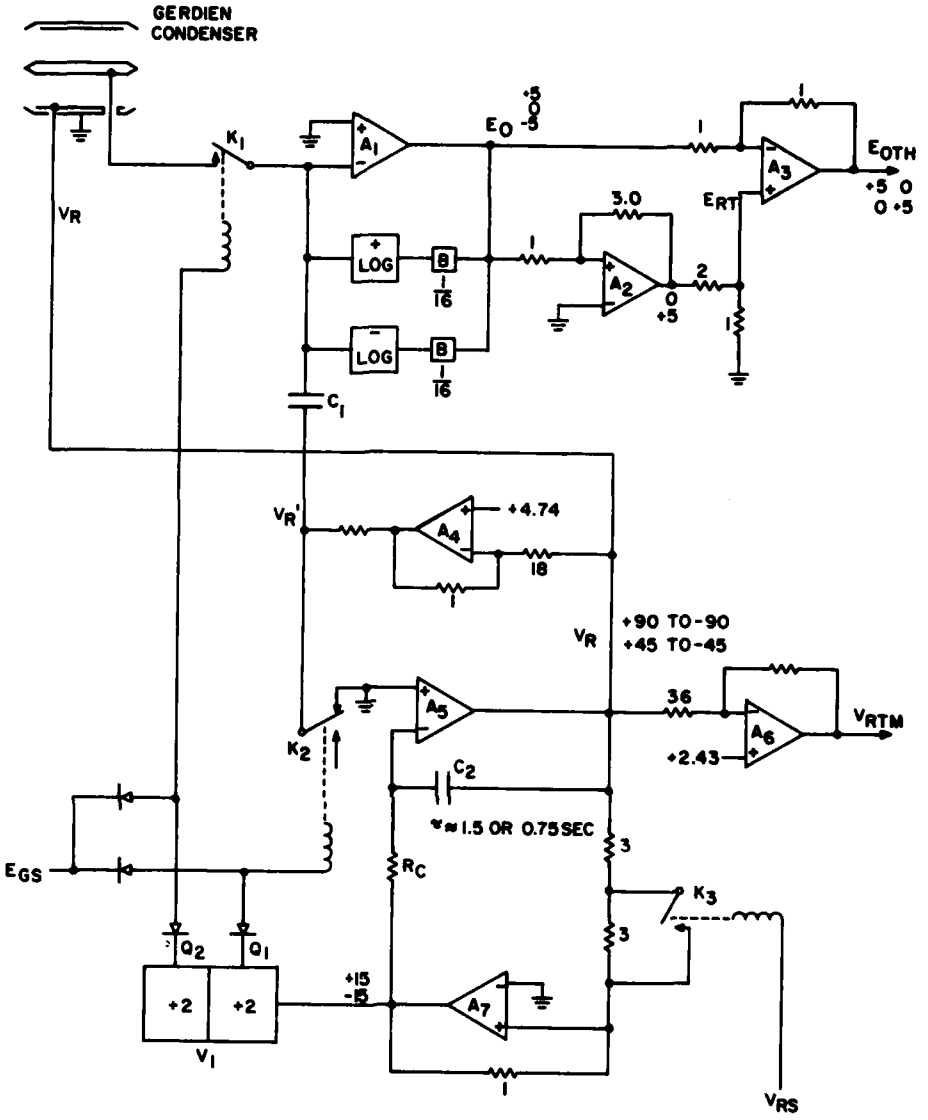

Figure D6. Gerdien Condenser Block Diagram

Appendix E

Retarding Potential Analyser (RPA)

SPE RPA SYSTEM NO. 1 (Figures E1-E7)

Electrometer calibration

Input current I_i	Output voltage E_{oTM}
$+ 10^{-7}$	5.3
$+ 10^{-8}$	4.2
$+ 10^{-9}$	3.1
$+ 10^{-10}$	2.05
$+ 10^{-11}$	1.0
$+ 10^{-12}$	0.45
0	0.4 or 4.65
$- 10^{-12}$	4.6
$- 10^{-11}$	4.05
$- 10^{-10}$	3.4
$- 10^{-9}$	2.65
$- 10^{-8}$	1.95
$- 10^{-7}$	1.25
$- 10^{-6}$	0.55
$- 10^{-5}$	0.05

V_R Sweep	+6.5 to -3.2
V_{RTM}	+0.7 to +3.2
Duration	0.35 sec/slope

Sensor Element Voltages

	(+) Mode	(-) Mode
V_A	-1.5	+5.1
V_o	-5.2	+8.0
V_k	-13.0	+13.0

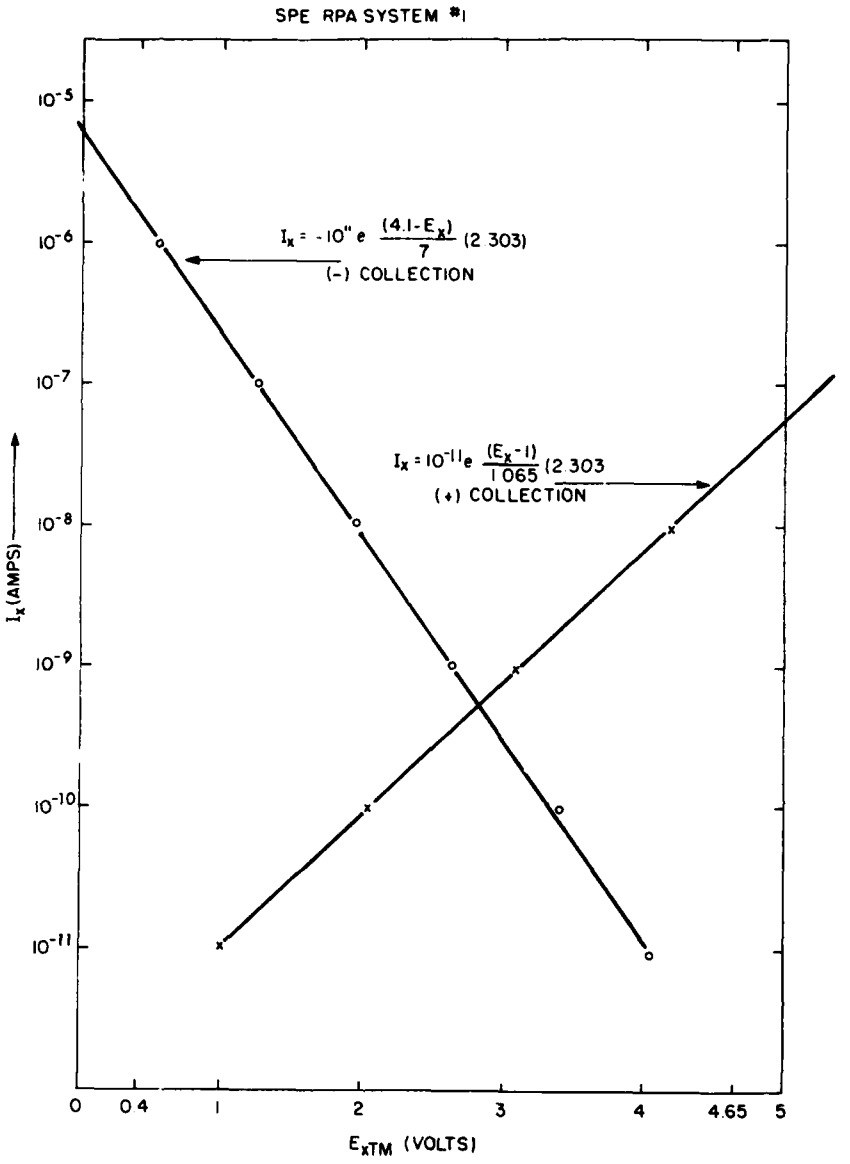

Figure E1. Retarding Potential Analyzer RPA

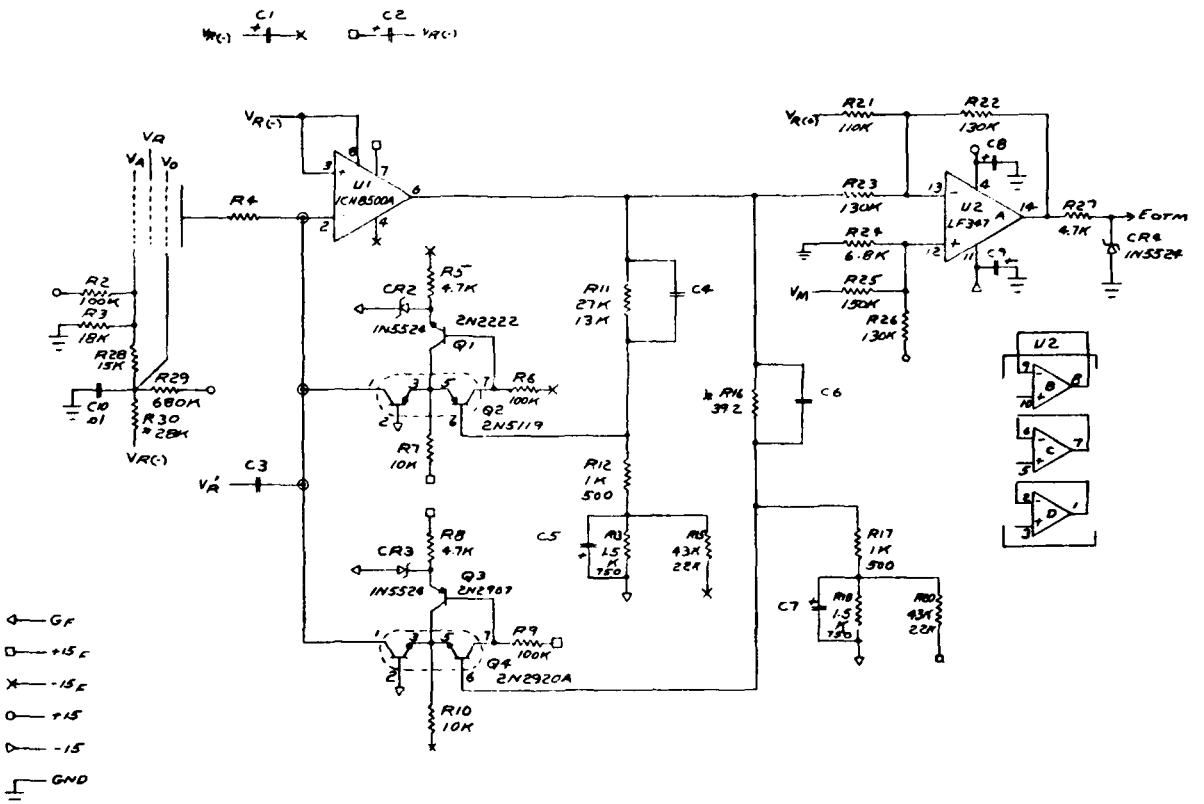

Figure E2. RPA Bipolar Logarithmic Amplifier

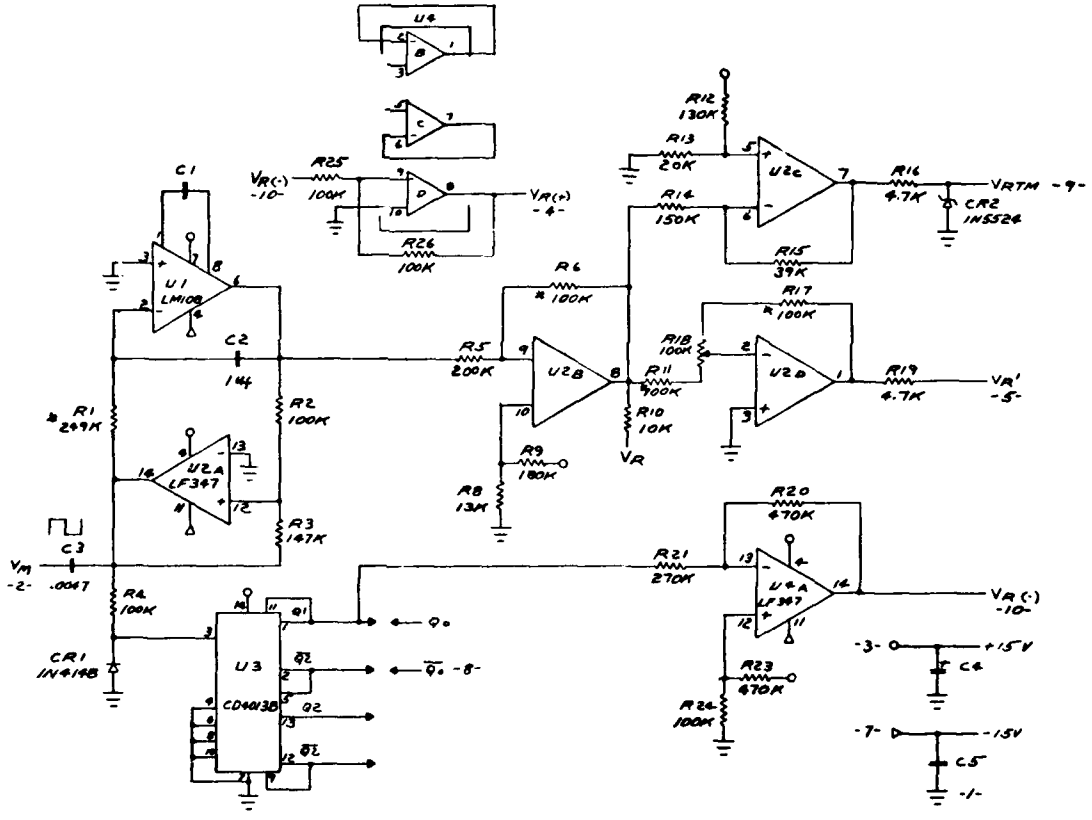

Figure E3. SPE RPA Sweep

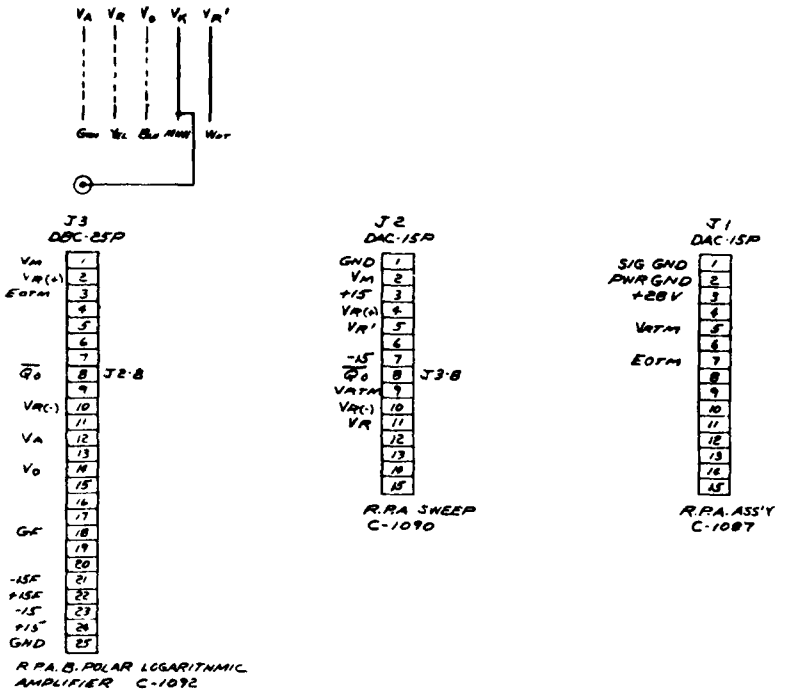

Figure E4. SPE Wiring Diagram

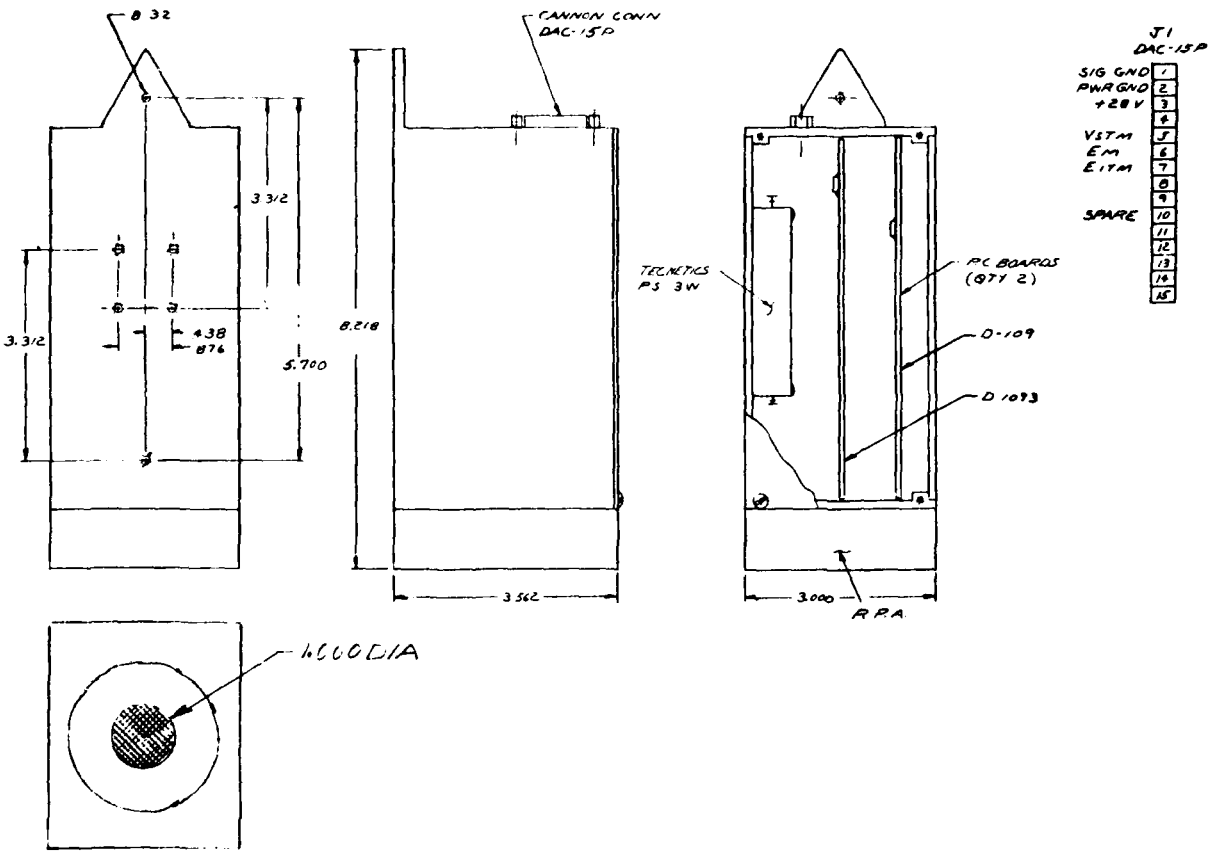

Figure E5. RPA Assembly

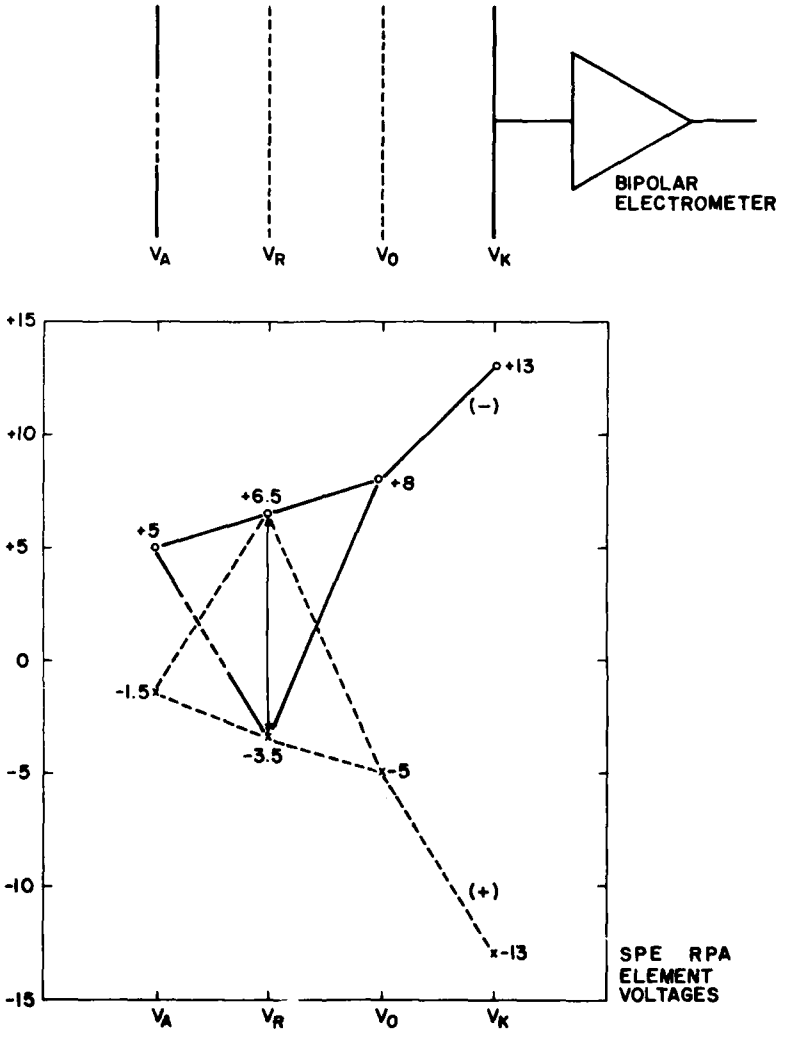

Figure E6. SPE RPA Element Voltages

AD-A118 752 AIR FORCE GEOPHYSICS LAB HANSCOM AFB MA F/G 7/4
DEVELOPMENT OF AN ION MASS SPECTROMETER AND SOUNDING ROCKET SYS--ETC(U)
JAN 82 A BAILEY, R NARCISI, L WLODYKA
UNCLASSIFIED AFGL-TR-82-0022 NL

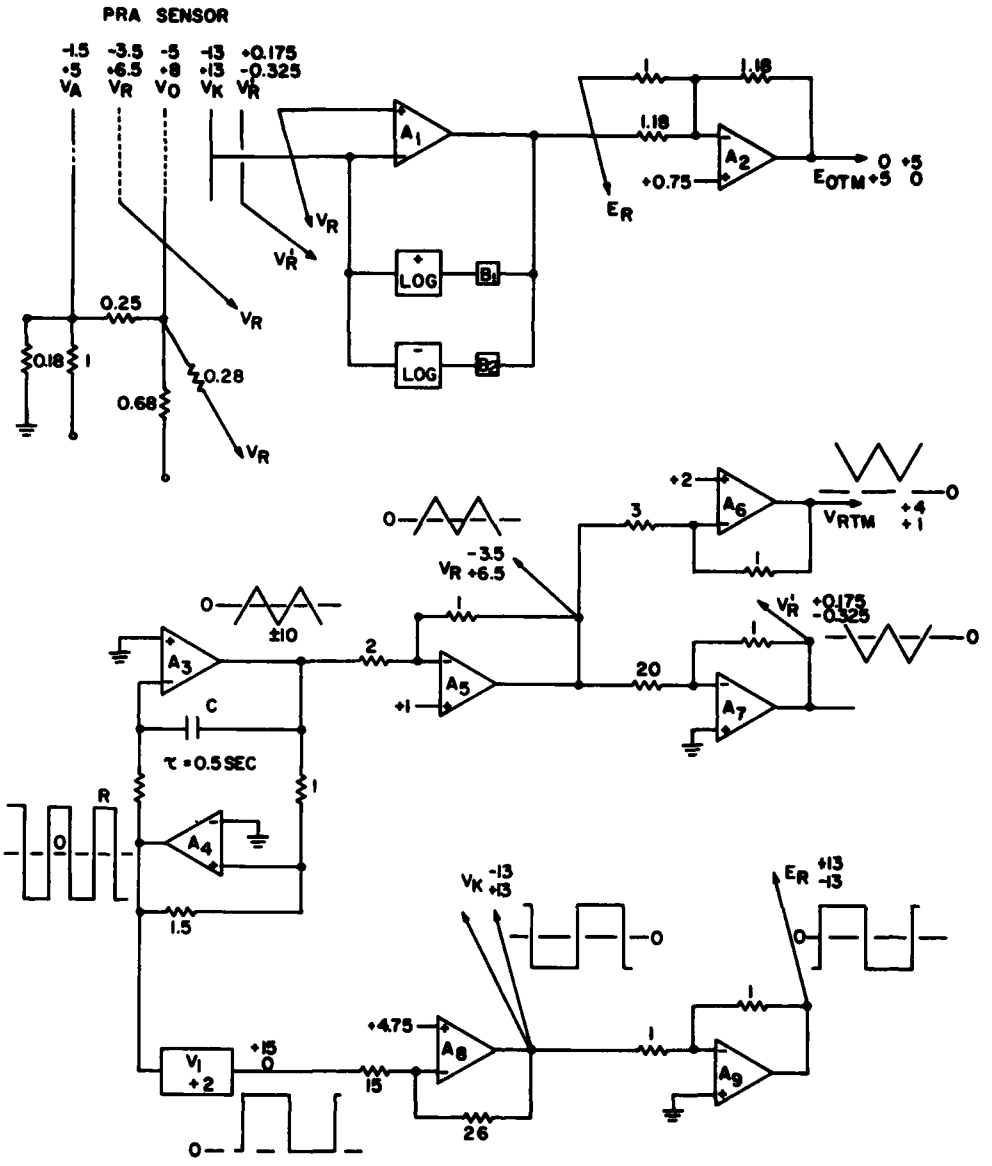

Figure E7. SPE RPA Block Diagram

Appendix F

Positive and Negative Ion Composition Measurements in the D and E Regions During the 26 February 1979 Solar Eclipse

A. Bailey, R. Narcisi, G. Federico and L. Wlodyka

Aeronomy Division, Air Force Geophysics Laboratory
Hanscom AFB, Massachusetts 01731

ABSTRACT

Two rockets carrying LHe, cryopumped quadrupole mass spectrometers capable of measuring both positive and negative ions and with shock-attaching conical samplers were launched from Red Lake, Canada during the solar eclipse. Attitude control systems always maintained the rockets at very low attack angles. The first rocket was launched so that the upleg D region was in darkness 35 ±8 sec and the downleg D region about 150 ± 15 sec after second contact. The second rocket was fired after totality in 75 percent solar illumination. The positive ion composition above 105 km exhibited a strongly increasing NO^+/O_2^+ ratio with time after second contact due to O_2^+ charge transfer with NO and a sharply diminished ionization rate. However, in both flights, the ionization rate below 105 km was dominated by energetic particle deposition exemplified by the increased ion concentration and the composition signatures of a particle event: a significant enhancement of O_2^+ at lower altitudes and large amounts of $H_5O_2^+$ ions in the D region that result from the O_2^+ clustering scheme. $H_5O_2^+$ was the major ion in the upper D region while $H_7O_3^+$, $H_9O_4^+$, and $H_5O_2^+$ were present at lower altitudes. The negative ion distributions in both flights exhibited a distinct shelf about 83 ±2 km dropping off by more than an order of magnitude by 90 km and with minima near 75 km. In the 75-90 km range a significant percentage of the negative ions had masses greater than 160 amu. Comparisons with prior flight results during daytime auroral zone absorption events will be made.

Note: This paper was presented at the 1980 Spring Meeting of the American Geophysical Union to be held in Toronto, Canada. Abstract Clearances: AFGL 38-80 and AFSC/OIS 80-197. (See Figure F1.)

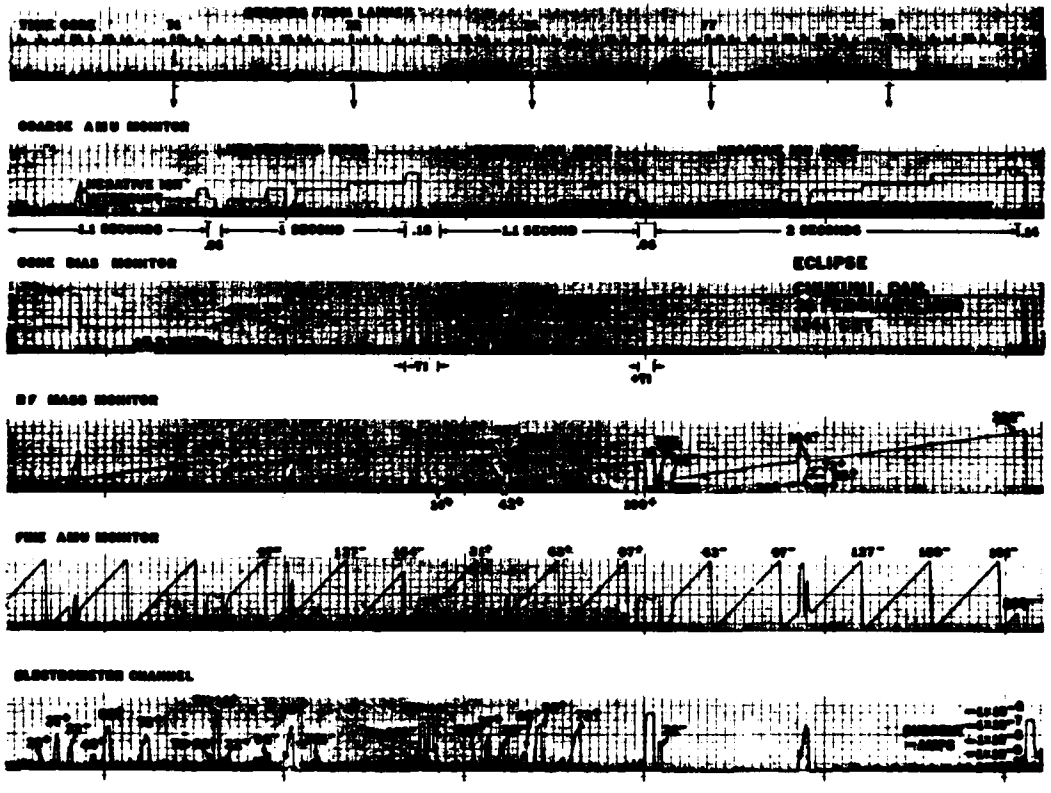

Figure F1. ECLIPSE-79 Flight Data Sample

ME

8